

**BIOPHYSICAL MODELS OF α -AMINO-3-
HYDROXY-5-METHYL-4-ISOXAZOLE-
PROPIONIC ACID RECEPTOR
TRAFFICKING IN
DENDRITES**

by

Berton A. Earnshaw

A dissertation submitted to the faculty of
The University of Utah
in partial fulfillment of the requirements for the degree of

Doctor of Philosophy

Department of Mathematics

The University of Utah

December 2007

Copyright © Berton A. Earnshaw 2007

All Rights Reserved

THE UNIVERSITY OF UTAH GRADUATE SCHOOL

SUPERVISORY COMMITTEE APPROVAL

of a dissertation submitted by

Berton A. Earnshaw

This dissertation has been read by each member of the following supervisory committee and by majority vote has been found to be satisfactory.

Chair: Paul C. Bressloff

James P. Keener

Alla Borisyuk

A. Villu Maricq

Gregory A. Clark

THE UNIVERSITY OF UTAH GRADUATE SCHOOL

FINAL READING APPROVAL

To the Graduate Council of the University of Utah:

I have read the dissertation of Berton A. Earnshaw in its final form and have found that (1) its format, citations, and bibliographic style are consistent and acceptable; (2) its illustrative materials including figures, tables, and charts are in place; and (3) the final manuscript is satisfactory to the Supervisory Committee and is ready for submission to The Graduate School.

Date

Paul C. Bressloff
Chair, Supervisory Committee

Approved for the Major Department

Aaron Bertram
Chair/Dean

Approved for the Graduate Council

David S. Chapman
Dean of The Graduate School

ABSTRACT

The trafficking of α -amino-3-hydroxy-5-methyl-4-isoxazolepropionic acid (AMPA) receptors in dendrites is emerging as a major postsynaptic mechanism for the expression of plasticity at glutamatergic synapses. AMPA receptors within a spine are in a continuous state of flux, being exchanged with local intracellular pools via exo/endocytosis and with the surrounding dendrite via lateral membrane diffusion. The precise mechanisms underlying the activity-dependent regulation of AMPA receptor trafficking are currently unknown. However, they are likely to involve one or more of the following processes: changes in the interaction between receptors and other synaptic proteins, changes in the rates of exo/endocytosis, and modifications in membrane or receptor structure that alter the surface transport of receptors. Here we present biophysical models of AMPA receptor trafficking at single dendritic spines and between multiple dendritic spines distributed along the surface of a dendrite that take into account these modes of receptor trafficking. Solutions of these models reproduce a variety of experimental data including trafficking during plasticity, and allow us to make predictions concerning the important targets of second-messenger pathways activated during plasticity. For example, scaffolding protein numbers must be up- or down-regulated during plasticity in order for there to be a persistent change in the number of AMPA receptors at a synapse. We also derive an effective “cable equation” for receptor trafficking whose solutions determine the distribution of synaptic receptor numbers across multiple spines. These solutions allow us to examine how lateral diffusion regulates the strength of a synapse. In particular, our analysis suggests that 1) lateral membrane diffusion alone is an insufficient synaptic delivery mechanism, 2) local changes in the constitutive recycling of AMPA receptors induce nonlocal changes in synaptic strength, and 3) AMPA receptor trafficking is not likely to mediate heterosynaptic forms of plasticity.

To Tiraje, the thrill of science is fleeting, the joy of love is eternal.

CONTENTS

ABSTRACT	iv
LIST OF FIGURES	viii
LIST OF TABLES	x
ACKNOWLEDGEMENTS	xi
CHAPTERS	
1. INTRODUCTION	1
2. AMPA RECEPTOR TRAFFICKING AND SYNAPTIC PLASTICITY	3
2.1 Neuronal communication	3
2.2 NMDA receptor-mediated LTP/LTD	6
2.3 AMPA receptors and trafficking	8
2.3.1 Basal trafficking	10
2.3.2 LTP trafficking	11
2.3.3 LTD trafficking	12
3. COMPARTMENTAL MODEL OF AMPA RECEPTOR TRAFFICKING AT A SINGLE DENDRITIC SPINE	14
3.1 Model equations	16
3.1.1 Steady-state solution	18
3.1.2 Model extensions during LTD	20
3.2 Analysis of model equations	20
3.2.1 Receptor trafficking under basal conditions	22
3.2.2 Increase of synaptic receptor concentration during LTP	26
3.2.3 Decrease of synaptic receptor concentration during LTD	30
3.3 Spatial model of AMPA receptor trafficking at a single spine	33
3.3.1 Model equations	35
3.3.2 Description of numerics	36
3.3.3 Steady-state AMPA receptor concentrations and fluxes	38
3.3.4 Blocking exo/endocytosis	41
3.3.5 Trafficking during LTP and LTD	41
3.4 Discussion of single-spine model	43
3.4.1 Effects of diffusion	47
3.4.2 Single-channel conductance	48
3.4.3 Slot proteins and synaptic stabilization	49

4.	TWO-DIMENSIONAL MODEL OF AMPA RECEPTOR TRAFFICKING ACROSS MULTIPLE DENDRITIC SPINES	50
4.1	Diffusion-trapping model on a cylinder	51
4.2	Steady-state analysis using asymptotic matching	55
4.2.1	Matching inner and outer solutions	56
4.2.2	Calculation of boundary concentrations U_j	59
4.2.3	Evaluation of Green's function	61
4.3	Comparison of singular perturbation solution with numerical and one-dimensional solutions	62
4.4	Mean first passage time for a receptor	64
4.4.1	Evaluation of Green's Function	68
4.4.2	Effective and anomalous diffusion	69
4.5	One-dimensional approximation of outer solution	71
5.	ONE-DIMENSIONAL CONTINUUM APPROXIMATION OF THE MULTISPINE MODEL	73
5.1	One-dimensional continuum multispine model	74
5.1.1	Model extensions during LTP and LTD	77
5.2	Steady-state analysis	80
5.2.1	Uniform background concentration	81
5.2.2	Nonuniform background concentration	81
5.3	Delivery of synaptic AMPA receptors from the soma via lateral diffusion	83
5.4	Nonlocal effects of constitutive recycling mediated by lateral diffusion	86
5.5	Lateral diffusion of AMPA receptors is unlikely to mediate heterosynaptic LTP/LTD	90
5.5.1	Long-term potentiation	91
5.5.2	Long-term depression	96
5.6	Discussion	96
5.6.1	Maintenance of LTP/LTD	98
5.6.2	Sharing endosomes	99
5.6.3	Spine morphology	100
5.6.4	Homeostatic synaptic scaling	100
6.	FUTURE DIRECTIONS	102
6.1	Extension of spatial single-spine model	102
6.2	Anomalous lateral diffusion of AMPA receptors at synapses	103
6.3	Intrinsic and extrinsic noise	105
6.4	Discrete synaptic states	106
	REFERENCES	108

LIST OF FIGURES

2.1 Schematic of a prototypical neuron	4
2.2 Electron micrograph and schematic of a dendritic spine showing various components	5
2.3 Schematic of synaptic transmission	5
2.4 Typical LTP/LTD recordings	6
2.5 Schematic of an NMDA receptor	7
2.6 Schematic of AMPA receptor subunit topology	9
2.7 Schematic of AMPA receptor trafficking at a dendritic spine	10
3.1 Simplified two-compartment model of a dendritic spine	14
3.2 LTD model	21
3.3 Steady-state synaptic receptor number as a function of model parameters . .	24
3.4 Time course of AMPA receptors after blocking exo/endocytosis	25
3.5 Time course of AMPA receptors during LTP	29
3.6 Exchange of GluR1/2 and GluR2/3 AMPA receptors	30
3.7 Time course of AMPA receptors during LTD	34
3.8 Model geometry	35
3.9 Steady-state behavior under basal conditions	40
3.10 Time course of AMPA receptors after blocking exo/endocytosis	41
3.11 Snapshots of GluR1/2 AMPA receptor concentration and flux during LTP .	42
3.12 Time course of AMPA receptors during LTP	44
3.13 Snapshots of GluR2/3-GRIP and GluR2/3-PICK AMPA receptor concentrations and fluxes during LTD	45
3.14 Time course of AMPA receptors during LTD	46
4.1 Diffusion-trapping model of receptor trafficking on a cylindrical dendritic cable	52
4.2 Solutions U , U_j , R_j and S_j	64
4.3 Effect of ϵ on the solution U	65
5.1 One-dimensional continuum model of AMPA receptor trafficking across multiple dendritic spines	76

5.2	Models of AMPA receptor trafficking during LTP/LTD	78
5.3	Steady-state distribution of AMPA receptors as a function of distance from the soma	87
5.4	Nonlocal effects of variations in constitutive recycling	89
5.5	Time course of AMPA receptor trafficking during LTP: insertion of receptor-scaffolding complexes into the ESM.....	93
5.6	Time course of AMPA receptor trafficking during LTP: insertion of scaffolding proteins into the PSD	95
5.7	Time course of AMPA receptor trafficking during LTD	97

LIST OF TABLES

3.1 Basal parameter values	22
5.1 Basal parameter values for dendritic spines	84
5.2 Parameters during LTP	91
5.3 Parameters during LTD	92

ACKNOWLEDGEMENTS

Many thanks to the faculty and staff of a most helpful and encouraging mathematics department. A heartfelt thank you to the members of my supervisory committee for their time, energy and enlightenment. An especial thank you to Paul, an extraordinary mathematician who took a chance on a pure math drop-out. Loving thanks to my parents for life, faith and opportunity. Finally, no amount of thanks can express my gratitude to my family: to Emerson, who ever reminds me that the world is mysterious and thrilling; to Adrienne, who can turn darkness into light with a single chubby smile; and to Tiraje, my Love, my Everything, life is empty without you.

Thanks to the National Science Foundation for funding my studies and this work (NSF grants VIGRE 0091675, RTG 0354259, and DMS 0515725).

CHAPTER 1

INTRODUCTION

Motor control, perception, learning, memory and other characteristic functions of the brain depend upon a neuron's ability to communicate with other neurons. Understanding neuronal communication has long been the subject of scientific research, beginning in the late nineteenth century with the work of Golgi and Ramón y Cajal [52]. It was recognized early in these studies that the network of neurons comprising the brain must in some sense be *plastic*, i.e., able to undergo modifications accounting for the experience-dependent adaptation of the brain's various functions. However, it took nearly eight decades before researchers demonstrated activity-dependent plasticity in the mammalian brain [7]. *Long-term potentiation* (LTP), as it was called, is a lasting increase in the efficacy of synaptic transmission induced by correlations in neural activity. A short time later, a similar plasticity with the opposite effect on synaptic efficacy was discovered, termed *long-term depression* (LTD) [74]. Since that time, LTP and LTD have been studied extensively in many organisms and in many parts of the nervous system. Various kinds of LTP/LTD have been identified, and many of the mechanisms involved in the induction, expression and maintenance of LTP/LTD have been elucidated (see [8, 76, 69, 75] for reviews). Because LTP/LTD is activity-dependent and ubiquitous at synapses throughout the mammalian nervous system, many hypothesize that LTP/LTD represents a prototypical mechanism for learning and memory (see [8, 76, 81, 82] for reviews).

Due in part to the study of LTP/LTD, the synapse is now understood to be a dynamic mosaic of highly-regulated proteins which are in a continuous state of flux, trafficking about the synapse and interacting with other proteins. In particular, a large body of experimental evidence suggests that the dendritic trafficking of α -amino-3-hydroxy-5-methyl-4-isoxazolepropionic acid (AMPA) receptors is responsible for the changes in synaptic efficacy observed during LTP/LTD (see [111, 13, 120, 78, 119, 125, 77, 19, 138, 36, 10, 22, 98, 139] for reviews). AMPA receptors mediate the majority of fast excitatory synaptic transmission in the central nervous system and their trafficking appears to

occur through a combination of two major mechanisms: exo/endocytic exchange of membrane-embedded receptors with intracellular receptor pools, and lateral diffusion of receptors between the synapse and the surrounding extrasynaptic membrane. Under basal conditions, the steady-state AMPA receptor concentration within a synapse is determined by a dynamical equilibrium in which the various receptor fluxes into and out of the synapse are balanced, and any change of one or more of these fluxes can subsequently modify the number of synaptic receptors in thus alter the efficacy of the synapse.

The precise mechanisms underlying the activity-dependent regulation of AMPA receptor trafficking are currently not known. However, they are likely to involve one or more of the following processes: changes in the interaction between receptors and other synaptic proteins, changes in the rates of exo/endocytosis, and modifications in membrane or receptor structure that alter the surface transport of receptors. In this thesis, we present mathematical models of receptor trafficking that take into account these processes. We analyze the solutions of these models in order to 1) determine the steady-state number of AMPA receptors at synapses under basal conditions, to 2) investigate the dependence of this steady-state number on local and nonlocal changes in AMPA receptor trafficking, and to 3) study the time-course of variations in synaptic receptor number induced by LTP/LTD in order to identify possible targets of second-messenger pathways that are activated at the onset of LTP/LTD.

The thesis is organized as follows. We begin in Chapter 2 with a review of AMPA receptor trafficking and N-methyl-D-aspartate (NMDA) receptor-mediated LTP/LTD. In Chapter 3 we present and analyze a compartmental model of AMPA receptor trafficking at a single dendritic spine. Employing this single-spine model, we propose in Chapter 4 a model of AMPA receptor trafficking across multiple dendritic spines distributed along the surface of cylindrical dendritic cable. For long cables this model is approximated very well by a one-dimensional continuum model of AMPA receptor trafficking, and in Chapter 5 we analyze this simplified model. We end the thesis with a proposal of future research (Chapter 6).

CHAPTER 2

AMPA RECEPTOR TRAFFICKING AND SYNAPTIC PLASTICITY

In this chapter we briefly review the fundamentals of neuronal communication including synaptic transmission. We also introduce the phenomenon of synaptic plasticity and some accompanying experimental data. AMPA receptors and their subunit composition are then discussed. Finally, we review the trafficking of AMPA receptors at synapses and its role in synaptic plasticity.

2.1 Neuronal communication

Prototypical neurons, such as the pyramidal neuron shown in Figure 2.1, are highly polarized, possessing a single long process called an *axon* and a larger number of ramified processes called *dendrites* which emanate from the soma. These processes are used to send and receive information encoded in the temporal dynamics of neuronal membrane potential. When a region of the somatic membrane called the *axon hillock* or *trigger zone* is sufficiently depolarized, a significant deviation in resting membrane potential called an *action potential* is initiated and actively propagated from the soma to terminals at the distal ends of the axon. These terminals form highly specialized contact sites called *synapses* with other neurons. Synapses are usually located on a dendrite of the postsynaptic neuron, but can occur on both the soma and axon. Excitatory synapses in the central nervous system are almost always formed on small protrusions of the dendrite called *dendritic spines* (see Figure 2.2).

The synapse is the locale of neuronal communication. When an action potential reaches an axon terminal, the accompanying change in membrane potential causes voltage-gated calcium channels to open. The subsequent increase in intracellular Ca^{2+} concentration initiates various second-messenger pathways, one of which causes vesicles containing chemicals called *neurotransmitters* to fuse with a specialized area of the presynaptic membrane called the *active zone*. The fused vesicles secrete neurotransmitter into the

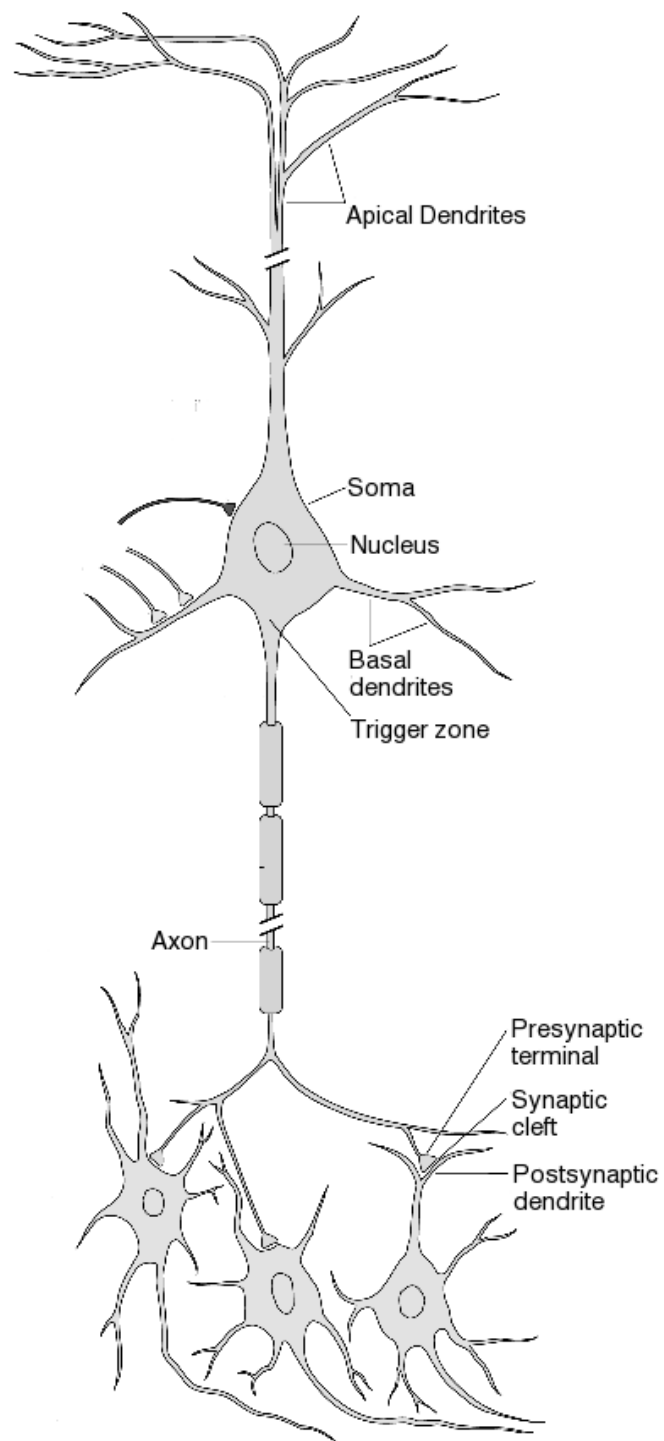


Figure 2.1. Schematic of a prototypical neuron, demonstrating the soma, axon, dendrites and synapses. (Adapted from [52])

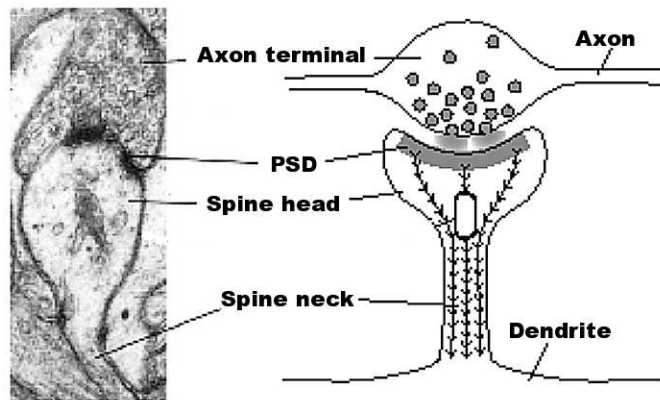


Figure 2.2. Electron micrograph and schematic of a dendritic spine showing various components. (Adapted from [85])

synaptic cleft, the extracellular space between the pre- and postsynaptic membranes. The neurotransmitter diffuses through the cleft and potentially binds with an appropriate receptor embedded in the postsynaptic membrane (see Figure 2.3). If the synapse is *excitatory* – that is, if it acts to propagate the action potential – then this binding affects a depolarization of the postsynaptic membrane. For example, the binding of glutamate (the major excitatory neurotransmitter in the central nervous system) to AMPA receptors begins a rapid influx of cations through the receptor pore, accounting for

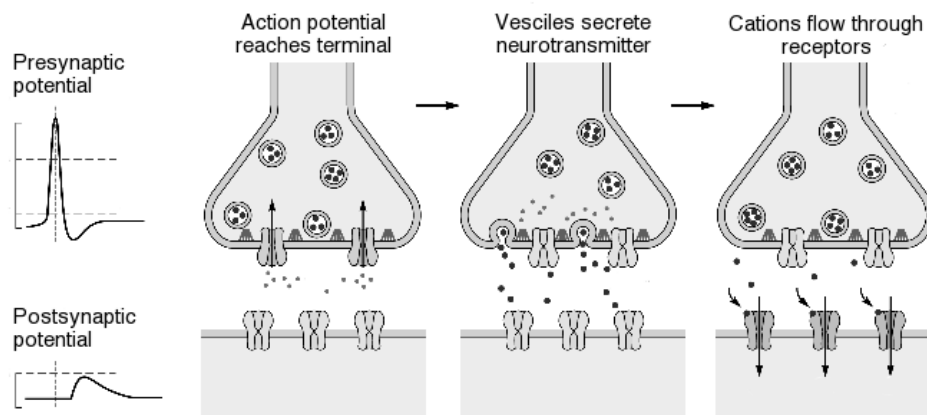


Figure 2.3. Schematic of synaptic transmission. The arrival of an action potential at an axon terminal causes a presynaptic release of neurotransmitter which binds to selective receptor channels on the postsynaptic membrane. These ligand-gated channels open and allow an influx of ions (typically Na^+ , Ca^{2+} and K^+), creating the synaptic potential. (Adapted from [52])

most of the depolarization. This *synaptic potential* then passively diffuses to the soma of the postsynaptic neuron, where it integrates with synaptic potentials from other synapses until a sufficiently depolarized trigger zone fires an action potential and starts again the communication pathway.

2.2 NMDA receptor-mediated LTP/LTD

A remarkable property of the synapse is its ability to regulate the efficacy of its own transmission, a phenomenon called *synaptic plasticity*. As mentioned above, LTP and LTD are well-studied, prototypical forms of synaptic plasticity. Typical recordings made during LTP/LTD experiments are shown in Figure 2.4. In slice preparations (e.g., from the CA1 region or dentate gyrus of the hippocampus) LTP is induced either by delivering a brief tetanic stimulus (e.g., 100 Hz for 1 s) to the postsynaptic neuron, or pairing stimulus delivery with significant membrane depolarization. LTD is induced either by delivering a low-frequency stimulus for many minutes (e.g., 1 Hz for 5-15 min) or pairing stimulus delivery with membrane depolarization. Both LTP and LTD can be divided into two phases. *Early-phase* LTP/LTD is characterized by a change in the amplitude of synaptic potentials lasting up to an hour after stimulus delivery, the amplitude increasing during LTP and decreasing during LTD. Studies suggest that these early-phase changes

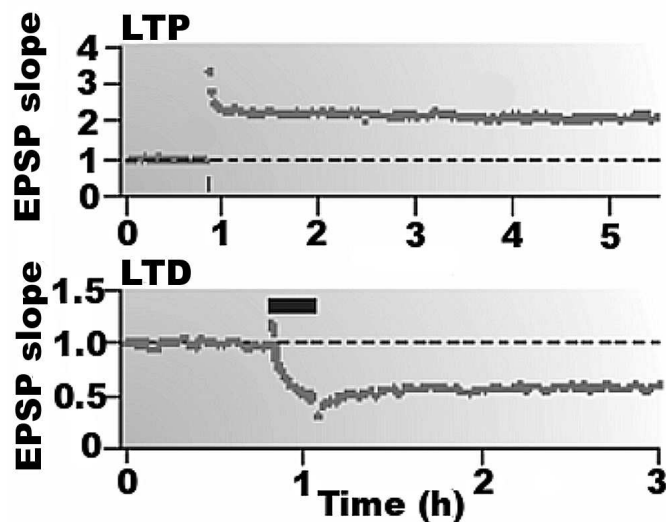


Figure 2.4. Typical LTP/LTD recordings. LTP is characterized by a lasting (> 1 hr) increase in the amplitude or slope of excitatory postsynaptic potentials (EPSPs), while LTD is characterized by a lasting decrease in the same. (Adapted from [22])

are due mainly to variations in the number and function of postsynaptic AMPA receptors [75]. In *late-phase LTP/LTD*, the change in synaptic potential amplitude lasts anywhere from a few hours to the entire lifetime of the synapse and requires new protein synthesis and gene transcription (see [51, 75] for reviews). Because of its dependence on AMPA receptor trafficking, this paper is mainly concerned with the early-phase of LTP/LTD. Also, the term *weight* of a synapse is often used to denote the amplitude of the synaptic potential, and one speaks of LTP and LTD as *up-* and *down-regulating* the synaptic weight, respectively.

A ubiquitous form of LTP/LTD at CNS excitatory synapses depends upon the activation of N-methyl-D-aspartate (NMDA) receptors (see Figure 2.5). NMDA receptors mediate the influx of Ca^{2+} into the dendritic spine, and the spatiotemporal pattern of this intracellular Ca^{2+} signal triggers second-messenger pathways within the neuron that affect the up- or down-regulation of the synaptic weight. Like AMPA receptors, NMDA receptors require glutamate to allow ion flow. Unlike AMPA receptors, however, the NMDA receptor possesses a voltage-sensitive magnesium binding site within its pore. At resting membrane potential, Mg^{2+} binds the site with high affinity, blocking all ion flow through the receptor. However, as the membrane potential depolarizes, the Mg^{2+} site releases the bound ion, allowing Ca^{2+} to flow if the receptor has already bound glutamate. These two ion gates make NMDA receptors the primary mechanism for indicating correlations in pre- and postsynaptic activity to the synapse: an NMDA receptor detects the coincidence of glutamate release from the presynaptic terminal and the accompanying depolarization

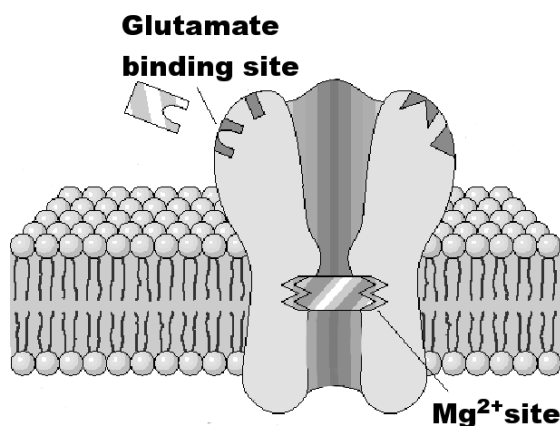


Figure 2.5. Schematic of an NMDA receptor, depicting glutamate and Mg^{2+} gates. (Adapted from [105])

of the postsynaptic membrane, and communicates this coincidence to the postsynaptic neuron through increased levels of intracellular Ca^{2+} concentration.

Throughout the rest of the paper, when we refer to LTP/LTD we will have NMDA receptor-mediated LTP/LTD at excitatory synapses in mind. It should be noted, however, that many varieties of LTP/LTD have been identified at various types of synapses throughout the nervous system, and that the modifications affecting LTP/LTD can be both pre- and postsynaptic [75].

2.3 AMPA receptors and trafficking

Glutamate receptors can be divided into two functional categories: metabotropic, which mediate their effects via coupling to G-protein second messenger systems, and ionotropic, which are ligand-gated cation channels. Ionotropic glutamate receptors can be further separated into three pharmacological groups: AMPA, NMDA, and kainate receptors, named for synthetic agonists which readily activate the receptors (see [27, 87] for reviews). AMPA receptors mediate the fast Na^+ influx that accounts for the majority of synaptic transmission at excitatory synapses in the central nervous system. AMPA receptors primarily gate Na^+ in preference to Ca^{2+} , due to subunit composition [27], and in preference to K^+ , due perhaps to their large pore size [133]. Topologically, AMPA receptors are hetero-tetramers of four subunits named GluR1 to GluR4 (see Figure 2.6). Each subunit is comprised of an extracellular N-terminal domain, four hydrophobic regions named TM1 to TM4, and an intracellular C-terminal domain. TM2 is a cytosolic hairpin loop which, together with the TM2 region of the other three subunits, forms the cation pore. The C-terminal domain contains a number of phosphorylation sites and conserved sequences that interact with other intracellular proteins (see [125, 10, 98] for reviews). The subunit composition of an AMPA receptor determines the manner in which it is trafficked, both under basal conditions and during the expression of LTP/LTD. This difference depends on whether the AMPA receptor contains a subunit with a long C-terminal domain (typically GluR1 or GluR4) or is comprised only of subunits with short C-terminal domains (typically GluR2 and GluR3). The majority of AMPA receptors at mature synapses are either GluR1/2 or GluR2/3 heteromers [27], and hence these two receptor classes play different trafficking roles under basal and activity-dependent conditions.

In dendritic spines there is an electron-dense thickening of the postsynaptic cytoskele-

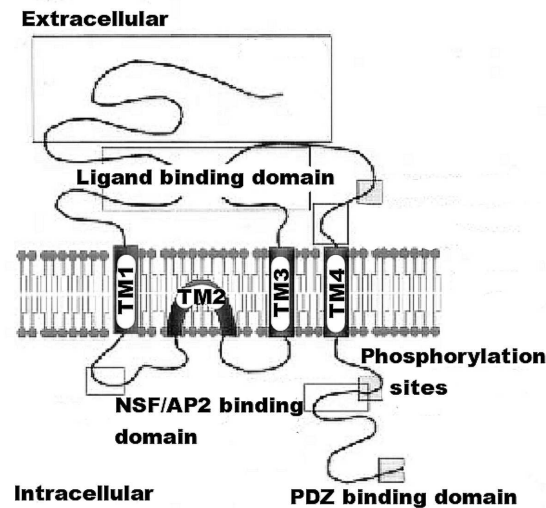


Figure 2.6. Schematic of AMPA receptor subunit (GluR) topology, demonstrating the the N- and C-terminal domains, the four regions TM1-4, ligand binding domain, PDZ interaction domains, and phosphorylation sites. (Adapted from [98])

ton just below the membrane that is directly apposed to the presynaptic active zone called the *postsynaptic density* (PSD) (see [151, 126, 118, 111] for reviews, also see Figure 2.2). The PSD is a subsynaptic scaffold that localizes and organizes the various receptors, ion channels, kinases, phosphatases and other signalling molecules present in the dendritic spine. Many of the proteins found in the PSD contain protein-to-protein interaction motifs, such as the PDZ domain (named for the first three proteins in which the domain was observed: PSD95, discs large, and zona occludens 1). Such interactions regulate the dynamics of the various proteins comprising the PSD, including AMPA receptors.

A schematic of AMPA receptor trafficking at a dendritic spine is shown in Figure 2.7. Receptors in the extrasynaptic membrane (ESM) of the spine diffuse freely, possibly as part of large receptor-scaffold complexes [138]. Due to the high density of scaffolding proteins constituting the PSD, the PSD acts as a confinement domain for surface AMPA receptors: the boundary of the PSD and ESM acts as a barrier to receptor entry/exit, and receptor diffusion within the PSD proceeds in a highly obstructed manner, with receptors often crosslinking to scaffolding proteins. [9, 132, 39, 139]. Estimates for the diffusivity range from 0.01 to $0.5\mu\text{m}^2/\text{sec}$ [9, 132, 39, 2, 3]. The narrow, highly curved spine neck also impedes receptor diffusion, slowing the exchange of receptors between the spine head and dendritic cable [3]. Surface receptors are continually exchanged with

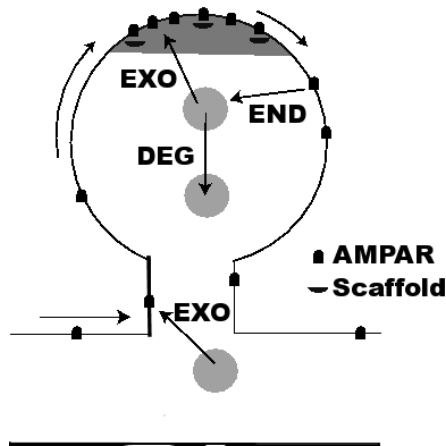


Figure 2.7. Schematic of AMPA receptor trafficking at a dendritic spine. Receptors stored in intracellular pools are continually exchanged with surface receptors through exo/endocytosis (EXO/END) and sorted for degradation (DEG). Surface receptors diffuse in the dendritic membrane and can be immobilized at the PSD (shaded region) through interactions with scaffolding proteins.

intracellular receptor pools through exo- and endocytosis, and are either reinserted into the membrane or sorted to lysosomes for degradation [73, 31, 100, 6, 99, 2]. Passafaro et al. (2001) estimate exocytosis into the PSD and ESM to have a time constant of 10 min and 30 min, respectively; however, data obtained by Adesnik et al. (2005) using different methods estimates the PSD exocytic time constant to be much longer, on the order of many hours. Ehlers (2000) found that the rate of endocytosis from the ESM is comparable to the faster exocytic rate found by Passafaro et al. (2001). It is thought that endocytosis does not occur in the PSD, but only in clathrin-coated “hot spots” found perisynaptically in the ESM [6]. The intracellular pool is probably large and may represent as much as 80% -90% of the total number of AMPA receptors at hippocampal neurons [10, 2].

2.3.1 Basal trafficking

Under basal conditions, AMPA receptor concentration in the postsynaptic membrane is high within the PSD, drops off dramatically at the boundary of the PSD, and remains low throughout the ESM [94, 23, 132, 131]. Estimates of receptor concentrations within the PSD range from 100 to 1000 receptors μm^{-2} , whereas within the ESM they range from 1 to 20 receptors μm^{-2} . The total number of receptors in the PSD depends on the size of the PSD and can vary from 1 to 200. The majority of AMPA receptors at the PSD are

GluR2/3 heteromers, due to an activity-independent exchange of synaptic AMPA receptors with GluR2/3 heteromers. This basal turnover creates a steady flux of receptors along the postsynaptic membrane from the PSD to the perisynaptic region where they enter the endocytic pathway. The PDZ domain-containing protein N-ethylmaleimide-sensitive factor (NSF), an ATPase involved in membrane-fusion events, is thought to mediate this exchange [78, 10] (although see Palmer et al. (2005)). The GluR2/3 heteromers are stabilized in the PSD through interactions with multi-PDZ-domain-containing glutamate-receptor-interacting proteins (GRIPs) and AMPA-receptor-binding proteins (ABPs), and are clustered together through interactions with neuronal-activity-regulated pentraxin (NARP) [78, 125]. While the association with GRIP/ABP is specifically with the GluR2 subunit, NARP interacts with all AMPA receptor subunits.

A few experiments give insight into the balance of the basal fluxes produced by exo/endocytosis and the mobility of receptors. Luscher et al. (1999) blocked separately both exo- and endocytosis pharmacologically and recorded the accompanying change in field potentials. Blocking exocytosis by loading synapses with BoTox caused a $\sim 50\%$ reduction in the population EPSPs over 10-20 min, while blocking endocytosis by loading synapses with the peptide D15 produced an $\sim 50\%$ increase in the population EPSPs over the same time period. With regards to mobility, Groc et al. (2004) and Ashby et al. (2006) both determined, by single-particle tracking, the diffusivity of mobile synaptic receptors in the PSD to be $\sim 0.01 \mu\text{m}^2/\text{sec}$, and that the fraction of mobile AMPA receptors within the PSD of mature dendritic spines is approximately one-half. Thus even under basal conditions, AMPA receptor concentrations are maintained by a dynamic balance of exo/endocytosis, diffusion, and immobilization by scaffolding proteins.

2.3.2 LTP trafficking

By definition, the induction of NMDA receptor-mediated LTP begins with the influx of Ca^{2+} into the dendritic spine through activated NMDA receptors. Although this rise in Ca^{2+} is essential for inducing LTP, little is known about the spatiotemporal properties of the Ca^{2+} signal required for induction [69, 75]. Also, though it is known that the increased levels of Ca^{2+} concentration activate second-messenger pathways within the neuron, there is little consensus on which pathways are involved [110]. It is almost certain, however, that calcium/calmodulin-dependent protein kinase II (CaMKII) is required for NMDA receptor-mediated LTP [70]. It is thought that CaMKII acts as a molecular switch for the

expression of LTP which is activated by the large rise in intracellular Ca^{2+} accompanying the induction of LTP [149, 71]. The activation of CaMKII by Ca^{2+} increases the rate of exocytosis of GluR1/2 heteromers into the ESM. Although the exact mechanism is unknown, it is thought that CaMKII phosphorylates synapse-associate protein 97 (SAP-97), the only PDZ-domain-containing protein known to bind with GluR1 and which has been implicated in the delivery of GluR1/2 heteromers to the postsynaptic membrane due to its interactions with the motor protein myosin-VI [42, 121, 148, 86]. Also, stargazin and other transmembrane AMPA receptor regulatory proteins (TARPs) play a crucial role in the membrane expression of GluR1/2 heteromers and their incorporation into the PSD [135, 134, 136]. Interestingly, stargazin binds with the PDZ-domain-containing protein PSD-95, a major scaffolding protein of the PSD, and evidence suggests that the concentration of PSD-95 at the PSD directly determines the number of AMPA receptors found there [33, 114]. It is hypothesized that the binding of PSD-95 to the actin cytoskeleton that accompanies the translocation of GluR1/2 heteromers into the PSD provides additional binding sites for constitutively recycling GluR2/3 heteromers, thereby maintaining the increase in AMPA receptor number [78, 119, 77, 19, 138].

2.3.3 LTD trafficking

As in the case of LTP, NMDA receptor-mediated LTD is induced by a rise in intracellular calcium levels. Although it is not well understood, the spatiotemporal properties of the Ca^{2+} signal determine whether LTP or LTD is induced: LTP is induced by a large, fast increase of intracellular Ca^{2+} concentration in the dendritic spine while LTD is induced by a moderate, slow increase which may be accompanied by Ca^{2+} release from intracellular stores [38, 75]. Just as LTP is associated with an increase in the number of synaptic AMPA receptors due to the influx of receptors from the ESM, LTD involves a loss of receptors from the PSD due to modifications in constitutive recycling [14, 15, 68, 5, 79]. A possible trigger for LTD expression is the activation of a phosphatase cascade involving calcineurin and protein phosphatase 1 (PP1) [90, 91]. Though the mechanisms underlying LTD expression are not as well understood as those for LTP, some possible candidates have been identified. First, induction of LTD triggers the phosphorylation of constitutive GluR2/3 heteromers by activated $\text{PKC}\alpha$ [20, 57, 101]. This disrupts their interactions with the stabilizing GRIP/ABP complexes and allows for association with protein interacting with kinase C 1 (PICK1). PICK1 mediates the

loss of AMPA receptors at the PSD, as the overexpression of PICK1 at synapses is correlated with a decrease in membrane expression of AMPA receptors [101]. Second, the clathrin adaptor protein AP2 is known to bind with AMPA receptors at a site that overlaps with the NSF binding site, the protein implicated in the constitutive recycling of GluR2/3 heteromers [67]. It is thought that an LTD induction trigger blocks NSF binding and promotes AP2 binding. In combination with the mechanism above, the free AMPA receptor with bound AP2 is recruited to perisynaptic clathrin-coated pits and endocytosed [79, 13, 6]. Third, there exists some indirect experimental evidence for the removal of scaffolding proteins from the PSD during LTD, namely, that NMDA receptor activation can lead to the ubiquitination and subsequent degradation of the scaffolding protein PSD-95 [21]. The removal of a scaffolding protein releases the associated bound receptor, which can then diffuse out of the PSD and be internalized through endocytosis.

CHAPTER 3

COMPARTMENTAL MODEL OF AMPA RECEPTOR TRAFFICKING AT A SINGLE DENDRITIC SPINE

In order to investigate the role of AMPA receptor trafficking in synaptic plasticity, we construct a simplified two-compartment model of the surface of a dendritic spine (see Figure 3.1). The first compartment represents the postsynaptic density (PSD) of the spine head and the second compartment represents the extrasynaptic membrane (ESM) of the remaining spine head and neck. We assume that AMPA receptors diffuse freely in the ESM. Within the PSD, however, AMPA receptor diffusion proceeds in a highly obstructed fashion, due to a number of factors including the binding of receptors to scaffolding

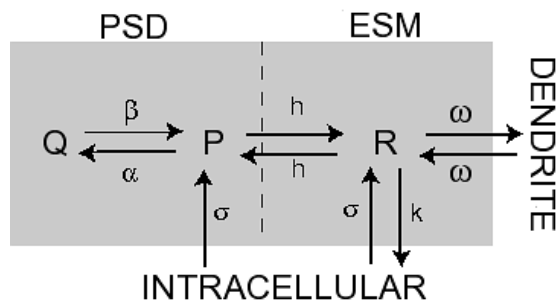


Figure 3.1. Simplified two-compartment model of a dendritic spine (see Figure 2.7 for schematic of AMPA receptor trafficking at a spine). Free receptors (concentration P) bind to scaffolding proteins within the PSD to form bound receptors (concentration Q) at a rate α (multiplied by the concentration of free binding sites) and unbind at a rate β . Free receptors flow between the PSD and ESM at a hopping rate h , and flow between the ESM and surface of the dendritic cable at a rate ω . Free receptors (concentration R) within the ESM are internalized at a rate k . Receptors are inserted into the PSD and ESM at a rate σ . Within each compartment there are two distinct types of receptor corresponding to GluR1/2 (type I) and GluR2/3 (type II) heteromers, respectively. The rates of binding/unbinding, hopping, and exo/endocytosis depend on receptor type. Only type II receptors undergo exocytosis in the PSD ($\sigma_I = 0$) and only type I receptors undergo exocytosis in the ESM ($\sigma_{II} = 0$).

proteins, the transient corralling of receptors to restricted domains by the underlying actin cytoskeleton, and the repulsion of receptors by picket-like transmembrane proteins (see Section 2.3). Single-particle tracking data suggests that the PSD acts as a confinement domain for diffusing receptors, and that about half of the AMPA receptors within the PSD are mobile [19, 39, 139, 3]. In order to model the confinement of diffusing particles within the PSD, we treat the boundary between the PSD and ESM compartments as a potential barrier over which receptors must hop in order to enter or exit the PSD. For simplicity, the net flux across the boundary is taken to be proportional to the difference in concentrations on either side of the barrier, with the hopping rate dependent on the barrier height. An alternative model of confinement is to assume that the boundary between the PSD and ESM is impermeable except for small openings within the boundary through which receptors can diffuse [45]. Receptors can also diffuse between the ESM and the surrounding membrane of the dendritic cable, with the net flux dependent on the geometry of the spine neck and the background concentration of receptors within the dendritic membrane. Indeed, it has recently been shown experimentally that there is a barrier to diffusion at the spine neck and thus changes in spine morphology could provide a mechanism for regulating receptor trafficking [3]. We model the effects of this barrier by assuming that receptors hop between the ESM and dendrite at a rate that depends on spine geometry.

In addition to the lateral movement of AMPA receptors within the plasma membrane, there is a continual exchange of surface receptors with pools of intracellular receptors through exo/endocytosis [15, 31, 68, 120, 6, 99, 125]. In fact there are at least two separate sources of intracellular AMPA receptors, one consisting of GluR1/2 heteromers that are inserted into the ESM and the other consisting of GluR2/3 heteromers that are inserted into the PSD during constitutive recycling. Since the expression of LTP and LTD is thought to involve changes in the trafficking of GluR1/2 and GluR2/3, respectively, it is important to distinguish explicitly between these two receptor types. We further assume that both receptor types undergo endocytosis from the ESM, and that there is no receptor endocytosis directly from the PSD [6]. The latter is consistent with the emerging picture that during constitutive recycling, receptors diffuse from the PSD to the ESM, are endocytosed, and either sorted to lysosomes for degradation or reinserted into the PSD [31]. Passafaro et al. (2001) find that under basal conditions, the rate of receptor insertion into the PSD is quantitatively similar to the rate of endocytosis, both

having a time constant of around 10 min. This is also consistent with changes in receptor number in response to blocking exo/endocytosis [76]. Passafaro et al. (2001) also find that the basal rate of exocytosis to the ESM is slower, having a time constant of at least 30 min. Note, however, that more recent data by Adesnik et al. (2005) suggests that constitutive recycling may take hours rather than minutes, and occur through exocytosis at the cell body followed by lateral membrane diffusion, rather than via direct insertion into dendritic spines. However, it is currently not clear how to reconcile these results with previous studies.

We assume that within the PSD each receptor type exists in one of two states, either bound to a scaffolding protein or free (unbound), whereas in the ESM all receptors are taken to be free. We also assume that under basal conditions there is a fixed concentration Z of binding sites within the PSD, which are taken to be nonspecific with respect to receptor type. There is experimental evidence to suggest that in mature synapses the trafficking of scaffolding proteins such as PSD-95, which play a major role in anchoring glutamate receptors to the PSD, is much slower than the fast trafficking of AMPA receptors, with the former taking place over a period of hours rather than minutes [97, 49]. Thus, to a first approximation, we can neglect the dynamics of Z associated with the turnover of scaffolding proteins. However, when considering changes in AMPA receptor trafficking during LTP/LTD, we will assume that there is an associated trafficking of “slot proteins” [121, 77] to or from the PSD that will be modeled in terms of a dynamical equation for Z (see Section 3.2.2).

3.1 Model equations

Experimental estimates for the diffusivity of mobile receptors in the PSD and ESM are on the order of 0.01 and $0.1\mu\text{m}^2\text{ s}^{-1}$ respectively [9, 39, 3]. Given that the surface areas of the PSD and ESM are on the order of 0.1 and $1\mu\text{m}^2$, respectively [126], it follows that the typical time-scale for diffusion within each compartment is on the order of 10 sec. This is orders of magnitude faster than the other components of AMPA receptor trafficking such as exo- and endocytosis, binding and unbinding, and synthesis and degradation, and is also faster the time courses of both LTP and LTD. Hence, by treating each compartment as spatially homogeneous, we can take the corresponding receptor concentrations to be spatially uniform and thus neglect the effects of intracompartamental diffusion. We will show later in this chapter that our results agree with a model of AMPA receptor trafficking

which accounts for spatial variations in receptor concentration (see Section 3.3). It follows that the temporal variation in receptor concentrations can be represented in terms of a system of ordinary differential equations that describe the following processes: the first-order kinetics associated with binding to and unbinding from scaffolding proteins within the PSD, the exocytosis of GluR1/2 receptors into the ESM and GluR2/3 receptors into the PSD, the endocytosis of both classes of receptor from the ESM, the hopping of free receptors between the PSD and ESM, and the hopping of free receptors between the ESM and dendritic cable.

For ease of notation we denote GluR1/2 heteromers as type I and GluR2/3 heteromers as type II. For each receptor type j , $j = I, II$, let P_j and Q_j denote, respectively, the free and bound receptor concentrations in the PSD, and let R_j represent the corresponding free receptor concentration in the ESM. We take the PSD to be a disc of radius $r = 0.2\mu\text{m}$ [126] and surface area $A = \pi r^2$, and take the ESM to have a surface area $a = 10A$. The dynamics of the free receptor concentrations in the PSD is described in terms of the kinetic equations

$$\frac{dP_I}{dt} = -\alpha_I(Z - Q_I - Q_{II})P_I + \beta_I Q_I - \frac{h_I}{a}(P_I - R_I), \quad (3.1)$$

$$\frac{dP_{II}}{dt} = -\alpha_{II}(Z - Q_I - Q_{II})P_{II} + \beta_{II} Q_{II} - \frac{h_{II}}{a}(P_{II} - R_{II}) + \frac{\sigma_{II}}{a}, \quad (3.2)$$

and the corresponding bound receptor concentrations satisfy the equations

$$\frac{dQ_I}{dt} = \alpha_I(Z - Q_I - Q_{II})P_I - \beta_I Q_I, \quad (3.3)$$

$$\frac{dQ_{II}}{dt} = \alpha_{II}(Z - Q_I - Q_{II})P_{II} - \beta_{II} Q_{II}. \quad (3.4)$$

The first two terms on the right-hand side of Equations (3.1)-(3.4) represent the binding and unbinding of receptors to and from scaffolding proteins, with $Z - Q_I - Q_{II}$ specifying the concentration of free binding sites. The rates of binding and unbinding are denoted by α_j and β_j respectively, for $j = I, II$. The third term on the right-hand side of Equations (3.1) and (3.2) represents the flux of receptors between the PSD and ESM with associated hopping rate h_j , $j = I, II$. Type II receptors also undergo exocytosis within the PSD at an insertion rate σ_{II} (last term in Equation (3.2)). The rate of exocytosis satisfies

$$\sigma_{II} = \sigma_{II}^{rec}(1 - f)S_{II},$$

where S_{II} is the number of type II receptors in the intracellular store, $1 - f$ is the fraction of intracellular receptors recycled to the surface (rather than degraded), and σ_{II}^{rec} is the

recycling rate per receptor. For simplicity we absorb $1 - f$ into σ_{II}^{rec} . We assume that the intracellular pool of GluR2/3 receptors is sufficiently large and the rate of receptor insertion is sufficiently slow so that the depletion of the pool due to exocytosis can be neglected, that is, S_{II} can be treated as a constant.

The receptor concentrations in the ESM evolve according to the kinetic equations

$$\frac{dR_I}{dt} = \frac{h_I}{A}(P_I - R_I) - \frac{\omega_I}{A}(R_I - U_I) - \frac{k_I}{A}R_I + \frac{\sigma_I}{A}, \quad (3.5)$$

$$\frac{dR_{II}}{dt} = \frac{h_{II}}{A}(P_{II} - R_{II}) - \frac{\omega_{II}}{A}(R_{II} - U_{II}) - \frac{k_{II}}{A}R_{II}. \quad (3.6)$$

The first term on the right-hand side of Equations (3.5) and (3.6) represents the flux of receptors between the PSD and ESM, and the second term is the corresponding flux between the ESM and the dendrite. The latter flux is taken to be proportional to the difference between the free receptor concentration R_j and a fixed background receptor concentration within the dendrite, which is denoted by U_j , $j = I, II$. The third term on the right-hand side of Equations (3.5) and (3.6) represents endocytosis at a rate k_j . Finally, type I receptors also undergo exocytosis at a rate σ_I (last term in Equation (3.5)), with

$$\sigma_I = \sigma_I^{rec} S_I,$$

where S_I is the number of type I receptors in the associated intracellular store and σ_I^{rec} is the insertion rate per receptor. S_I evolves according to the first-order equation

$$\frac{dS_I}{dt} = -\sigma_I^{rec} S_I + \delta_I \quad (3.7)$$

where δ_I is the net rate of receptor synthesis. In steady state, we have $S_I = \delta_I / \sigma_I^{rec}$. However, during LTP, the rapid exocytosis of GluR1/2 into the ESM will significantly deplete the corresponding intracellular pool so that σ_I cannot be treated as time-independent. Also, note that endocytosed receptors do not enter the intracellular pools but are instead removed altogether from the spine, producing an effective degradation of receptors. This is a simplification which we employ for this chapter only. In Chapters 4 and 5 we forgo this simplification in exchange for more elaborate models of receptor recycling.

3.1.1 Steady-state solution

For fixed parameter values there is a unique steady state solution, which is obtained by setting the right-hand sides of Equations (3.1)-(3.7) to zero. First, Equations (3.3)

and (3.4) imply that in steady-state the free and bound receptor concentrations within the PSD are related according to

$$Q_I = \frac{\rho_I}{1 + \rho_I + \rho_{II}} Z, \quad Q_{II} = \frac{\rho_{II}}{1 + \rho_I + \rho_{II}} Z, \quad (3.8)$$

where

$$\rho_I = \frac{\alpha_I P_I}{\beta_I}, \quad \rho_{II} = \frac{\alpha_{II} P_{II}}{\beta_{II}}. \quad (3.9)$$

Equations (3.1), (3.2), (3.5) and (3.6) then imply that

$$P_I = R_I, \quad P_{II} = R_{II} + \frac{\sigma_{II}}{h_{II}} \quad (3.10)$$

with

$$R_I = \frac{\sigma_I + \omega_I U_I}{k_I + \omega_I}, \quad R_{II} = \frac{\sigma_{II} + \omega_{II} U_{II}}{k_{II} + \omega_{II}}. \quad (3.11)$$

Given the steady-state receptor concentrations, the total number of AMPA receptors in the PSD is $N = N_I + N_{II}$ with $N_j = a(P_j + Q_j)$. If we assume that the strength of the synapse is roughly proportional to the total number of synaptic receptors N , then we can determine how the steady-state synaptic strength depends on the various parameters of the model.

A number of qualitative features of the steady-state receptor concentrations can be immediately deduced from Equations (3.8)-(3.11). First, Equations (3.8) and (3.9) imply that in the regime where the rate of binding is sufficiently large relative to the rate of unbinding, that is, $\alpha_j/\beta_j \gg P_j$, almost all the binding sites are occupied and $Q_I + Q_{II} \approx Z$. On the other hand, if $\alpha_j/\beta_j \ll P_j$ then the binding sites are unsaturated and the number of bound receptors varies linearly with the number of unbound receptors according to $Q_j \approx \rho_j Z$. Second, Equation (3.10) shows that in order to maintain a larger concentration of free GluR2/3 receptors in the PSD compared to the ESM [94, 131], the hopping rate h_{II} must be sufficiently small. In other words, there needs to be some form of barrier to diffusion between the PSD and ESM. Finally, Equation (3.11) implies that if receptors hop freely between the ESM and surrounding dendritic membrane (large ω_j), then the receptor concentration in the ESM is approximately equal to the background concentration, $R_j \approx U_j$. It then follows from Equation (3.10) that the receptor concentrations within the PSD are independent of the rates of endocytosis k_j (as well as the rate of exocytosis σ_j), which contradicts the experimental results of Luscher et al. (1999). Therefore, there should also be an effective barrier to diffusion between the ESM and dendritic membrane, as recently observed experimentally by Ashby et al. (2006).

3.1.2 Model extensions during LTD

We briefly describe the extension of our model used in the study of LTD. Both free and bound GluR2/3 receptors in the PSD are now assumed to be in two distinct phosphorylation states which are labeled by a and b . (These states could correspond to association with the proteins GRIP/ABP and PICK1, respectively, see Figure 3.2). Receptors in the a state behave as in the previous model, whereas those in the b state are assumed to have a faster unbinding rate β^* , zero binding rate ($\alpha^* = 0$), and a faster rate h_{II}^* of hopping between the PSD and the ESM. Decomposing the free and bound GluR2/3 receptor concentrations according to $P_{II} = P_{II,a} + P_{II,b}$ and $Q_{II} = Q_{II,a} + Q_{II,b}$, we have the following modified system of equations for the dynamics of GluR2/3 receptor concentrations within the PSD:

$$\begin{aligned} \frac{dP_{II,a}}{dt} = & -\alpha_{II}(Z - Q_I - Q_{II})P_{II,a} + \beta_{II}Q_{II,a} - \frac{h_{II}}{a}(P_{II,a} - R_{II}) + \frac{\sigma_{II}}{a} \\ & - \mu P_{II,a} + \nu P_{II,b}, \end{aligned} \quad (3.12)$$

$$\frac{dP_{II,b}}{dt} = \beta_{II}^*Q_{II,b} - \frac{h_{II}^*}{a}P_{II,b} + \mu P_{II,a} - \nu P_{II,b}, \quad (3.13)$$

and the corresponding bound receptor concentrations satisfy the equations

$$\frac{dQ_{II,a}}{dt} = \alpha_{II}(Z - Q_I - Q_{II})P_{II,a} - \beta_{II}Q_{II,a} - \mu Q_{II,a} + \nu Q_{II,b}, \quad (3.14)$$

$$\frac{dQ_{II,b}}{dt} = -\beta_{II}^*Q_{II,b} + \mu Q_{II,a} - \nu Q_{II,b}. \quad (3.15)$$

Here μ and ν denote the transition rates between the a and b states, respectively, which for simplicity are taken to be the same for free and bound receptors. We assume that within the ESM receptors in the b state are rapidly endocytosed so that $R_{II} = R_{II,a}$ and the dynamics for R_{II} is the same as in the base model, see Equation (3.6). The GluR1/2 dynamics is unaltered.

3.2 Analysis of model equations

We analyze our two-compartment model of a dendritic spine (see Figure 3.1) in terms of the corresponding set of differential equations describing the time evolution of the receptor concentrations in the PSD and ESM (see Section 3.1). Solutions of the model equations are used to investigate how receptor trafficking depends on the various biophysical parameters, including the rates of exo/endocytosis (σ_j, k_j), the rates of binding/unbinding to scaffolding proteins (α_j, β_j), and the concentration of scaffolding proteins (Z) within the PSD. Here the subscript j denotes the receptor type with $j = \text{I}$

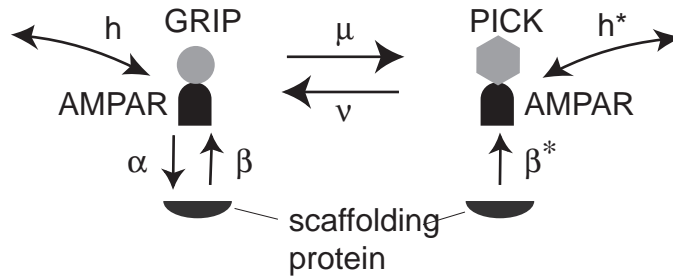


Figure 3.2. LTD model. GluR2/3 receptors are assumed to exist in two distinct states corresponding to association with GRIP and PICK proteins, respectively. Under basal conditions the transition rate μ from the GRIP-associated state to the PICK-associated state is zero so that only GRIP-associated receptors exist and the model dynamics reduces to the kinetic scheme shown in Figure 3.1. However, during the presentation of an LTD stimulus, μ increases so that some GRIP-associated receptors are converted to PICK-associated receptors. The latter are assumed to rapidly unbind from scaffolding proteins at a rate β^* and hop from the PSD to the ESM at a rate h^* where they are endocytosed. This results in a net loss of receptors from the PSD.

for GluR1/2 and $j = \text{II}$ for GluR2/3. These parameters are possible targets of second-messenger pathways initiated by a rise in intracellular Ca^{2+} during the induction phase of LTP/LTD. A basic assumption of our modeling approach is that there is a separation of time-scales between the activation of the signaling pathways by the postsynaptic calcium signal during induction (seconds) and the subsequent expression of LTP/LTD (minutes). Under such an assumption, it is possible to study the mechanisms underlying the expression of LTP/LTD independently of the particular signaling pathways involved in induction. In order to interpret the results of our model in terms of experimentally determined changes in EPSPs during LTP/LTD, we identify the strength of a synapse with the total number of synaptic receptors. Thus we neglect possible contributions to synaptic plasticity arising from changes in single-channel conductances (see Section 3.4 for a discussion of this point).

Note that there have been a number of other biophysically motivated models of LTP/LTD [59, 16, 124, 123, 1, 53, 43, 108, 122]. However, these have tended to focus on the role of Ca^{2+} as an induction signal for bidirectional synaptic plasticity, rather than on the role of AMPA receptor trafficking in the expression of synaptic plasticity. A few of the models however do include receptor trafficking between the PSD and intracellular pools [124, 43, 122].

3.2.1 Receptor trafficking under basal conditions

The parameter values chosen for receptor trafficking under basal conditions are listed in Table 3.1. As some of the model parameters have yet to be determined experimentally (e.g., the rate at which AMPA receptors bind to and are released from scaffolding proteins), we select values for these parameters that produce results consistent with the known experimental data. Our choice for the rate of exocytosis is based on the work of Passafaro et al. (2001), which suggests time constants for exocytosis of ~ 10 -30 min. Given a basal rate of exocytosis $\sigma \approx \sigma^{rec} S$, where S is the steady-state number of receptors in the intracellular pool, we take σ^{rec} to be the reciprocal of this time constant. For GluR2/3 receptors, we choose the rate of endocytosis k_{II} to approximately balance the flux due to exocytosis, which yields the constitutive recycling of GluR2/3 heteromers at the dendritic spine. This is consistent with the experimental data of Ehlers (2000). We choose the hopping rate h of receptors flowing between the PSD and ESM so that approximately half of all synaptic receptors are mobile, consistent with the data of Groc et al. (2004) and Ashby et al. (2006). Since GluR2/3 receptors are inserted directly into the PSD, the majority of basal free receptors found in the PSD in our model are of this type. The steady state is thus maintained primarily by the constitutive recycling of GluR2/3 receptors, which involves a constant flux of receptors from the PSD to the ESM where they are endocytosed and either reinserted into the membrane surface or degraded. We select the basal number of binding sites to approximately match the number of free

Table 3.1. Basal parameter values

Parameter	Symbol	Value _I	Value _{II}	Units	Reference
Area of PSD	a	0.1257*		μm^2	[126]
Area of ESM	A	1.257*		μm^2	[126]
Concentration of scaffolding proteins	Z	159.15*		μm^{-2}	[30]
Number of intracellular receptors	S	500	100		[30]
Recycling rate	σ^{rec}	0.0005556	0.001667	s^{-1}	[118]
Rate of exocytosis	σ	0.2778	0.1667	s^{-1}	[118]
Rate of endocytosis	k	0.01667	0.01667	$\mu\text{m}^2\text{s}^{-1}$	[31]
PSD-ESM hopping rate	h	0.001257	0.001257	$\mu\text{m}^2\text{s}^{-1}$	[30]
ESM-dendrite hopping rate	ω	0.001257	0.001257	$\mu\text{m}^2\text{s}^{-1}$	[30]
Background receptor concentration	U	10	0	μm^{-2}	[23]
Binding rate	α	10^{-6}	10^{-4}	$\mu\text{m}^2\text{s}^{-1}$	[30]
Unbinding rate	β	10^{-5}	10^{-5}	s^{-1}	[30]

*The nontrafficking parameters do not have particular type I and II values.

receptors, and choose basal binding and release rates so that (1) nearly all of the binding sites are filled by GluR2/3 receptors, and (2) they are consistent with other known systems [63]. Note that taking the synapse to be unsaturated, that is, to have a significant fraction of free binding sites, would require unrealistically low binding affinities. This, in turn, makes it difficult to match the range of experimental data presented below. Estimates of receptor concentrations within the PSD range from 100 to 1000 receptors μm^{-2} , whereas within the ESM they range from 1 to 20 receptors μm^{-2} [94, 23, 131]. The total number of receptors in the PSD depends on the size of the PSD and can vary from 1 to 200. We choose a parameter regime in which there are approximately 40 synaptic receptors under basal conditions and the concentration of extrasynaptic receptors is approximately $25 \mu\text{m}^{-2}$. Finally, the background concentration of GluR1/2 receptors in the dendrite is taken to be $U_I = 10\mu\text{m}^{-2}$ whereas the corresponding background concentration of GluR2/3 receptors is taken to be zero. This is based on the assumption that GluR2/3 receptor trafficking is local to the synapse, whereas trafficking of GluR1/2 receptors occurs extrasynaptically. In Chapters 4 and 5 we present models in which U_j is self-consistently determined. However, in our current model we cannot do this.

In Figure 3.3 we show how the steady-state number of GluR1/2 and GluR2/3 receptors in the PSD depends on various trafficking parameters as determined by Equations (3.8)-(3.11). Figures 3.3A-D show how total receptor number varies with the rates of exocytosis and endocytosis. As one expects, the number of receptors is an increasing (decreasing) function of the rate of exocytosis (endocytosis). However, this dependence is weak unless free receptors tend to be confined within their compartment, that is, the hopping rates h_j have to be sufficiently small. Note that the number of free and bound receptors within the PSD are approximately equal. In Figure 3.3E we show how the PSD binding sites become saturated with GluR2/3 receptors as the ratio of binding to unbinding rates α_{II}/β_{II} increases.

The dependence of synaptic strength on exo- and endocytosis has been investigated experimentally by pharmacologically blocking the insertion or internalization of receptors in a CA1 hippocampal cell [73]. For example, loading a cell with Botox disrupts exocytosis by inactivating v-SNAREs, and causes a 40% reduction in AMPA receptor EPSCs over 20 min. On the other hand, a targeted inhibition of endocytosis results in a two-fold increase in the AMPA receptor EPSCs over a similar time-scale. If we assume that the amplitude of a recorded EPSP is roughly proportional to the number of AMPA receptors

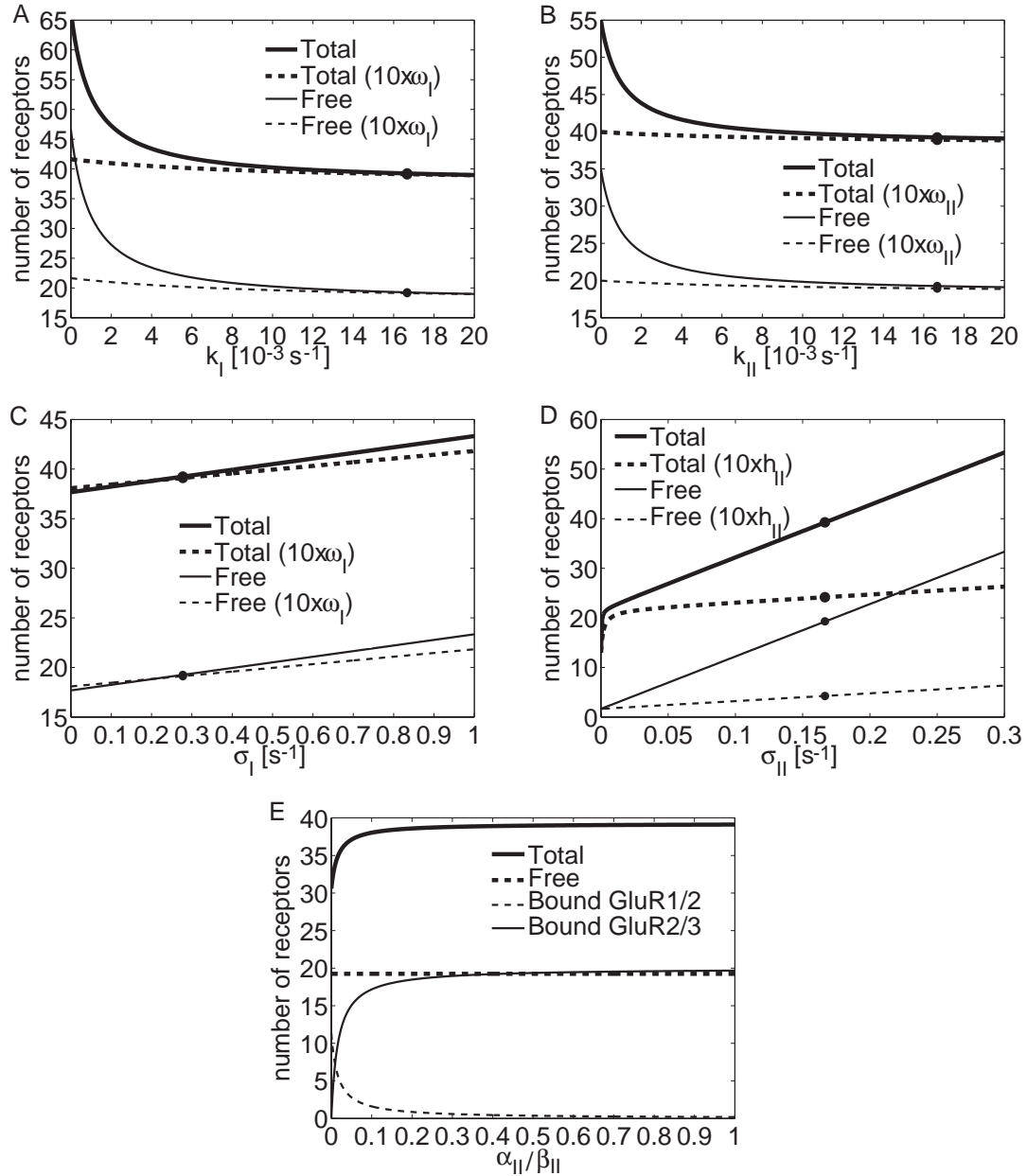


Figure 3.3. Steady-state synaptic receptor number as a function of parameters. Parameters values are as in Table 1 unless stated otherwise. (A,B) Receptor number as function of endocytic rates k_I and k_{II} at basal hopping rate ω_j (solid) and when ω_j is increased 10x (dashed). (C) Receptor number as function of exocytic rate σ_I at basal hopping rate ω_I (solid) and when ω_I is increased 10x (dashed). (D) Receptor number as function of exocytic rate σ_{II} at basal hopping rate h_{II} (solid) and when h_{II} is increased 10x (dashed). In A-D filled circles indicate basal values. (E) Receptor number as function of the ratio of binding to unbinding rate. The total number saturates near $\alpha_{II}/\beta_{II} = 1$ when all binding sites are filled. Dependence is weak near the basal value of $\alpha_{II}/\beta_{II} = 10$ (not shown), indicating a strong affinity of GluR2/3 receptors for binding sites. Receptor numbers are relatively insensitive to α_I/β_I (not shown).

from which the recording is made, then the time course of the number of AMPA receptors should roughly follow the time course of the recorded EPSPs. Thus the Luscher et al. (1999) data suggests that when exocytosis is blocked, the number of AMPA receptors at the PSD should approximately halve, and when endocytosis is blocked, the number of receptors should approximately double.

We can reproduce the results of Luscher et al. (1999) in our model by setting to zero either exocytosis ($\sigma_I = \sigma_{II} = 0$) or endocytosis ($k_I = k_{II} = 0$), and determining the resulting time-dependent decrease or increase in the number of synaptic receptors. We find that blocking exocytosis without changing any other parameters of the model leads to a loss of about half of the receptors in the PSD (see Figure 3.4A), whereas we find a doubling of receptors in the PSD after endocytosis is blocked (see Figure 3.4B). Note that in the latter case, one might expect blocking of endocytosis within the dendrite of a cell to raise the background concentrations U_j of AMPA receptors. However, the results shown in Figure 3.4B are insensitive to increases in background concentration, at least at the given basal hopping rates. Interestingly, the time courses predicted by our model are similar to those found by Luscher et al., although the reduction in response to exocytic blockage is slightly faster in our model and the increase in response to endocytic blockage

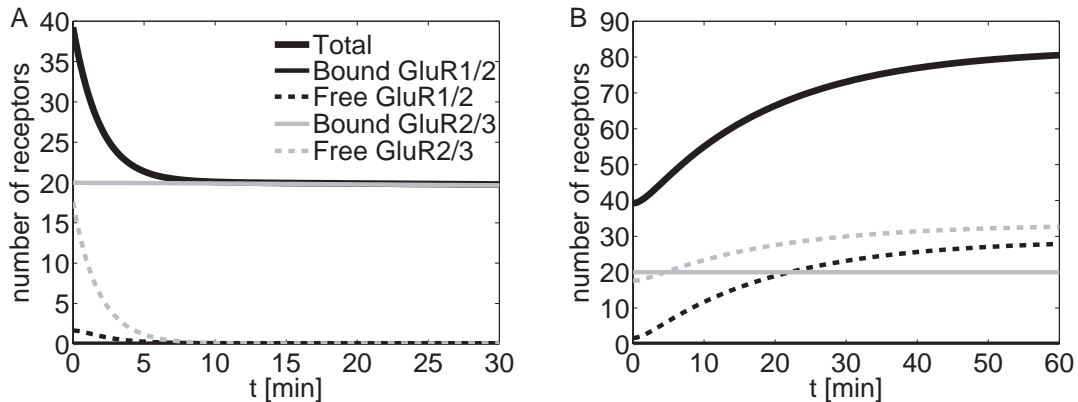


Figure 3.4. Time course of AMPA receptors after blocking exo/endocytosis. (A) Blocking exocytosis. With receptors at basal steady-state at time $t < 0$, exocytosis is blocked by setting $\sigma_j = 0$ ($j = 1, 2$) at $t = 0$. The number of AMPA receptors in the PSD almost halves in less than 10 min (due to the loss of free receptors) and decreases to ~ 1 over ~ 10 days (not shown). (B) Blocking endocytosis. Endocytosis is blocked by setting $k_j = 0$ ($j = 1, 2$) at $t = 0$. The number of AMPA receptors in the PSD nearly doubles within 1 hr (due to the addition of free receptors) and reaches a new steady-state value of ~ 84 . These results are consistent with Luscher et al. (1999).

is slightly slower. It should be noted that over the time course shown in Figure 3.4A the receptor concentration has not yet reached a steady state, that is, the asymptotic value shown in Figure 3.4A is larger than the steady-state value shown in Figure 3.3D for zero exocytosis. Our model thus predicts that when exocytosis is completely blocked the number of synaptic receptors should continue to decrease at a slow rate over several hours in order to reach steady-state. This slower component represents the unbinding of receptors from scaffolding proteins and their ultimate escape from the PSD to the ESM boundary.

3.2.2 Increase of synaptic receptor concentration during LTP

There is growing experimental evidence to suggest that a major contribution to the expression of early-phase LTP is the trafficking of GluR1/2 receptors into the PSD [125, 19, 10, 22]. This is likely to involve an activity-dependent increase in the rate of exocytosis of GluR1/2 receptors into the extrasynaptic membrane, and a corresponding increase in the number and/or affinity of receptor binding sites within the PSD. A number of PDZ-domain-containing proteins have been identified as playing a role in the regulation of AMPA receptor trafficking. For example, the PDZ-domain-containing protein synapse-associated protein 97 (SAP-97) binds directly to GluR1/2, and SAP-97 has been implicated in the trafficking of AMPA receptors into dendritic spines following phosphorylation by calcium/calmodulin-dependent protein kinase II (CaMKII) [42, 121, 148, 86]. CaMKII is itself activated by an activity-dependent rise in intracellular Ca^{2+} concentration under LTP stimulus protocols [69, 75].

GluR1/2 receptors also associate with transmembrane AMPA receptor regulatory proteins (TARPs) such as stargazin. Interestingly, stargazin binds with the PDZ-domain-containing protein PSD-95, a major scaffolding protein of the PSD [17, 114]. Disrupting the ability of stargazin to interact with PSD-95 leads to a massive decrease in synaptic AMPA receptors and an increase in extrasynaptic receptors. Moreover, an overexpression of PSD-95 enhances the number of synaptic AMPA receptors [33, 114], whereas removal of PSD-95 from the synapse by depalmitoylation depletes synaptic AMPA receptors [34]. On the other hand, increasing the expression of stargazin without changing the level of PSD-95 increases the number of extrasynaptic AMPA receptors without changing the strength of a synapse [114]. It is thus hypothesized that the interaction between stargazin and AMPA receptor subunits is important for the surface delivery of AMPA receptors,

whereas the interaction between stargazin and PSD-95 is important for the synaptic targeting of the receptors. Recent evidence suggests that phosphorylation of stargazin by CaMKII facilitates the interaction with PSD-95 and is a critical component of LTP [136].

Motivated by the above experimental findings, we numerically solve the kinetic Equations (3.1)-(3.7) of our receptor trafficking model in order to determine the time-dependent variation in the GluR1/2 receptor concentration in response to increases in the rate of exocytosis σ_I , the affinity α_I of binding sites in the PSD, and the hopping rate h_I between the PSD and ESM (under the assumption that the interaction between PSD-95 and stargazin facilitates the entry of receptors into the PSD). We assume that such changes occur rapidly relative to the time-course associated with the redistribution of AMPA receptors. This is based upon experimental data indicating that CaMKII, one of the crucial components of the signaling pathways involved in the induction of LTP, acts like a rapid molecular switch [149, 71, 70]. It is important to emphasize, however, that the detailed molecular mechanisms underlying the trafficking of AMPA receptors during LTP are still far from clear. One of the useful features of our mathematical model is that it allows us to explore a given hypothesis regarding the regulation of receptor trafficking during LTP.

In order to model changes in the rate of exocytosis we set $\sigma_I = \sigma_I^{rec} S_I$. We assume that in steady state the rate of exocytosis is equal to the rate of receptor synthesis δ_I . A sudden increase in σ_I^{rec} , and hence σ_I , results in the rapid insertion of intracellular receptors into the extrasynaptic membrane, and a corresponding reduction in S_I so that after an initial transient, the rate of exocytosis returns to the steady-state value. (Increasing the rate of receptor synthesis would lead to a persistent change in the rate of receptor insertion, but does not produce realistic time courses for LTP). Therefore, in order to maintain an increase in the number of synaptic receptors, we further assume that LTP involves an increase in the concentration Z of binding sites. One proposal for how this could occur is that AMPA receptors delivered to the synapse bring with them so called ‘‘slot’’ proteins that provide the additional binding sites [77]. We model this by supplementing Equations (3.1)-(3.7) with the following dynamical equation for the concentration Z of binding sites:

$$\frac{dZ}{dt} = -c \frac{dS_I}{dt} = c(\sigma_I^{rec} S_I - \delta_I) \quad (3.16)$$

That is, the rate of increase in Z is taken to be proportional to the rate at which the intracellular store of GluR1/2 receptors is depleted, with c a dimensionless constant.

Solving Equations (3.7) and (3.16) shows that Z increases asymptotically to a new steady-state value. It is important to note that Z only satisfies Equation (3.16) while the rate of exocytosis per receptor is maintained above basal levels. When the latter returns to its basal value, perhaps due to deactivation of the CaMKII switch, the number of intracellular receptors S_I recovers according to Equation (3.7) whereas Z is now held fixed. (Over longer time-scales of hours and days additional mechanisms are needed to stabilize Z with respect to the constitutive recycling of scaffolding proteins, see Section 3.4).

In Figures 3.5A,B we plot the resulting time courses for the total number of receptors in the PSD and ESM, respectively. Also shown in Figure 3.5A is the increase in the number of scaffolding proteins within the PSD, which asymptotically approaches a new steady-state value over the time course of a few minutes. The corresponding depletion of the intracellular pool is shown in Figure 3.5B. If we assume that the number of synaptic AMPA receptors is proportional to the size of EPSPs, then the profile shown in Figure 3.5A is consistent with recordings from single synapses [102, 96] and field EPSPs [7, 40]. That is, typical EPSPs recorded during LTP show a sharp, initial rise that peaks in ~ 30 - 60 sec at ~ 200 - 300% of the baseline response, then settles at a slower rate to ~ 150 - 200% of baseline response. In Figures 3.5C,D we show the time-dependent variation in the number of synaptic and extrasynaptic receptors in response to changes in the rate of exocytosis alone, without a corresponding increase in binding sites, binding affinity or hopping rate. It can be seen that there is a large increase in the number of extrasynaptic receptors but only a small transient increase in the number of synaptic receptors. This is consistent with what happens when there is an overexpression of stargazin without a corresponding increase in PSD-95 [114]. That is, stargazin can facilitate transport of AMPA receptors to the surface but is not able to target synapses unless it can interact with PSD-95.

It is important to emphasize that the distribution of receptors has not reached a steady state over the time course of a few minutes shown in Figures 3.5A,B. For during this period the rate of exocytosis σ_I has returned to its basal level, which implies that there are not enough free GluR1/2 receptors to maintain equilibrium with the receptors bound to the newly activated binding sites within the PSD. Thus over a longer time period of several hours, the GluR1/2 receptors are slowly exchanged with GluR2/3 receptors through the process of constitutive recycling (see Figure 3.6). Such an exchange has been observed experimentally, and has been suggested as a mechanism for maintaining bidirectional

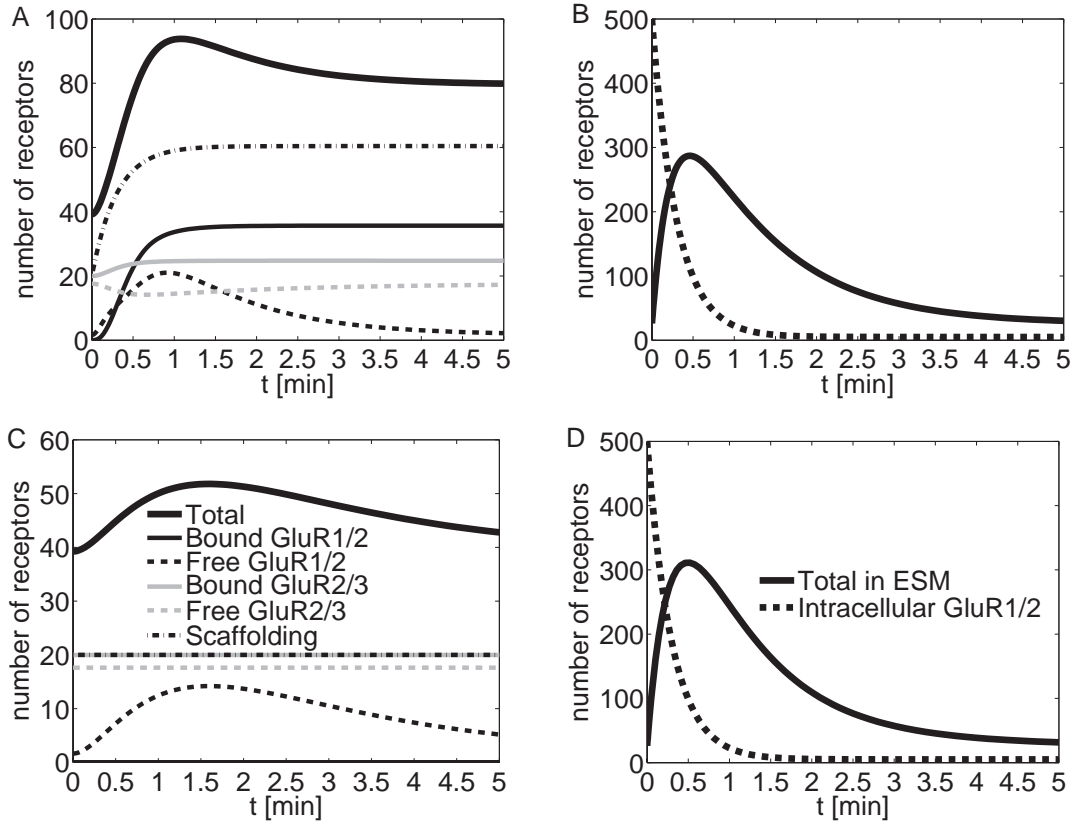


Figure 3.5. Time course of AMPA receptors during LTP. (A, B) With receptors at basal steady-state for $t < 0$, LTP is induced at time $t = 0$ by making the following changes to the basal GluR1/2 parameter values listed in Table 3.1 and numerically solving Equations (3.1)-(3.7): binding rate $\alpha_I = 0.001\mu\text{m}^2\text{s}^{-1}$, recycling rate $\sigma_I^{rec} = 0.0556\text{s}^{-1}$, and hopping rate $h_I = 0.01257\mu\text{m}^2\text{s}^{-1}$. Binding site trafficking is also activated according to Equation (3.16) with $c = 0.65$. Figure (A) shows the variation in the total number of receptors (thick solid black) and the number of binding sites (dash-dot black) within the PSD, whereas Figure (B) shows the corresponding variation in the total number of receptors in the ESM (solid) and the number of intracellular receptors (dash). The number of receptors in the ESM rises transiently due to the exocytosis of intracellular GluR1/2 receptors. Some enter the PSD and are immobilized by newly-available binding sites. These results are consistent with experimentally recorded EPSPs after LTP induction, see e.g. [40, 96]. (C,D) Time course of synaptic receptors (C) and extrasynaptic receptors (D) without synaptic targeting. Labeling of various curves is as in Figures (A,B). With receptors at basal steady-state at time $t < 0$, the rate of GluR1/2 exocytosis is increased by setting $\sigma_I^{rec} = 0.0556\text{s}^{-1}$ at time $t = 0$. However, the hopping rate and binding affinity of GluR1/2 receptors, and the number of binding sites remain at basal levels. The concentration in the ESM rises transiently as GluR1/2 receptors from the intracellular pool are exocytosed there, as in the case of LTP, but now there is only a small transient rise in the number of synaptic receptors. This is consistent with the suggestion that stargazin plays a role in transporting GluR1/2 receptors to the membrane surface, whereas its interaction with PSD-95 is required for synaptic targeting [114].

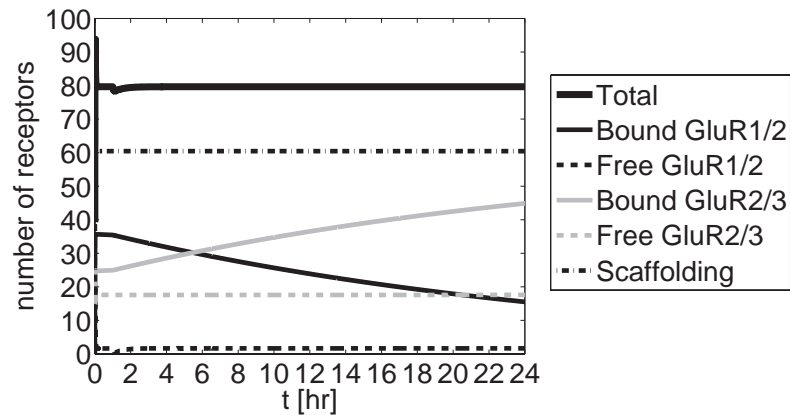


Figure 3.6. Exchange of GluR1/2 and GluR2/3 AMPA receptors. After 1 hr of maintaining LTP parameters as in Figure 3.5, all parameters are returned to their basal values except the binding site concentration Z , at which time GluR2/3 receptors begin to replace GluR1/2 receptors at the binding sites. These results are consistent with the work of McCormack et al. (2006).

synaptic plasticity [88]. However, in order to stabilize the strength of a synapse over these longer time-scales additional mechanisms are necessary. In particular, the slow turnover of scaffolding proteins within the PSD [97, 49] suggests that the increase in the concentration Z of binding sites through the trafficking of slot proteins is only temporary and that Z eventually returns to basal levels. One possible way of maintaining the increased number of binding sites is through structural changes in the dendritic spine (see Section 3.4).

3.2.3 Decrease of synaptic receptor concentration during LTD

Many synapses that exhibit LTP also exhibit LTD under appropriate stimulus conditions. A common stimulus protocol for inducing LTD is a prolonged repetitive synaptic stimulation at 0.5-5 Hz involving around 900 stimuli [29, 28]. Whether LTP or LTD occurs depends on the spatiotemporal properties of the intracellular Ca^{2+} signal [75, 108]. LTP is induced by a large, fast increase of intracellular Ca^{2+} concentration in the dendritic spine while LTD is induced by a moderate, slow increase that may be accompanied by Ca^{2+} release from intracellular stores [38]. The LTD induction signal triggers signaling cascades that involve the activation of enzymes such as PKC, PP1 and calcineurin [147, 125, 127]. Just as LTP is associated with an increase in the number of synaptic

AMPA receptors due to the influx of receptors from the extrasynaptic membrane, LTD appears to involve a loss of receptors from the PSD due to modifications in constitutive recycling [14, 15, 68, 5, 79]. One triggering mechanism is thought to be phosphorylation of GluR2/3 synaptic receptors, which disrupts the interactions with the stabilizing scaffolding protein GRIP/ABP and allows for association with PICK1 [84, 20, 101, 57, 72]. PICK1 mediates the loss of AMPA receptors at the PSD, as the overexpression of PICK1 at synapses is correlated with a decrease in membrane expression of AMPA receptors. It has been suggested that the switch from association with GRIP/ABP to PICK1 plays a role in untethering receptors from PSD binding sites, escorting them out of the PSD, and then facilitating internalization of the receptors once they have reached the ESM [125, 127]. Another possible mechanism for reducing the number of synaptic AMPA receptors during LTD is through the removal of scaffolding proteins from the PSD. There is some indirect experimental evidence for this, namely that NMDA receptor activation can lead to the ubiquitination and subsequent degradation of the scaffolding protein PSD-95 [32]. The removal of a scaffolding protein releases the associated bound receptor, which can then diffuse out of the PSD and be internalized through endocytosis.

The above role of GluR2/3 receptor trafficking in LTD is consistent with data suggesting that under basal conditions the majority of receptors within the PSD are of this type [121, 88]. On the other hand, experimental studies in knockout mice provide evidence that dephosphorylation of GluR1 subunits is an essential component of hippocampal LTD [64, 65, 66]. This suggests that there may be a number of distinct mechanisms for the removal of synaptic receptors during LTD [10, 75]. As in the case of LTP, we can use our model to explore various hypotheses regarding how changes in receptor trafficking generate responses that are consistent with those observed during LTD. Here we will focus on the role of GluR2/3 under the assumption that basal levels of GluR1/2 within the PSD are low. In order to proceed, we extend our basic model by assuming that GluR2/3 receptors within the PSD exist in two distinct states corresponding to association with GRIP/ABP and PICK1 respectively (see Section 3.1.2). Suppose that under basal conditions the transition rate μ from the GRIP-associated state to the PICK-associated state is negligible ($\mu = 0$) so that the number of receptors in the PICK-associated state is approximately zero. The receptor concentrations then satisfy the original set of Equations (3.1)-(3.7). We now assume that during the induction phase of LTD the transition rate μ increases, leading to the conversion of some bound receptors to the

PICK-associated state. We further assume that the change in μ is rapid compared to the time-scale of receptor trafficking, and is maintained during the presentation of the LTD stimulus (μ rapidly returns to zero once the stimulus is removed). The combined system of GRIP-associated and PICK-associated GluR2/3 receptors within the PSD now evolves according to Equations (3.12)-(3.15). In particular, PICK-associated receptors rapidly untether from their binding sites and hop to the ESM where they are endocytosed, resulting in a reduction in the number of receptors within the PSD. However, on its own, this mechanism cannot maintain LTD once the low frequency stimulus is removed, for there is currently no evidence for a bistable switch analogous to CaMKII that would allow levels of phosphorylation to persist. Therefore, receptors would convert back to the GRIP-associated state and the synapse would recover. In order to have a persistent reduction in synaptic strength, we assume that as receptors untether from binding sites, these sites are removed at some rate γ . We thus supplement Equations (3.1), (3.3), and (3.12)-(3.15) of the extended model by the following equation for the concentration Z of binding sites:

$$\frac{dZ}{dt} = -\gamma(Z - Q_I - Q_{II,a} - Q_{II,b}) \quad (3.17)$$

where Q_I is the concentration of bound GluR1/2 receptors and $Q_{II,a}$ and $Q_{II,b}$ are, respectively, the concentrations of bound GRIP-associated and PICK-associated GluR2/3 receptors. This equation, which takes the rate of decrease of Z to be proportional to the concentration of free binding sites within the PSD, only holds during the presentation of the LTD stimulus; once the stimulus is removed Z stops decreasing. Under basal conditions the binding sites are almost fully occupied. On the other hand, during LTD GRIP-associated receptors are converted to PICK-associated receptors so that $Q_{II,a}$ decreases and $Q_{II,b}$ increases. Since PICK-associated receptors are more likely to unbind from scaffolding proteins we find that $Q_{II,a}$ decreases faster than $Q_{II,b}$ increases. The net result is that Z decreases due to the freeing of binding sites. Once the LTD stimulus is removed, all receptors convert back to the GRIP-associated state and all the remaining binding sites become reoccupied.

We numerically solve the extended receptor trafficking model given by Equations (3.1), (3.3), (3.12), (3.15) and (3.17) in order to determine the time-dependent variation in synaptic receptor concentration during LTD. Figure 3.7A shows the time course of the total number of receptors for the various receptor types. The synapse is assumed to be in steady-state under basal conditions for $t < 0$, with a negligible concentration

of PICK-associated receptors ($\mu = 0$). We assume that a low frequency stimulus is applied for 900 sec during which $\mu > 0$. It can be seen that there is a conversion of GRIP-association to PICK-association during the presentation of the stimulus, with a partial recovery after the stimulus is removed. The steady-state receptor concentration has decreased, however, due to the removal of binding sites. Interestingly, our model can reproduce a variety of experimental results. For example Dudek and Bear (1992) showed that increasing the frequency of the stimulus from 3Hz to 10Hz, say, can lead to a transient reduction in synaptic strength rather than LTD. One way to generate this in our model is to assume that the stimulus induces the conversion of GRIP to PICK but the number of binding sites is not reduced (see Figure 3.7B). In another experiment, Dudek and Bear (1993) showed how a sequence of low frequency stimulations each separated by around 45 min can induce a saturating sequence of LTD. This result can also be reproduced by our model, with the saturation arising from the fact that even if most binding sites are removed, there are still free receptors present (see Figure 3.7C).

3.3 Spatial model of AMPA receptor trafficking at a single spine

In this section we present a model of AMPA receptor trafficking model at a single spine which does not treat receptor concentrations as spatial uniform but rather allows for spatial variation. The spine is treated as a uniform cylinder of radius r_0 and length z_0 with one end open and the other closed (see Figure 3.8).

The first compartment represents the PSD region of the spine head, and is modeled by the flat disc at the sealed end of the cylinder. The second compartment represents the ESM of the remaining spine head and neck, and is modeled by the curved surface of the cylinder. The circular boundary at the open end of the cylinder represents the junction of the spine with the surface of the dendritic shaft. We take both the PSD and ESM to be radially symmetric, with r the radial distance from the center of the PSD and z the axial distance along the cylinder from the PSD. The variables P , Q and R are defined as in Section 3.1 except that they are now functions of $r \in [0, r_0]$ or $z \in [0, z_0]$. As before we take $r_0 = 0.2\mu\text{m}$, and $z_0 = 1\mu\text{m}$. We denote the diffusivity of AMPA receptors in the PSD and ESM by D_a and D_A , respectively, and take $D_a = 0.01$ and $D_A = 0.1\mu\text{m}^2 \text{ s}^{-1}$ [39, 3].

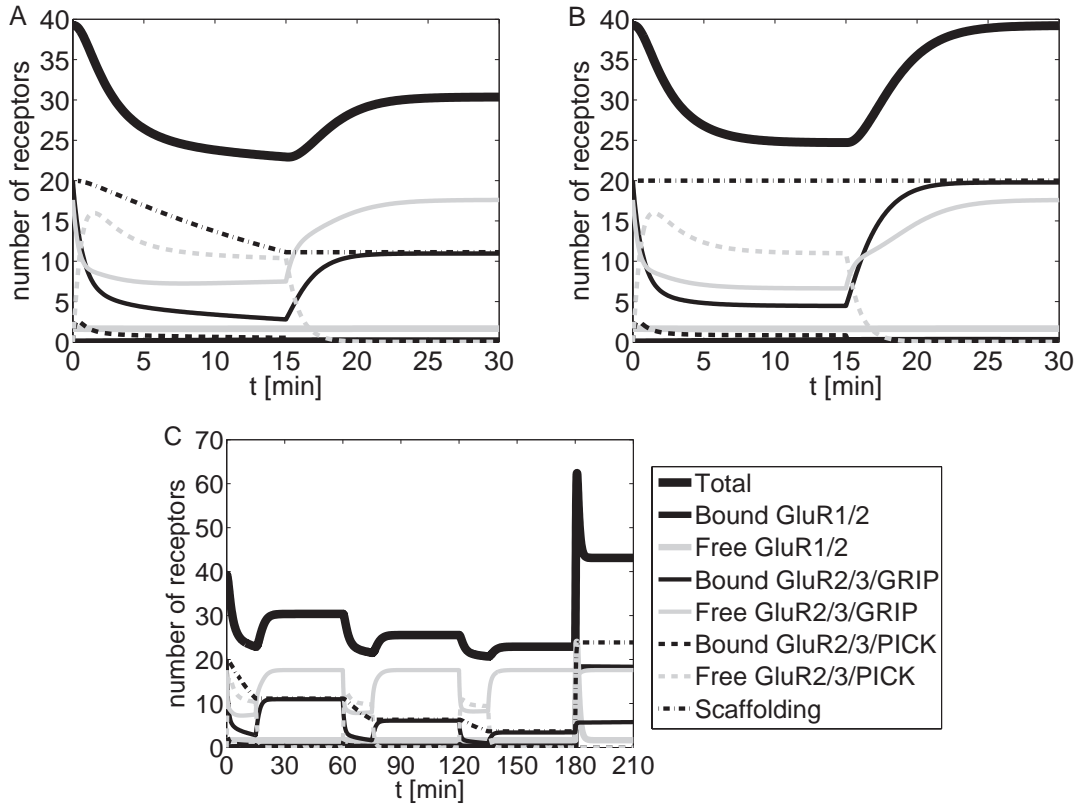


Figure 3.7. Time course of AMPA receptors during LTD. The total number of receptors (solid black curves) and binding sites (solid green curves) in the PSD are plotted together with contributions from various receptor types. (A) With receptors at steady-state for $t < 0$, LTD is induced at time $t = 0$ by increasing from zero the transition rate μ from GluR2/3-GRIP to GluR2/3-PICK and maintaining this for 15 min. LTD parameter values are $\mu = \nu = 0.01 \text{ s}^{-1}$, $\beta_{II}^* = 0.1 \text{ s}^{-1}$, $k_{II}^* = k_{II} = 0.1667 \mu\text{m}^2\text{s}^{-1}$, and $\gamma = 0.001 \text{ s}^{-1}$. All other parameters are as in Table 3.1. GluR2/3-GRIP is rapidly converted to GluR2/3-PICK during the first few minutes; afterward, this conversion occurs at a slower rate. Bound GluR2/3- PICK releases from binding sites and free GluR2/3-PICK exits the PSD and is endocytosed. The number of binding sites follows the loss of bound receptors. When at 900 sec LTD induction ends and μ is set to zero again, GluR2/3-PICK converts back to GluR2/3-GRIP at the rate ν . However, the new steady-state synaptic receptor number is lower due to the loss of binding sites. These results are consistent with typical recordings of EPSPs during LTD [29]. (B) Time course of receptors in the PSD during LTD with moderate frequency stimulus. LTD is induced as in A, except that $\gamma = 0 \text{ s}^{-1}$ throughout. Since the number of binding sites remains unchanged, the number of AMPA receptors in the PSD returns to its initial steady-state value. This result is consistent with Dudek and Bear (1992). (C) Saturation of LTD. LTD is induced as in A, except that it is followed by 45 min of basal activity, and this one hour epoch is repeated three times, followed by the induction of LTP. (LTP is induced as in Figure 3.5, except $c = 0.325$). Notice that the loss of PSD receptors decreases in each consecutive epoch. Saturation occurs because only bound, and not free, receptors are lost during LTD. This result is consistent with Dudek and Bear (1993)

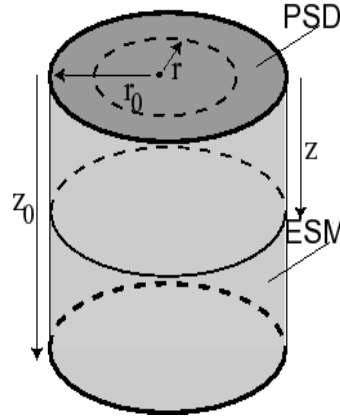


Figure 3.8. Model geometry. Model of a dendritic spine. The PSD is modeled as a disk at the end of a cylinder, while the extrasynaptic membrane (ESM) of the spine head is modeled as the curved surface of the cylinder. The open end of the cylinder represents the junction of the spine head with the dendritic shaft.

3.3.1 Model equations

The free receptor concentrations in the PSD ($0 \leq r < r_0$) satisfy the equations

$$\frac{\partial P_I}{\partial t} = \frac{D_a}{r} \frac{\partial}{\partial r} \left(r \frac{\partial P_I}{\partial r} \right) - \alpha_I (Z - Q_I - Q_{II}) P_I + \beta_I Q_I, \quad (3.18)$$

$$\frac{\partial P_{II}}{\partial t} = \frac{D_a}{r} \frac{\partial}{\partial r} \left(r \frac{\partial P_{II}}{\partial r} \right) - \alpha_{II} (Z - Q_I - Q_{II}) P_{II} + \beta_{II} Q_{II} + \frac{\sigma_{II}}{a}. \quad (3.19)$$

The first term on the right side of Equations (3.18) and (3.19) represents radial diffusion in the PSD with diffusivity D_a while the the rest of the terms are similar to those in Equations (3.1) and (3.2). The bound receptor concentrations continue to satisfy Equations (3.3) and (3.4). The receptor concentrations in the ESM ($0 < z < z_0$) satisfy the equations

$$\frac{\partial R_I}{\partial t} = D_A \frac{\partial^2 R_I}{\partial z^2} - \frac{k_I}{A} R_I + \frac{\sigma_I}{A}, \quad (3.20)$$

$$\frac{\partial R_{II}}{\partial t} = D_A \frac{\partial^2 R_{II}}{\partial z^2} - \frac{k_{II}}{A} R_{II}. \quad (3.21)$$

The first term on the right-hand side of Equations (3.20) and (3.21) represents axial diffusion in the ESM with diffusivity D_A . S_I continues to satisfy Equation 3.7.

The above equations must be supplemented by the hopping boundary conditions employed in the compartmental model (see Section 3.1). They are

$$J_{a,j}(r_0) = J_{A,j}(0) = \frac{h_j}{2\pi r_0} [P_j(r_0) - R_j(0)] \quad (3.22)$$

for $j = I, II$, where the receptor fluxes are defined according to

$$J_a = -D_a \frac{\partial P}{\partial r}, \quad J_A = -D_A \frac{\partial R}{\partial z}. \quad (3.23)$$

Here J_a denotes the flux within the PSD with $2\pi r J_a(r)$ corresponding to the rate at which receptors cross a circle of radius r concentric with the PSD. Similarly, J_A denotes the flux within the ESM with $2\pi r_0 J_A(z)$ corresponding to the rate at which receptors cross a circumference of radius r_0 at an axial distance z from the PSD. We also impose the following boundary condition at the ESM-dendrite junction,

$$J_{A,j}(z_0) = \frac{\omega_j}{2\pi r_0} [R_j(z_0) - U_j] \quad (3.24)$$

for $j = I, II$, which represents hopping across the spine neck between the ESM and dendrite at a rate ω_j . The total number of AMPA receptors in the PSD is $N = N_I + N_{II}$, with

$$N_j = 2\pi \int_0^{r_0} r (P_j(r) + Q_j(r)) dr. \quad (3.25)$$

3.3.2 Description of numerics

All figures in this section were produced using Matlab. Steady-state figures were produced by plotting their analytic formulations. Figures containing time-evolution data were produced using a finite area numerical approximation of our model partial differential equations. A finite area method was chosen to conserve surface receptors, as the paradigm of this method computes the total flux into and out of an area, rather than computing the change in concentration at a single point. For updating, we employed the standard backward Euler method, discretizing the diffusion operator and time derivative in the standard way.

Backward Euler is known to be second-order accurate in space. Our finite area method requires the computation of flux at the junctions in our model (at $r = r_0$ and $z = z_0$), yet the method does not have a data point at any junction, since the data points are always interior to their representative areas and the junctions are always area boundaries. However, we can still maintain second-order accuracy at these junctions in the following way. At $r = r_0$, we use a weighted harmonic mean of the diffusion coefficients D_a and D_A as an effective diffusion coefficient D_{eff} ; i.e.,

$$D_{eff} = \frac{2D_a D_A (\Delta r + \Delta z)}{D_a \Delta z + D_A \Delta r}$$

where Δr and Δz are the spacial step lengths in the disk and on the cylinder, respectively. It is well-known that this choice of effective diffusion coefficient for spatially inhomoge-

nous diffusion coefficients preserves second-order accuracy. Because the surface receptor concentration may be discontinuous at $r = r_0$, we compute the flux there by extrapolating the concentrations in the PSD and ESM simultaneously, as follows. Let P_K be the last point in our discretization of P (so that the boundary of the area containing P_K includes the junction of the PSD and the ESM) and let R_1 be the first point in our discretization of R (so that the boundary of the area containing R_1 includes the same junction). A discretization of the boundary conditions (3.22) yields the following system of equations for P_{K+1} and R_0 :

$$\begin{aligned} -D_{eff} \frac{P_{K+1} - P_K}{\Delta r} &= h \left(\frac{P_{K+1} + P_K}{2} - \frac{R_1 + R_0}{2} \right) \\ -D_{eff} \frac{R_1 - R_0}{\Delta z} &= h \left(\frac{P_{K+1} + P_K}{2} - \frac{R_1 + R_0}{2} \right) \end{aligned}$$

The left-hand sides of these equations represent discretizations of the flux at $r = r_0$ (equivalently, at $z = 0$), and the values $(P_{K+1} + P_K)/2$ and $(R_1 + R_0)/2$ are midpoint interpolations of the concentrations $P(r_0)$ and $R(0)$, respectively, using the points P_{K+1} and R_0 that we are attempting to extrapolate. The solution to these equations is

$$\begin{aligned} P_{K+1} &= \frac{\theta_a \theta_A + \theta_a - \theta_A}{\theta_a \theta_A + \theta_a + \theta_A} P_K + \frac{2}{\theta_a \theta_A + \theta_a + \theta_A} R_1 \\ R_0 &= \frac{2}{\theta_a \theta_A + \theta_a + \theta_A} P_K + \frac{\theta_a \theta_A - \theta_a + \theta_A}{\theta_a \theta_A + \theta_a + \theta_A} R_1 \end{aligned}$$

where $\theta_a = 2D_a/(h\Delta r)$ and $\theta_A = 2D_A/(h\Delta z)$. We can now compute the discretized flux:

$$-D_{eff} \frac{P_{K+1} - P_K}{\Delta r} = -D_{eff} \frac{R_1 - R_0}{\Delta z} = \frac{P_K - R_1}{1/h + (\Delta r + \Delta z)/(2D_{eff})}.$$

Notice that this approximation is independent of the extrapolated values P_{K+1} and R_0 . This method of computing the flux inherits second-order accuracy from the midpoint interpolation used above.

The flux at $z = z_0$ was computed in a similar way. Let R_L be the last point in our discretization of R (so that the boundary of the area containing R_L includes the junction of the ESM with the dendritic shaft). Then a discretization of the boundary condition (3.24) yields the following equation for R_{L+1} :

$$-D_A \frac{R_{L+1} - R_L}{\Delta z} = \omega \left(\frac{R_{L+1} + R_L}{2} - R_0 \right)$$

where this time R_0 represents the concentration of receptors on the dendritic shaft. The solution of this equation is

$$R_{L+1} = \frac{(\theta - 1)R_L + 2R_0}{\theta + 1},$$

where $\theta = 2D_A/\omega\Delta z$. The discretized flux is therefore

$$-D_A \frac{R_{L+1} - R_L}{\Delta z} = \frac{2D_A\omega(R_L - R_0)}{2D_A + \omega\Delta z}$$

which is again second-order accurate and independent of the extrapolated value R_{L+1} .

3.3.3 Steady-state AMPA receptor concentrations and fluxes

The steady-state bound receptor concentrations Q_j still satisfy Equation 3.8. It remains to solve the following steady-state diffusion equations for P_j and R_j :

$$0 = \frac{D_a}{r} \frac{\partial}{\partial r} \left(r \frac{\partial P_j}{\partial r} \right) + \frac{\sigma_{II}}{A_a} \delta_{j,II}, \quad 0 \leq r < r_0 \quad (3.26)$$

and

$$0 = D_A \frac{\partial^2 R_j}{\partial z^2} + \frac{\sigma_I}{A_A} \delta_{j,I} - k_j R_j, \quad 0 < z < z_0 \quad (3.27)$$

subject to the boundary conditions (3.22) and (3.24). Here $\delta_{i,j}$ is the Kroncker delta function. The general steady-state solution for type I receptors is

$$P_I(r) = c_1 \ln(r) + c_2, \quad (3.28)$$

$$R_I(z) = c_3 e^{\kappa_I z} + c_4 e^{-\kappa_I z} + \Sigma_I, \quad (3.29)$$

where $\kappa_I = \sqrt{k_I/D_A}$ and $\Sigma_I = \sigma_I/(A_A k_I)$. Finiteness of P_I requires $c_1 = 0$, and hence the vanishing of the steady-state flux at the boundary between the PSD and ESM. The boundary condition (3.22) for $j = I$ implies $c_3 = c_4$ and $c_2 = 2c_3 + \Sigma_I$. The boundary condition (3.24) for $j = I$ yields the result

$$c_3 = \frac{\omega_I(U_I - \Sigma_I)}{2(\omega_I \cosh(\kappa_I z_0) + D_A \kappa_I \sinh(\kappa_I z_0))}.$$

Similarly, the steady-state solution for type II receptors is given by

$$P(r) = d_1 \ln(r) + d_2 - \Sigma_{II} r^2 \quad (3.30)$$

$$R(z) = d_3 e^{\kappa_{II} z} + d_4 e^{-\kappa_{II} z} \quad (3.31)$$

where $\kappa_{II} = \sqrt{k_{II}/D_A}$ and $\Sigma_{II} = \sigma_{II}/(4A_a D_a)$. Finiteness of P_{II} requires $d_1 = 0$. The boundary conditions (3.22) and (3.24) for $j = II$ then show that

$$d_2 = d_3 + d_4 + \Sigma_{II} r_0^2 + \frac{2D_a \Sigma_{II} r_0}{h_{II}}, \quad (3.32)$$

$$d_3 = d_4 - \frac{2D_a \Sigma_{II} r_0}{D_A \kappa_{II}}, \quad (3.33)$$

$$d_4 = \frac{\omega_{II} U_{II} + 2D_a \Sigma_{II} r_0 e^{\kappa_{II} z_0} (1 + \omega_{II}/(D_A \kappa_{II}))}{2(\omega_{II} \cosh(\kappa_{II} z_0) + D_A \kappa_{II} \sinh(\kappa_{II} z_0))}. \quad (3.34)$$

Typical steady-state concentration profiles are shown in Figure 3.9A for parameter values corresponding to a synapse operating under basal conditions (listed in Table 3.1).

The total receptor concentration in the PSD is high and almost entirely composed of GluR2/3 receptors (number of GluR1/2 receptors in PSD is ~ 1 , number of GluR2/3 receptors is ~ 37), with about half of these bound (number of bound receptors ≈ 20). The concentration drops dramatically into the ESM and is almost entirely composed of GluR1/2 receptors (number of GluR2/3 receptors in ESM ~ 1 , number of GluR1/2 receptors ~ 16). These steady-state profiles is maintained primarily by the constitutive recycling of GluR2/3 receptors, which involves a constant flux of receptors from the PSD to the ESM where they are endocytosed and either reinserted into the membrane surface or degraded. The spatial dependence of the surface receptor flux is also shown in Figure 3.9A, where a positive (negative) flux represents flow away from (toward) the PSD. The receptor flux is positive throughout the membrane, increasing from zero at the center of the PSD, peaking at $\sim 0.13 \mu\text{m}^{-1}\text{s}^{-1}$ at the PSD-ESM junction and decreasing to $\sim 0.003 \mu\text{m}^{-1}\text{s}^{-1}$ at the ESM-shaft junction. Note that the flux of free receptors is continuous at the boundary between the PSD and ESM. The discontinuous jump in receptor concentration at this boundary is due to two factors: bound receptors within the PSD do not equilibrate with the free receptor concentration in the ESM, and the boundary acts as a barrier to receptor movement. All of these features of the concentration and flux are consistent with experimental data (see Section 2.3) and with our compartmental model (see Section 3.2). In particular, note how nearly uniform the concentrations in both the PSD and ESM are, suggesting that in the steady-state our compartmental model is an appropriate simplification.

Given the steady-state receptor concentrations, it is straightforward to calculate the total number of type I and type II AMPA receptors in the PSD and ESM by integrating over the corresponding spatial domain. If we assume that the strength of the synapse is proportional to the total number of synaptic receptors, then we can determine how the steady-state synaptic strength depends on the various parameters of the model. The results are shown in Figures 3.9B-F. Since we are assuming that the constitutive recycling of GluR2/3 receptors predominates under basal conditions, the total receptor number in the PSD tends to be insensitive to changes in parameters associated with GluR1/2 trafficking except for the rates of exo/endocytosis σ_I and k_I . On the other hand, the receptor number is strongly dependent on parameters associated with GluR2/3 trafficking, including the rates of exo/endocytosis, σ_{II} , k_{II} , the ratio of the binding and unbinding rates, α_{II}/β_{II} , and the hopping rate h_{II} . These results agree well with similar results

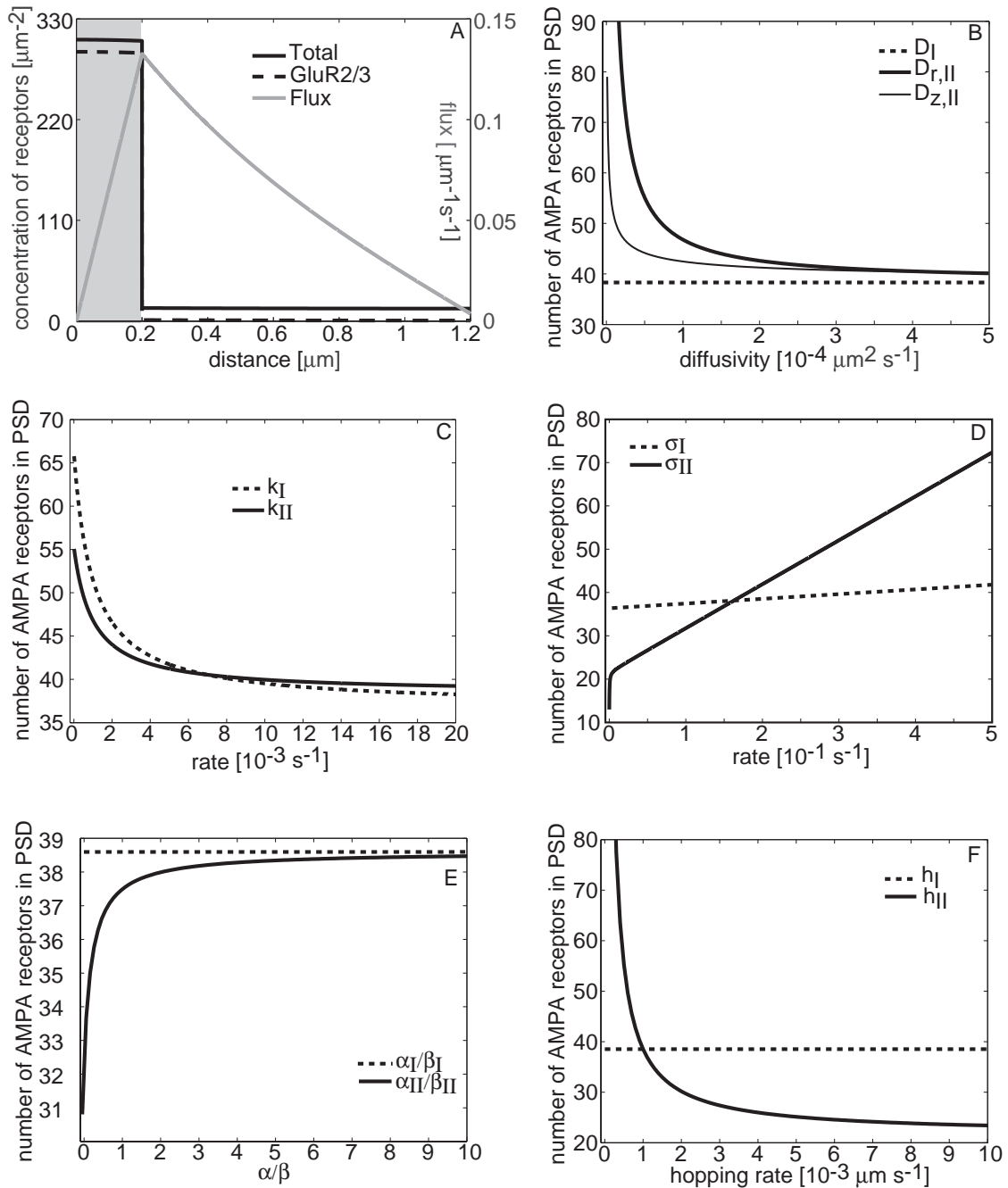


Figure 3.9. Steady-state behavior under basal conditions (see Table 3.1 for parameter choices). (A) Steady-state concentration and flux of surface AMPA receptors. The shaded and unshaded regions are the PSD and ESM, respectively. Distance is measured from the center of the PSD, and is given by the radial coordinate r within the PSD (0 to 0.2 μm) and by $r_0 + z$ within the ESM (0.2 to 1.2 μm), where z is the axial distance from the PSD (see Figure 3.8). (B-F) Dependence of the steady-state number of AMPA receptors in the PSD on model parameters. Compare with Figure 3.3

obtained from our compartmental model (see Figure 3.3).

3.3.4 Blocking exo/endocytosis

Figure 3.10 shows the results of blocking exo/endocytosis. Notice how closely these figures resemble those obtained from the compartmental model (see Figure 3.4) again showing how well the compartmental model approximates the spatial model.

3.3.5 Trafficking during LTP and LTD

In Figure 3.11 we show snapshots of the GluR1/2 receptor concentration profile and the associated flux in response to the induction of LTP (see Section 3.2 for details). For simplicity we do not include the dynamical Equation (3.16) for the scaffolding concentra-

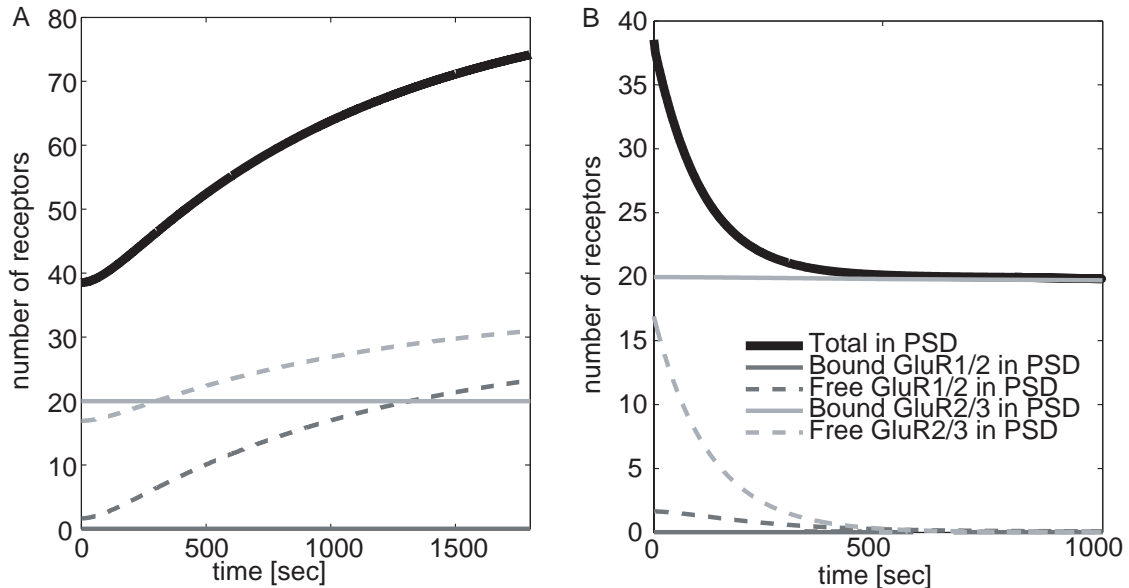


Figure 3.10. Time course of AMPA receptors after blocking exo/endocytosis. (A) Blocking endocytosis. With receptors at basal steady-state at time $t < 0$, endocytosis is blocked by setting $k_j = 0$ ($j = I, II$) at $t = 0$. The background concentration U_{II} is also set to $10\mu\text{m}^{-2}$ at the same time, representing concurrent blockage at nearby synapses. The number of AMPA receptors in the PSD nearly doubles within 30 min (due to an increase in the number of free receptors) and reaches a new steady-state value of ≈ 84 receptors in 1 hr (not shown). (B) Blocking exocytosis. This time, exocytosis is blocked by setting $\sigma_j = 0$ ($j = I, II$) at $t = 0$. The number of AMPA receptors in the PSD almost halves in less than 10 min (due to a loss of free receptors). These results are consistent with Luscher et al. (1999) and with those obtained from the simplified two-compartment model (see Figure 3.4).

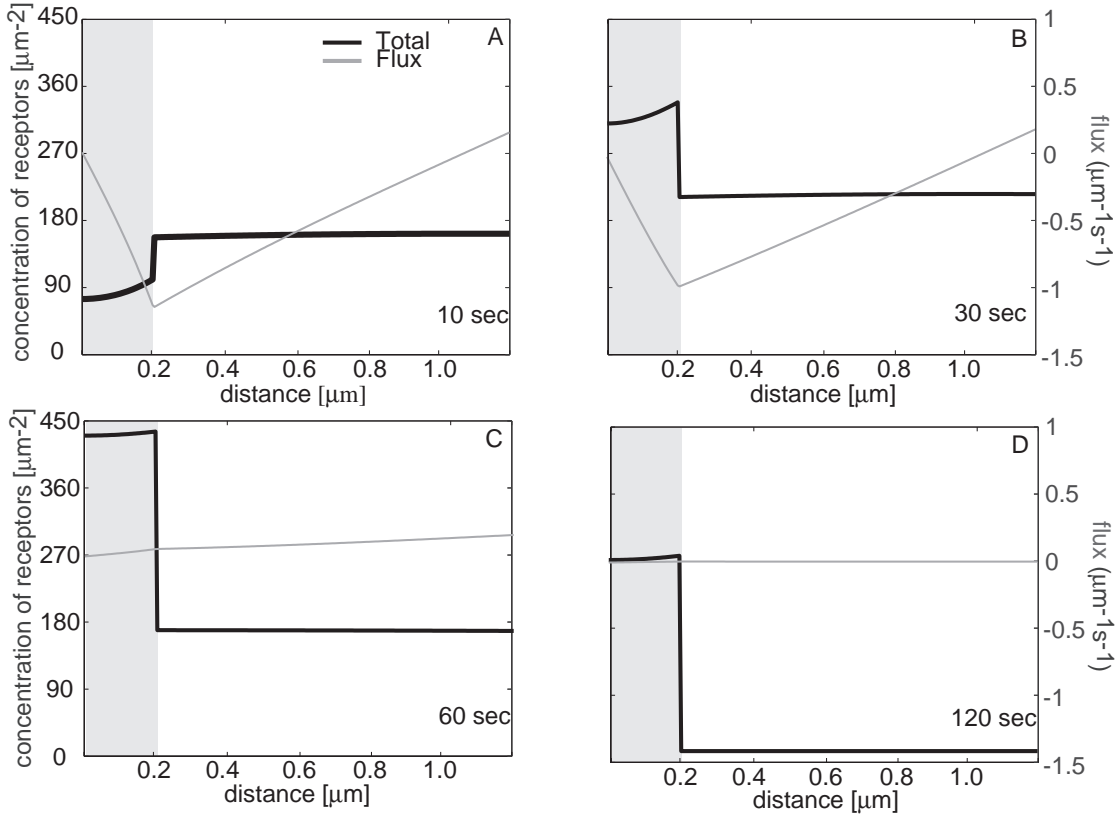


Figure 3.11. Snapshots of GluR1/2 AMPA receptor concentration and flux during LTP at (A) 10 sec, (B) 30 sec, (C) 60 sec, and (D) 120 sec after induction. Distance is defined as in Figure 3.9A. With receptors at basal steady-state at time $t < 0$, LTP is induced by setting $Z = 477 \mu\text{m}^{-2}$, $\alpha_I = 0.001 \mu\text{m}^2\text{s}^{-1}$, $\kappa_I = 0.0556\text{s}^{-1}$, and $h_I = 0.01 \mu\text{m s}^{-1}$ at time $t = 0$. The concentration in the ESM rises transiently as GluR1/2 receptors from the intracellular pool are exocytosed there. Mediated by diffusion and barrier hopping, the concentration in the PSD rises as receptors from the ESM enter the PSD, and a portion of these receptors are immobilized by the newly-activated binding sites.

tion Z , but simply step Z to its asymptotic value at time $t = 0$. Figures 3.11A-D show a sequence of events in which GluR1/2 receptors are rapidly inserted into the ESM due to a transient increase in the rate of exocytosis, after which they laterally diffuse into the PSD. This leads to a large transient increase in the free synaptic receptor concentration. The free receptors then bind to the newly-activated binding sites within the PSD, leading to a persistent increase in the concentration of bound receptors in the PSD. The trafficking of GluR1/2 receptors into the PSD accounts almost fully for the doubling of the total number of synaptic receptors in the PSD. In addition, note how the concentration profiles

in both the PSD and ESM remain relatively uniform throughout the expression of LTP. In Figures 3.12A-B we plot the corresponding time courses for the total number of receptors in the PSD and ESM. Also, in Figure 3.12C-D we plot the corresponding time courses without synaptic targeting and in Figure 3.12E we plot the exchange of GluR1/2 receptors for GluR2/3 after LTP. Again, these results obtained from the spatial model are nearly identical to the compartmental model (see Figures 3.5 and 3.6).

In Figures 3.13A-D we show snapshots of the resulting GluR2/3-GRIP and GluR2/3-PICK receptor concentration profiles within the PSD, and the associated fluxes after the induction of LTD (see Section 3.2). It can be seen that there is a conversion of GRIP to PICK during the presentation of the stimulus, with a partial recovery after the stimulus is removed. The steady-state receptor concentration has decreased, however, due to the removal of active binding sites. This is further illustrated in Figure 3.14A-C, where the time course of the total number of receptors is plotted for the various receptor types. Again, these simulations agree with those obtained using the compartmental model. Again, note how similar these results are compared to those of the simplified two-compartmental model (see Figure 3.7).

3.4 Discussion of single-spine model

In this chapter we presented a mathematical model of AMPA receptor trafficking at a single spine that provides a general theoretical framework for investigating the role of trafficking in the expression of synaptic plasticity. The behavior of the model depends on various trafficking parameters that could be targets of second-messenger pathways activated by the postsynaptic calcium signal during the induction of LTP/LTD. We used our model to explore the consequences of targeting different sets of trafficking parameters, and showed how this can reproduce a wide range of experimental data: 1) The increase/decrease in synaptic strength after pharmacologically blocking endocytosis/exocytosis [73]. 2) The time course of changes in synaptic strength during the expression of LTP [7, 40, 96]. 3) The slow exchange of GluR1/2 receptors with GluR2/3 receptors after potentiation [88]. 4) The time course of changes in synaptic strength during the expression of LTD and its dependence on frequency of stimulation [29, 28]. 5) The saturation of LTD induced by a sequence of low frequency stimuli [28].

Constraining our model to reproduce these results using physiologically reasonable parameter values allows us to make experimentally testable predictions regarding AMPA

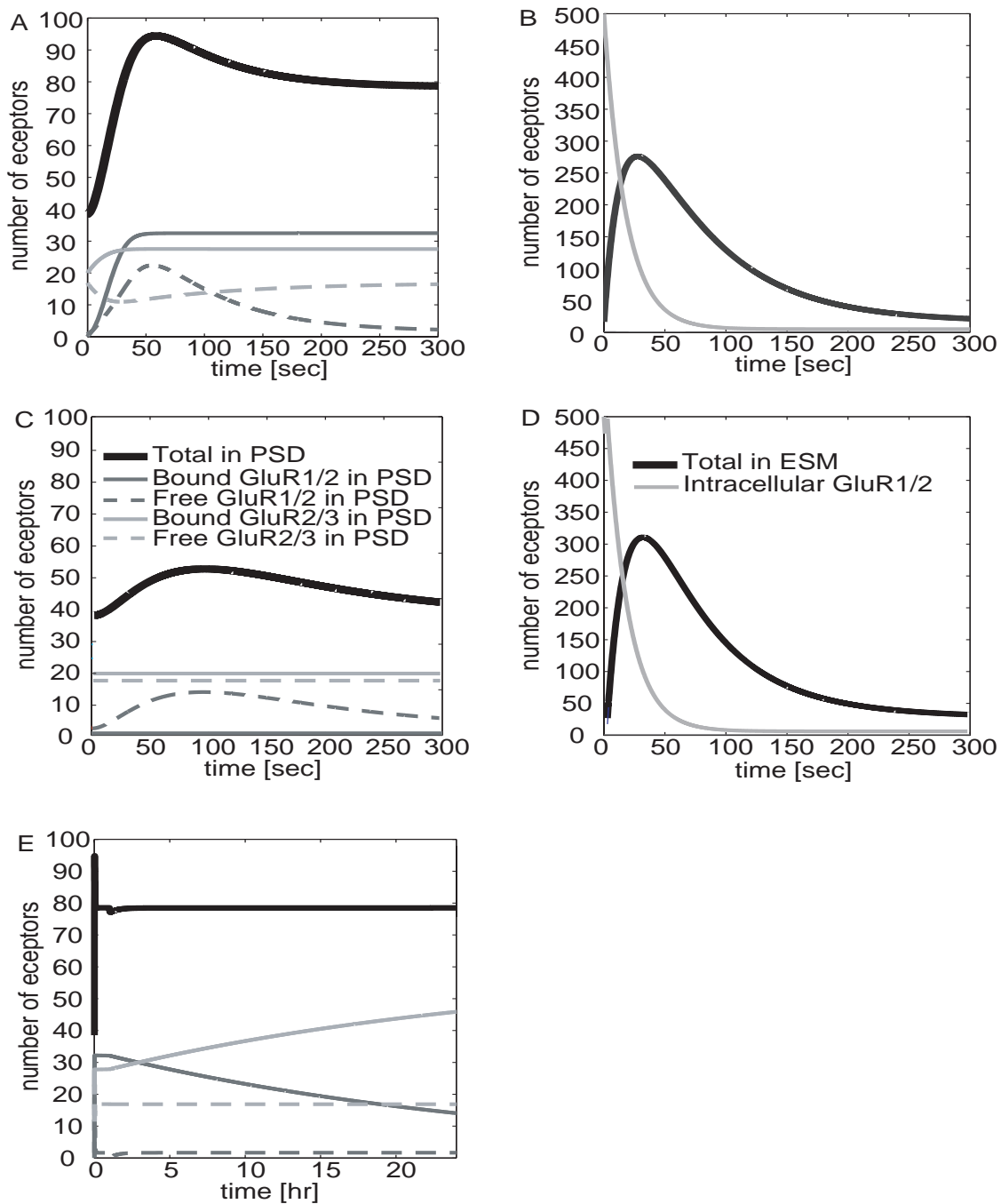


Figure 3.12. Time course of AMPA receptors during LTP. (A,B) Time course of receptors after induction of LTP using same conditions as Figure 3.11. These results are nearly identical to those obtained with the simplified two-compartment model, see Figures 3.5A,B. (C,D) Time course of receptors without synaptic targeting. These results are nearly identical to those obtained with the simplified two-compartment model, see Figures 3.5C,D. (E) Exchange of GluR1/2 and GluR2/3 AMPA receptors. These results are nearly identical with those obtained with two-compartment model, see Figure 3.6.

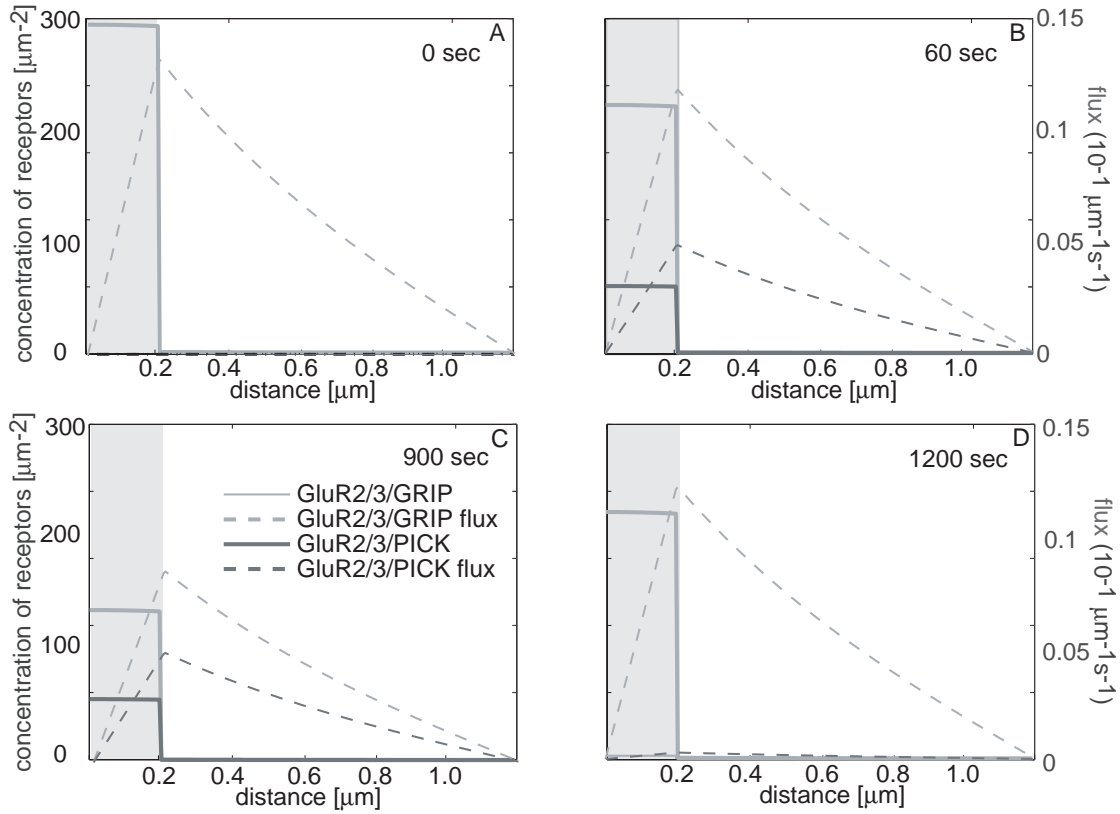


Figure 3.13. Snapshots of GluR2/3-GRIP and GluR2/3-PICK AMPA receptor concentrations and fluxes during LTD at (A) 0 sec, (B) 60 sec, (C) 900 sec, and (D) 1200 sec after onset of a low frequency stimulus that lasts 900 sec. Distance is defined as in Figure 3.9A. With receptors at basal steady-state at time $t < 0$, LTD is induced by simulating the extended LTD model for 900 sec, beginning at time $t = 0$. LTD parameter values are $\mu = 10^{-4}\text{s}^{-1}$, $\nu = 0.01\text{s}^{-1}$, $\beta_{II}^* = 0.1\text{s}^{-1}$, $k_{II}^* = k_{II} = 0.1667\text{s}^{-1}$, and $\gamma = 0.001\text{s}^{-1}$. After 900 sec, μ is set to zero so that the remaining PICK is converted back to GRIP. The concentration of GluR2/3-GRIP decreases while GluR2/3-PICK increases during the early course of LTD, and then both decrease together until 900 sec, when GluR2/3-PICK begins to convert back to GluR2/3-GRIP. However, the final concentration of GluR2/3-GRIP is lower than the initial concentration, due to a loss of active binding sites.

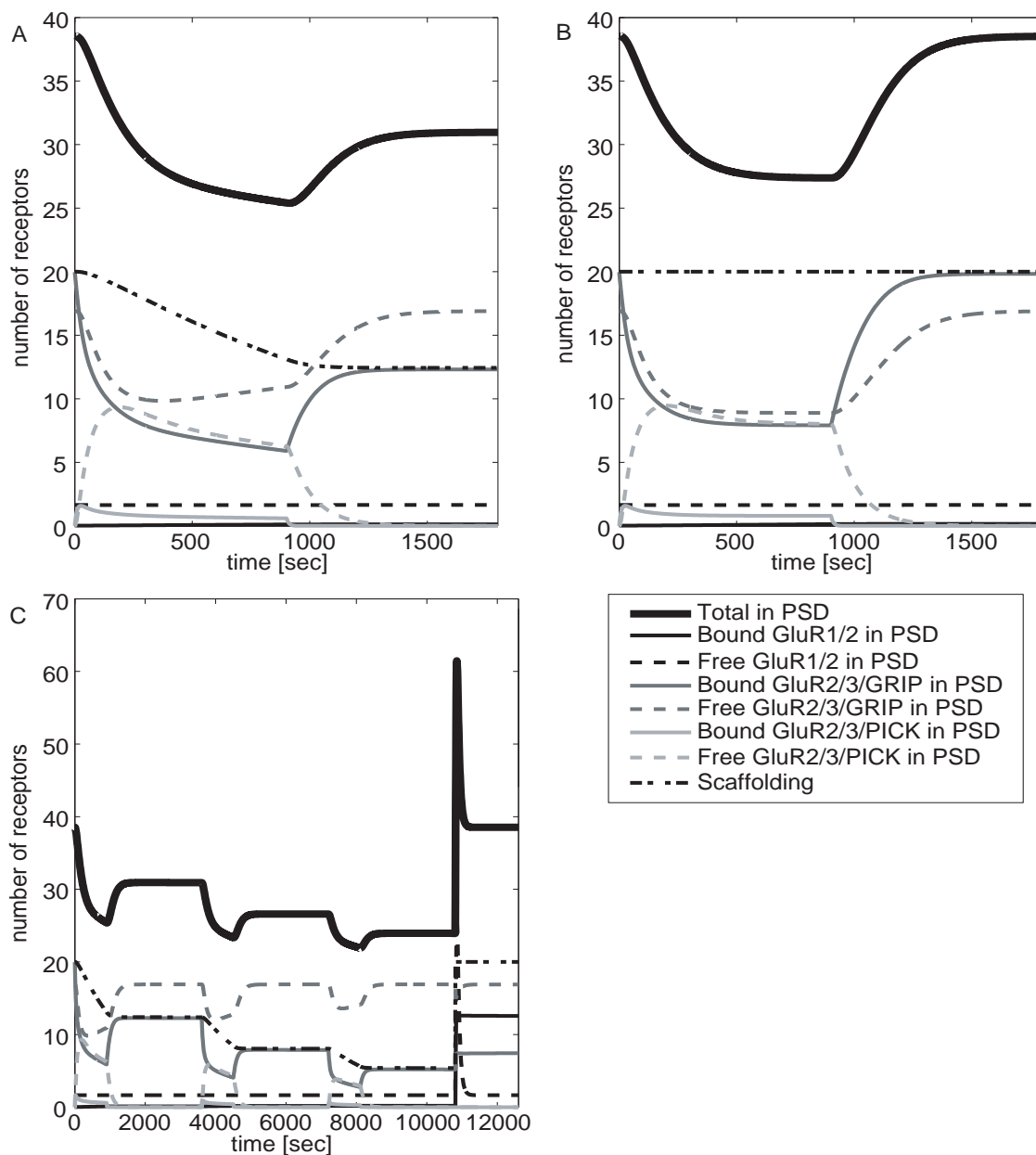


Figure 3.14. Time course of AMPA receptors during LTD. (A) Time course of receptors in the PSD during LTD with low frequency stimulus. LTD is induced as in Figure 3.13. These results are nearly identical to those obtained with the simplified two-compartment model, see Figure 3.7A. (B) Time course of receptors in the PSD during LTD with moderate frequency stimulus. LTD is induced as in Figure 3.13, except $\gamma = 0$. These results are nearly identical to those obtained with the simplified two-compartment model, see Figure 3.7B. (C) Saturation of LTD. LTD is induced as in Figure 3.13, except that it is followed by 45 min of basal activity, and this one hour epoch is repeated three times, followed by the induction of LTP. These results are nearly identical to those obtained with the simplified two-compartment model, see Figure 3.7C.

receptor trafficking and its regulation during LTP/LTD. First, there should be a significant fraction of mobile receptors in the PSD under basal conditions, consistent with the data of Groc et al. (2004) and Ashby et al. (2006). This, in turn, requires a barrier to diffusion at the PSD-ESM boundary, as previously suggested by Triller and Choquet (2003, 2005). Second, the exocytosis of intracellular GluR1/2 receptors during LTP only generates realistic time courses if it is combined with synaptic targeting (e.g. increases in the hopping rate across the PSD-ESM barrier and the rate of binding to scaffolding proteins). This is consistent with the suggested role of stargazin and its interaction with PSD-95 [114]. Moreover, depletion of the intracellular pool suggests that the increased rate of exocytosis is only temporary. Therefore, in order to have persistent early-phase LTP, it is necessary to increase the number of binding sites within the PSD, perhaps via the delivery of “slot” proteins by incoming AMPA receptors [77]. Third, the unbinding of GluR2/3 receptors from scaffolding proteins in the PSD (perhaps by exchange of GRIP with PICK) and subsequent endocytosis from the ESM is not sufficient to generate persistent LTD. A realistic LTD time course can be generated, however, if there is also a gradual decrease in the number of binding sites, that is, a removal of “slot” proteins. One of the interesting features of our model is that a number of experimental results can be obtained without any further tuning of the model. These include the slow exchange of GluR1/2 with GluR2/3 receptors during LTP, and the saturation of LTD. Of course, our results may be a consequence of the various simplifying assumptions of our model, which we now discuss in more detail.

3.4.1 Effects of diffusion

One major simplification of our two-compartment model is to ignore the effects of diffusion within the PSD and ESM. This was motivated by the observation that given physiologically reasonable values for the diffusivity of mobile receptors in each of the compartments [39], lateral membrane diffusion is relatively fast. Indeed, comparison with our spatial model showed nearly exact agreement in all cases (see Section 3.3). In particular, the fluxes involved in receptor trafficking are maintained by small concentration gradients so that the distribution of receptors within a compartment is approximately spatially uniform (see Figure 3.9). One consequence of fast diffusion is that the relatively high levels of free receptors found in the PSD cannot be maintained without some form of barrier between the PSD and ESM. Such a barrier was incorporated into our model

by requiring that the diffusive flux across the boundary between the PSD and ESM is proportional to the difference in concentrations on either side of the boundary. The associated hopping rate limits the flux across the PSD-ESM junction and allows the free receptor concentrations to be discontinuous there. An alternative mechanism for localizing free receptors within the PSD would be to have a sufficiently small diffusivity. Numerical simulations of our spatial model suggest that the required diffusivity lies outside the range of measured values for mobile receptors within the PSD [39].

One important aspect of dendritic spines that an extension of our spatial model could address is the effect of spine geometry on receptor-trafficking, in particular the role of the spine neck in restricting the flow of receptors from the ESM to the dendritic shaft, as recently observed experimentally [3] (see Section 6.1). In our simplified two-compartment model we represented the effect of the spine neck phenomenologically as an effective hopping rate ω . A diffusion model that takes into account the curvature of a spine's surface could be used to determine ω from first principles. In fact, in Section 6.1 we show from a preliminary calculation that

$$\omega \approx \frac{2\pi r_n D_n}{L_n}$$

where L_n and r_n are the average length and radius of the spine neck, respectively, and D_n is the diffusivity of AMPA receptors in the spine neck. Using $L_n = 0.45$ and $r_n = 0.075\mu\text{m}$ [41] and $D_n = 6.7 \times 10^{-3}\mu\text{m}^2\text{s}^{-1}$ [3], we find that $\omega \approx 7 \times 10^{-3}\mu\text{m}^2\text{s}^{-1}$, which is approximately our baseline value.

3.4.2 Single-channel conductance

In order to interpret the results of our model in terms of experimentally determined EPSP amplitudes we assumed that the size of an EPSP is roughly proportional to the total number of synaptic receptors. However, there is experimental evidence to suggest that direct phosphorylation of existing AMPA channels and a resulting increase in single-channel conductance can also contribute to LTP expression [4, 104]. An analogous result may hold for LTD, since dephosphorylation of AMPA receptors can lead to a decrease in single-channel conductance [4]. Recently, a combined experimental and modeling study of LTP in CA1 neurons explored how experimentally observed EPSP amplitudes in LTP can be accounted for by changing receptor number, channel conductance, or glutamate release in a detailed computational model of CA1 cells [47]. The size of an EPSP was found to depend sublinearly on the number of AMPA receptors, leading to the conclusion that the

change in receptor number required to account for the largest observed EPSPs in LTP is unrealistically high and, hence, that more than one mechanism is likely to be involved in the expression of LTP. Note that this study was concerned with the static dependence of synaptic strength on fixed synaptic receptor numbers and conductances, rather than with dynamical mechanisms that account for the time course of LTP expression. Developing an extension of our own model that includes both the dynamics of receptor trafficking and changes in single-channel conductances could provide further insights into the relative contributions of these two processes to LTP/LTD.

3.4.3 Slot proteins and synaptic stabilization

Although many scaffolding-related proteins have been identified [125], little is known about how these proteins act in concert to regulate and maintain AMPA receptor numbers at synapses. We modeled these proteins phenomenologically in terms of binding sites, which represent complexes able to immobilize AMPA receptors, much like the “slot” proteins hypothesized by Shi et al. (2001). We found that in order to stabilize changes in synaptic AMPA receptor numbers with respect to receptor turnover (which occurs on the order of minutes), it was necessary to transport binding sites to or from the synapse. However, it is known that scaffolding proteins themselves undergo constitutive recycling over a period of several hours [97, 49]. This implies that without additional processes the number of binding sites would eventually return to basal values. Therefore, another level of synaptic stabilization is required in order to maintain changes in synaptic strength over hours and days. One such mechanism could involve structural changes in the dendritic spine driven by F-actin and protein synthesis [85, 54, 62]. For example, enlargement of the spine head could accommodate an increase in the number of binding sites during LTP, with the associated increase in the production of F-actin providing additional anchoring points for scaffolding proteins. Interestingly, one of the mechanisms for increasing the production of F-actin and stabilization of a synapse is enhanced AMPA receptor expression [85]. An alternative mechanism for stabilizing a synapse has recently been proposed in a modeling study by Shouval (2005), based on the clustering of interacting receptors within the PSD. Under the hypothesis that receptor clusters can modify the exo/endocytic rate of individual receptors, it is shown how receptor clusters can form metastable states that significantly increases the stability of a synapse.

CHAPTER 4

TWO-DIMENSIONAL MODEL OF AMPA RECEPTOR TRAFFICKING ACROSS MULTIPLE DENDRITIC SPINES

In the previous chapter we presented a model of AMPA receptor trafficking at a single spine. However, there are hundreds or even thousands of synapses and their associated spines distributed along the surface of a dendrite. It follows that neurons must traffic receptors and other postsynaptic proteins over long distances (several 100 μm) from the soma. This can occur by two distinct mechanisms: either by lateral diffusion in the plasma membrane [19, 139, 2, 18] or by motor-driven intracellular transport along microtubules followed by local insertion into the surface membrane (exocytosis) [58, 116, 146]. It is likely that both forms of transport occur in dendrites, depending on the type of receptor and the developmental stage of the organism.

In this chapter we extend our model of AMPA receptor trafficking at a single spine to the more realistic case of multiple spines distributed along the surface a two-dimensional cylindrical dendrite. In this model the junction of spine and dendrite will be represented as a small, partially absorbing hole in the cylinder surface. Receptors can enter and exit a spine at this junction or they can diffuse laterally between spines within the dendritic surface. Note that the steady-state solutions for such a diffusion process are singular in the radius of the junctions, since when the radius is zero (i.e., there are no spines) we expect uniform concentrations of receptors throughout the dendritic membrane, and for any positive radius we expect receptor concentrations to change rapidly near the junctions in order to satisfy boundary conditions there. Furthermore, it is well-known that the two-dimensional Green's function for Laplace's equation has logarithmic singularities, and we will see that these singularities develop at the center of each junction. Given these facts we construct an approximate solution to the steady-state diffusion equation for AMPA receptor trafficking between multiple spines by matching appropriate 'inner' and 'outer' asymptotic expansions [145, 144, 128] (see Section 4.2). This leads to a

system of linear equations that determines the dendritic receptor concentration at each spine-dendrite junction. Solving this system of equations yields the 'outer' solution for the steady-state distribution of AMPA receptors along the dendrite. Finally, we compare our results with numerical solutions of the full model, and with a reduced one-dimensional model (see Sections 4.3 and 4.5) and find good agreement among all three.

It should be noted that diffusion-trapping problems arise in many areas of physics, chemistry and biology, and a variety of different modeling techniques have been developed to study them. For example, in random porous media a particle diffuses freely in a pore region until it encounters the boundary of a partially absorbing trap region (pore-trap interface) where it is absorbed with some probability. Here the spatial extent of the trap regions are not negligible so that one has to solve the diffusion equation in a heterogeneous medium using techniques such as homogenization theory [109, 137]. Another important class of model is that of continuous time random walks [113, 48], which have been used to study anomalous transport in a wide range of systems including motor proteins [60]. In these spatially discrete models the effect of a trap is to generate a non-exponential waiting time distribution. In terms of a spatially discrete version of our receptor trafficking model, only a fraction of sites (corresponding to spines) would have waiting time distributions that differ from a simple exponential.

4.1 Diffusion-trapping model on a cylinder

Schematic diagrams of the diffusion-trapping model are shown in Figure 4.1. Consider a population of M dendritic spines distributed along a cylindrical dendritic cable of length L and radius l , see Figure 4.1A. Since protein receptors are much smaller than the length and circumference of the cylinder, we can neglect the extrinsic curvature of the membrane. Therefore, we represent the cylindrical surface of the dendrite as a long rectangular domain Ω_0 of width $2\pi l$ and length L , see Figure 4.1B:

$$\Omega_0 = \{(x, y) : 0 < x < L, y < |\pi l|\}.$$

The cylindrical topology is preserved by imposing periodic boundary conditions along the circumference of the cylinder, that is, at $y = \pm\pi l$. At one end of the cylinder ($x = 0$) we impose a nonzero flux boundary condition, which represents a constant source of newly synthesized receptors from the soma, and at the other end ($x = L$) we impose a no-flux boundary condition. Each spine neck is assumed to intersect the dendritic surface transversely such that the intersection is a circle of radius $\varepsilon\rho$ centered about the point

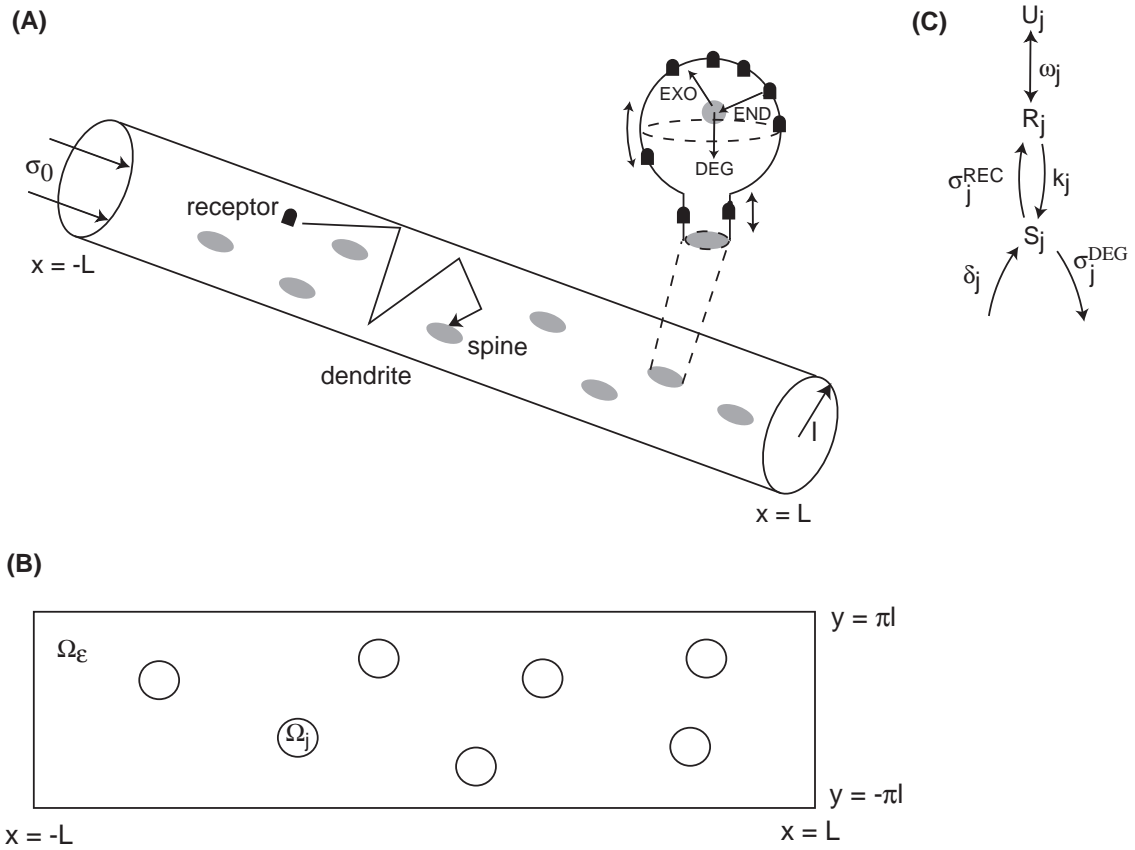


Figure 4.1. Diffusion–trapping model of receptor trafficking on a cylindrical dendritic cable (diagram not to scale). (A) A population of dendritic spines is distributed on the surface of a cylinder of length L and radius l . Each receptor diffuses freely until it encounters a spine where it may become trapped. Within a spine receptors may be internalized via endocytosis (END) and then either recycled to the surface via exocytosis (EXO) or degraded (DEG), see inset. Synthesis of new receptors at the soma and insertion into the plasma membrane generates a surface flux σ_0 at one end of the cable. (B) Topologically equivalent rectangular domain with opposite sides $y = \pm\pi l$ identified. (C) State transition diagram for a simplified one-compartment model of a dendritic spine. Here R_j denotes the concentration of surface receptors inside the j th spine, U_j is the mean dendritic receptor concentration on the boundary between the spine neck and dendrite, and S_j is the number of receptors within the corresponding intracellular pool. Freely diffusing surface receptors can enter/exit the spine at a hopping rate ω_j , be endocytosed at a rate k_j , exocytosed at a rate σ_j^{rec} and degraded at a rate σ_j^{deg} . New intracellular receptors are produced at a rate δ_j .

$\mathbf{r}_j = (x_j, y_j) \in \Omega_0$, where $j = 1, \dots, M$ labels the j th spine. For simplicity, we take all spines to have the same radius. Since a dendrite is usually several hundred μm in length, we will assume the separation of length-scales $\varepsilon\rho \ll l \ll L$ and treat ε as a small parameter. We denote the surface of the cylinder excluding the small discs arising from the spines by Ω_ε , where

$$\Omega_\varepsilon = \Omega_0 \setminus \bigcup_{j=1}^M \Omega_j, \quad \Omega_j = \{\mathbf{r} : |\mathbf{r} - \mathbf{r}_j| \leq \varepsilon\rho\}.$$

Let $U(\mathbf{r}, t)$ denote the concentration of surface receptors within the dendritic membrane at position $\mathbf{r} \in \Omega_\varepsilon$ at time $t \in [0, \infty)$, and as before let $R_j(t)$ denote the concentration of surface receptors in the j th spine. For the moment we make no distinction between different classes of receptors, although the equations that follow are based on those given in Chapter 3 for the trafficking of GluR2/3 heteromers. We exclude the trafficking of GluR1/2 heteromers since they constitute a negligible portion of the total AMPA receptor population during basal trafficking. The dendritic surface receptor concentration evolves according to the diffusion equation

$$\frac{\partial U}{\partial t} = D\nabla^2 U, \quad (\mathbf{r}, t) \in \Omega_\varepsilon \times [0, \infty) \quad (4.1)$$

for a homogeneous surface diffusivity D , with periodic boundary conditions at the ends $y = \pm\pi l$,

$$U(x, \pi l, t) = U(x, -\pi l, t), \quad \partial_y U(x, \pi l, t) = \partial_y U(x, -\pi l, t), \quad (4.2)$$

and non-zero or zero flux conditions at the ends $x = 0, L$,

$$\partial_x U(0, y, t) = -\frac{\sigma_0}{2\pi l D}, \quad \partial_x U(L, y, t) = 0. \quad (4.3)$$

Here σ_0 denotes the number of receptors per unit time entering the surface of the cylinder from the soma. At each interior boundary $\partial\Omega_j$ we impose the mixed boundary condition

$$\varepsilon \partial_n U(\mathbf{r}, t) = -\frac{\omega_j}{2D\pi\rho} (U(\mathbf{r}, t) - R_j), \quad \mathbf{r} \in \partial\Omega_j, \quad j = 1, \dots, M. \quad (4.4)$$

where $\partial_n U$ is the outward normal derivative to Ω_ε . The flux of receptors across the boundary between the dendrite and j th spine is taken to depend on the difference in concentrations on either side of the boundary with ω_j a hopping rate (the same as in Chapter 3). It follows that the total number of receptors crossing the boundary per unit

time is $\omega_j[U_j(t) - R_j(t)]$, where $U_j(t)$ is the mean dendritic receptor concentration on the boundary $\partial\Omega_j$ of length $2\pi\epsilon\rho$:

$$U_j = \frac{1}{2\pi\epsilon\rho} \int_{\partial\Omega_j} U(\mathbf{r}, t) d\mathbf{r}. \quad (4.5)$$

For simplicity, in this chapter we treat each spine as a single homogeneous compartment instead of two, eliminating the compartment corresponding to the PSD. This simplifies our calculations while retaining the important aspects of trafficking at spines. In Chapter 5 we will again include the PSD in our single-spine model. Also, recall that in the single-spine model of Chapter 3 we took a time-independent rate of local exocytosis under basal conditions, assuming that there exists a local intracellular pool of receptors whose state is maintained either by some form of local receptor synthesis or by the targeted delivery of intracellular receptors transported from the soma along microtubules. The necessary secretory machinery for AMPA receptor synthesis has been found in some dendrites [103], and there is growing evidence that synaptic plasticity-inducing stimuli can promote the local synthesis of proteins [55, 50, 129]. However, it is not yet known whether there exists an activity-independent component to local protein synthesis that contributes to receptor trafficking under basal conditions. If AMPA receptors are primarily synthesized at the soma, then they can be transported to dendritic sites either by lateral diffusion in the plasma membrane [2] or intracellularly via motor-driven transport along microtubules [71, 116]. In the latter case this provides a local source of intracellular receptors for delivery to the surface via exocytosis, which supplements the constitutive recycling of receptors via local endosomes [31]. At the simplest level, constitutive recycling at a spine can be modeled in terms of the concentration R_j of receptors on the membrane of the j th spine and the number S_j of receptors in the associated intracellular pool [63]:

$$\frac{dR_j}{dt} = \frac{\omega_j}{A_j}[U_j - R_j] - \frac{k_j}{A_j}R_j + \frac{\sigma_j^{rec}S_j}{A_j}, \quad (4.6)$$

$$\frac{dS_j}{dt} = -\sigma_j^{rec}S_j - \sigma_j^{deg}S_j + k_jR_j + \delta_j. \quad (4.7)$$

where σ_j^{rec} is the rate of recycling, σ_j^{deg} is the rate of degradation and k_j the rate of endocytosis from the ESM of j th spine. The final term δ_j on the right-hand side of Equation (5.6) represents the local rate of accumulation of new (rather than recycled) receptors within the intracellular pool of the j th spine, supplied, for example, by the targeted delivery of intracellular receptors from the soma (or possibly by local receptor synthesis). Identifying σ_j as the net rate of exocytosis, we have $\sigma_j = \sigma_j^{rec}S_j$. Note that

Equation (4.6) for R_j is of the same form as Equations (3.5) and (3.6). Equation (4.7) for S_j is, however, different from Equation (3.7) as it now includes exo- and endocytic terms that balance those of Equation (4.6), a degradation term σ_j^{deg} and a production term δ_j . The various processes described by Equations (4.6) and (4.7) are summarized in Fig. 4.1C.

4.2 Steady-state analysis using asymptotic matching

In steady-state one can solve Equations (4.6) and (4.7) for R_j in terms of the mean concentration U_j :

$$R_j = \frac{\omega_j U_j + \lambda_j \delta_j}{\omega_j + k_j(1 - \lambda_j)}, \quad (4.8)$$

with

$$\lambda_j = \frac{\sigma_j^{rec}}{\sigma_j^{rec} + \sigma_j^{deg}}, \quad S_j = \frac{k_j \lambda_j R_j}{\sigma_j^{rec}}. \quad (4.9)$$

U_j is then determined from Equation (4.5) and the steady-state version of Equation (4.1):

$$\nabla^2 U = 0, \quad \mathbf{r} \in \Omega_\varepsilon \quad (4.10)$$

with boundary conditions

$$U(x, \pi l) = U(x, -\pi l), \quad \partial_y U(x, \pi l) = \partial_y U(x, -\pi l), \quad (4.11)$$

$$\partial_x U(0, y) = -\kappa, \quad \partial_x U(L, y) = 0, \quad (4.12)$$

where $\kappa = \sigma_0/(2\pi l D)$ and

$$\varepsilon \partial_n U(\mathbf{r}) = -\frac{\omega_j}{2\pi \rho D} (U(\mathbf{r}) - R_j), \quad \mathbf{r} \in \partial\Omega_j, \quad j = 1, \dots, M. \quad (4.13)$$

We now make the simplification that $U(\mathbf{r}) = U_j$ on $\partial\Omega_j$. Substitution of Equation (4.8) into Equation (4.13) then yields the reduced boundary condition

$$\varepsilon \partial_n U(\mathbf{r}) = -\frac{\hat{\omega}_j}{2\pi \rho D} (U_j - \hat{R}_j), \quad \mathbf{r} \in \partial\Omega_j, \quad j = 1, \dots, M. \quad (4.14)$$

where

$$\hat{\omega}_j = \frac{\omega_j k_j (1 - \lambda_j)}{\omega_j + k_j (1 - \lambda_j)}, \quad \hat{R}_j = \frac{\sigma_j^{rec}}{k} \frac{\delta_j}{\sigma_j^{deg}}. \quad (4.15)$$

One can view $\hat{\omega}_j$ as an effective hopping rate and \hat{R}_j as an effective receptor concentration within the spine.

Integrating the diffusion Equation (4.10) over the domain Ω_ε and imposing the boundary conditions (4.11), (4.12) and (4.14) leads to the solvability condition

$$\sigma_0 = \sum_{j=1}^M \hat{\omega}_j [U_j - \hat{R}_j] \quad (4.16)$$

This expresses the condition that the rate at which receptors enter the dendrite from the soma is equal to the effective rate at which receptors exit the dendrite into spines and are degraded. Note that if there were no degradation of receptors in the intracellular pools ($\sigma_j^{deg} = 0$), then $\lambda_j = 1$ and $\hat{\omega}_j = 0$ for all $j = 1, \dots, M$, see Equations (4.9) and (4.15). Hence, it would not be possible to satisfy Equation (4.16) for $\sigma_0 > 0$; the number of receptors in the dendrite would grow without bounds. Blow-up of the solution would also occur in the limit $\varepsilon \rightarrow 0$, since the spine neck resistance becomes infinite ($\omega_j \rightarrow 0$) as the radius of the neck shrinks to zero. Newly synthesized receptors at the soma would then not be able to flow from the dendrite to a spine and be degraded.

Our method of solution for the boundary-value problem given by Equations (4.10), (4.11), (4.12) and (4.14), which we denote by BVPI, proceeds in two steps. First, we solve a related problem BVPII, in which the mixed boundary conditions (4.14) are replaced by the inhomogeneous Dirichlet conditions

$$U(\mathbf{r}) = U_j, \quad \mathbf{r} \in \partial\Omega_j, \quad j = 1, \dots, M \quad (4.17)$$

under the assumption that the U_j are known. The resulting solution will be determined up to an arbitrary constant χ due to the fact that we have imposed Neumann boundary conditions at the ends $x = 0, L$. Second, we substitute our solution to BVPII into the M mixed boundary conditions (4.14) which together with the conservation equation (4.16) yield $M + 1$ equations in the $M + 1$ unknowns χ and $U_j, j = 1, \dots, M$. This closed system of equations can be solved to generate the full solution to the original boundary value problem BVPI. In order to solve BVPII, we match appropriate ‘inner’ and ‘outer’ asymptotic expansions, following along similar lines to previous studies of boundary-value problems in domains with small holes [145, 144, 128].

4.2.1 Matching inner and outer solutions

Around each small circle $\partial\Omega_j$ we expect the solution of BVPII to develop a boundary layer where it changes rapidly from its value U_j at $\partial\Omega_j$ in order to match the solution in the bulk of the domain. Therefore, Ω_ε may be decomposed into a set of $j = 1, \dots, M$

‘inner’ regions where $|\mathbf{r} - \mathbf{r}_j| = \mathcal{O}(\varepsilon)$, and an ‘outer’ region where $|\mathbf{r} - \mathbf{r}_j| \gg \mathcal{O}(\varepsilon)$ for all $j = 1, \dots, M$. In the j th inner region, we introduce the stretched local variable $\mathbf{s} = \varepsilon^{-1}(\mathbf{r} - \mathbf{r}_j)$ and set $V(\mathbf{s}; \varepsilon) = U(\mathbf{r}_j + \varepsilon\mathbf{s}; \varepsilon)$ so that to leading order (neglecting far-field boundary conditions)

$$\begin{aligned}\nabla_{\mathbf{s}}^2 V &= 0, & |\mathbf{s}| > \rho \\ V &= U_j, & |\mathbf{s}| = \rho.\end{aligned}\tag{4.18}$$

This has an exact solution of the form $V = U_j + B_j \log(|\mathbf{s}|/\rho)$ with the unknown amplitude B_j determined by matching inner and outer solutions. This leads to an infinite logarithmic expansion of B_j in terms of the small parameter [145, 144, 128]

$$\nu = -\frac{1}{\log(\varepsilon\rho)}.\tag{4.19}$$

Thus we write $B_j = \nu A_j(\nu)$, where the function $A_j(\nu)$ is to be found, and the inner solution becomes

$$V = U_j + \nu A_j(\nu)[\log(|\mathbf{s}|) - \log(\rho)]\tag{4.20}$$

In terms of the outer variable $|\mathbf{r} - \mathbf{r}_j|$, we obtain the following far-field behavior of the inner solution:

$$V \sim U_j + A_j(\nu) + \nu A_j(\nu) \log(|\mathbf{r} - \mathbf{r}_j|).\tag{4.21}$$

This far-field behavior must then match the near-field behavior of the asymptotic expansion of the solution in the outer region away from the M holes. The corresponding outer problem is given by

$$\nabla^2 U = 0, \quad \mathbf{r} \in \Omega_0\tag{4.22}$$

with boundary conditions

$$\begin{aligned}U(x, \pi l) &= U(x, -\pi l), & \partial_y U(x, \pi l) &= \partial_y U(x, -\pi l) \\ \partial_x U(0, y) &= -\kappa, & \partial_x U(L, y) &= 0\end{aligned}$$

and asymptotic conditions

$$U \sim U_j + A_j(\nu) + \nu A_j(\nu) \log |\mathbf{r} - \mathbf{r}_j| \quad \text{as } \mathbf{r} \rightarrow \mathbf{r}_j\tag{4.23}$$

Equations (4.22) and (4.23) can be reformulated in terms of an outer problem with homogeneous boundary conditions and a constant forcing term by taking

$$U(\mathbf{r}) = \mathcal{U}(\mathbf{r}) + u(\mathbf{r}), \quad u(x, y) \equiv \frac{\kappa}{2L}(x - L)^2.\tag{4.24}$$

We then obtain

$$\nabla^2 \mathcal{U} = -\frac{\kappa}{L}, \quad \mathbf{r} \in \Omega_\varepsilon \quad (4.25)$$

with boundary conditions

$$\begin{aligned} \mathcal{U}(x, \pi l) &= \mathcal{U}(x, -\pi l), & \partial_y \mathcal{U}(x, \pi l) &= \partial_y \mathcal{U}(x, -\pi l) \\ \partial_x \mathcal{U}(0, y) &= 0, & \partial_x \mathcal{U}(L, y) &= 0 \end{aligned}$$

and asymptotic conditions

$$\mathcal{U} \sim -u(\mathbf{r}_j) + U_j + A_j(\nu) + \nu A_j(\nu) \log |\mathbf{r} - \mathbf{r}_j| \quad \text{as } \mathbf{r} \rightarrow \mathbf{r}_j. \quad (4.26)$$

In order to handle the logarithmic behavior of the outer solution around the points \mathbf{r}_j , we introduce the Neumann Green's function $G(\mathbf{r}; \mathbf{r}')$, defined according to

$$\begin{aligned} \nabla^2 G &= \frac{1}{|\Omega_0|} - \delta(\mathbf{r} - \mathbf{r}'), & (4.27) \\ G(x, \pi l; \mathbf{r}') &= G(x, -\pi l; \mathbf{r}'), & \partial_y G(x, \pi l; \mathbf{r}') &= \partial_y G(x, -\pi l; \mathbf{r}') \\ \partial_x G(0, y; \mathbf{r}') &= 0, & \partial_x G(L, y; \mathbf{r}') &= 0, \\ \int_{\Omega_0} G(\mathbf{r}; \mathbf{r}') d\mathbf{r} &= 0. \end{aligned}$$

Here $|\Omega_0| = 2\pi lL$ is the area of the rectangular domain Ω_0 . It is well known that the Green's function has a logarithmic singularity as $\mathbf{r} \rightarrow \mathbf{r}'$ so that we can decompose G as

$$G(\mathbf{r}; \mathbf{r}') = -\frac{1}{2\pi} \log |\mathbf{r} - \mathbf{r}'| + \mathcal{G}(\mathbf{r}; \mathbf{r}'), \quad (4.28)$$

where \mathcal{G} is the regular part of G (see Section 4.2.3). The properties of the Neumann Green's function suggest that we replace Equations (4.25) and (4.26) by the single equation

$$\nabla^2 \mathcal{U} = -\frac{\kappa}{L} + \sum_{j=1}^M 2\pi\nu A_j(\nu) \delta(\mathbf{r} - \mathbf{r}_j) \quad (4.29)$$

Integrating this equation over the domain Ω_0 using homogeneous boundary conditions then yields the solvability condition

$$\frac{\sigma_0}{D} = \sum_{j=1}^M 2\pi\nu A_j(\nu) \quad (4.30)$$

It follows that Equation (4.29) has the solution

$$\mathcal{U}(\mathbf{r}) = -\sum_{j=1}^M 2\pi\nu A_j(\nu) G(\mathbf{r}; \mathbf{r}_j) + \chi, \quad (4.31)$$

where χ is a constant to be found, as can be checked by applying the Laplacian to both sides and imposing the solvability condition (4.30). The outer solution for \mathcal{U} has the near-field behavior

$$\mathcal{U} \sim -2\pi\nu A_j(\nu) \left[-\frac{1}{2\pi} \log |\mathbf{r} - \mathbf{r}_j| + \mathcal{G}(\mathbf{r}_j; \mathbf{r}_j) \right] - \sum_{i \neq j} 2\pi\nu A_i(\nu) G(\mathbf{r}_j; \mathbf{r}_i) + \chi \quad (4.32)$$

as $\mathbf{r} \rightarrow \mathbf{r}_j$. Comparison with Equation (4.26) yields the following system of equations:

$$(1 + 2\pi\nu \mathcal{G}_{jj}) A_j + \sum_{i \neq j} 2\pi\nu G_{ji} A_i = u_j - U_j + \chi \quad (4.33)$$

where $u_j = u(\mathbf{r}_j)$, $G_{ji} = G(\mathbf{r}_j; \mathbf{r}_i)$ and $\mathcal{G}_{jj} = \mathcal{G}(\mathbf{r}_j; \mathbf{r}_j)$.

4.2.2 Calculation of boundary concentrations U_j

Equations (4.20) and (4.31) are the inner and outer solutions of BVPII, with the $M + 1$ coefficients χ and A_j , $j = 1, \dots, M$, determined from the M linear equations (4.33) together with the solvability condition (4.30). We can now generate the solution to the original BVPI by substituting the inner solution (4.20) into the mixed boundary conditions (4.14). This gives

$$2\pi\nu A_j(\nu) = \frac{\hat{\omega}_j}{D} [U_j - \hat{R}_j] \equiv V_j \quad (4.34)$$

Substituting Equation (4.34) into the solvability condition (4.30) shows that the latter is equivalent to the conservation equation (4.16). Furthermore, substituting Equation (4.34) into Equation (4.33) gives the system of linear equations

$$((2\pi\nu)^{-1} + \mathcal{G}_{jj}) \frac{\hat{\omega}_j}{D} [U_j - \hat{R}_j] + \sum_{i \neq j} G_{ji} \frac{\hat{\omega}_i}{D} [U_i - \hat{R}_i] = u_j - U_j + \chi \quad (4.35)$$

This, together, with the conservation Equation (4.16) gives $M + 1$ equations for the $M + 1$ unknowns χ and U_j , $j = 1, \dots, M$. Having solved these equations for U_j and χ , the dendritic receptor concentration in the bulk of the dendritic membrane is given by

$$U(\mathbf{r}) = u(\mathbf{r}) - \sum_{j=1}^M \frac{\hat{\omega}_j}{D} [U_j - \hat{R}_j] G(\mathbf{r}; \mathbf{r}_j) + \chi \quad (4.36)$$

and the distribution of receptors within the spines is given by Equation (4.8). Note that we will derive a one-dimensional version of Equations (4.16), (4.35) and (4.36) in Section 4.5. In contrast to the two-dimensional case, the one-dimensional Neumann Green's

function is non-singular so that one can represent the spines as point sources/sinks on the dendrite, and singular perturbation theory is not needed.

We can obtain a matrix solution to Equation (4.35). Introducing the matrix \mathbf{B} with elements

$$B_{jj} = 2\pi \left(\frac{D}{\hat{\omega}_j} + \mathcal{G}_{jj} \right), \quad B_{ji} = 2\pi G_{ji}, \quad j \neq i, \quad (4.37)$$

Equation (4.35) can be written in the compact form

$$\sum_{i=1}^M (\delta_{i,j} + \nu B_{ji}) V_i = 2\pi\nu [u_j - \hat{R}_j + \chi]$$

with V_i defined in Equation (4.34). Setting $\mathbf{M} = (\mathbf{I} + \nu\mathbf{B})^{-1}$, where \mathbf{I} is the $M \times M$ identity matrix, we have

$$V_j = 2\pi\nu \sum_{i=1}^M M_{ji} (u_i - \hat{R}_i + \chi). \quad (4.38)$$

The constant χ is then determined by substituting Equation (4.38) into the solvability condition (4.30):

$$\frac{\sigma_0}{D} = \sum_{j=1}^M V_j = 2\pi\nu \sum_{i,j=1}^M M_{ji} (u_i - \hat{R}_i + \chi),$$

which gives

$$\chi = \frac{\frac{\sigma_0}{2\pi\nu D} - \sum_{i,j=1}^M M_{ji} (u_i - \hat{R}_i)}{\sum_{i,j=1}^M M_{ji}} \quad (4.39)$$

Since $M_{ji} = \delta_{i,j} + \mathcal{O}(\nu)$, it follows that to lowest order in ν

$$\chi = \frac{\sigma_0}{2\pi M D \nu} + \mathcal{O}(1), \quad U_j = \hat{R}_j + \frac{\sigma_0}{M \hat{\omega}_j} + \mathcal{O}(\nu). \quad (4.40)$$

The singular nature of the constant χ , and hence of the solution $U(\mathbf{r})$, reflects the fact that for fixed somatic flux σ_0 , the flux in the neighborhood of each spine boundary $\partial\Omega_j$ diverges as $\varepsilon \rightarrow 0$. This is necessary in order to maintain the solvability condition (4.16). Note, in particular, that $\hat{\omega}_j [U_j - \hat{R}_j]$ gives the number of receptors flowing across the boundary per unit time, and its size essentially remains fixed as ε decreases. Thus the flux through the boundary increases resulting in a steeper concentration gradient in a neighborhood of the boundary. If the hopping rate $\hat{\omega}_j$ decreases as ε decreases, then the boundary concentration U_j will also diverge in order to maintain Equation (4.16).

4.2.3 Evaluation of Green's function

To evaluate the Green's function G satisfying Equation (4.27), we begin with its Fourier series representation,

$$G(\mathbf{r}; \mathbf{r}') = \frac{2}{|\Omega_0|} \sum_{n=1}^{\infty} \frac{\cos\left(\frac{\pi n x}{L}\right) \cos\left(\frac{\pi n x'}{L}\right)}{\left(\frac{\pi n}{L}\right)^2} + \frac{2}{|\Omega_0|} \sum_{m=1}^{\infty} \frac{\cos\left(\frac{m(y-y')}{l}\right)}{\left(\frac{m}{l}\right)^2} + \frac{4}{|\Omega_0|} \sum_{m=1}^{\infty} \sum_{n=1}^{\infty} \frac{\cos\left(\frac{\pi n x}{L}\right) \cos\left(\frac{\pi n x'}{L}\right) \cos\left(\frac{m(y-y')}{l}\right)}{\left(\frac{\pi n}{L}\right)^2 + \left(\frac{m}{l}\right)^2}. \quad (4.41)$$

Recalling the formula

$$\sum_{k=1}^{\infty} \frac{\cos(k\theta)}{k^2 + b^2} = \frac{\pi}{2b} \frac{\cosh(b(\pi - |\theta|))}{\sinh(\pi b)} - \frac{1}{2b^2}, \quad |\theta| \leq 2\pi, \quad (4.42)$$

we can sum the third term of Equation (4.41) over the index n , yielding

$$\frac{1}{2\pi} \sum_{m=1}^{\infty} \frac{\cos\left(\frac{m(y-y')}{l}\right) \left[\cosh\left(\frac{m(L-|x-x'|)}{l}\right) + \cosh\left(\frac{m(L-|x+x'|)}{l}\right) \right]}{m \sinh\left(\frac{Lm}{l}\right)} - \frac{2}{|\Omega_0|} \sum_{m=1}^{\infty} \frac{\cos\left(\frac{m(y-y')}{l}\right)}{\left(\frac{m}{l}\right)^2}. \quad (4.43)$$

Notice that the second sum of Equation (4.43) cancels the second sum of Equation (4.41). Using the angle addition formula for hyperbolic cosine, $\cosh(x) - \sinh(x) = e^{-x}$, and the identity

$$\coth\left(\frac{Lm}{l}\right) = \frac{1 + q^m}{1 - q^m}, \quad q = e^{-2L/l}, \quad (4.44)$$

we find

$$\frac{\cosh\left(\frac{m(L-|x-x'|)}{l}\right) + \cosh\left(\frac{m(L-|x+x'|)}{l}\right)}{\sinh\left(\frac{Lm}{l}\right)} = (1 - q^m)^{-1} \left[e^{-m|x-x'|/l} + e^{-m|x+x'|/l} + e^{(m|x-x'|-2L)/l} + e^{(m|x+x'|-2L)/l} \right]. \quad (4.45)$$

Therefore,

$$G(\mathbf{r}; \mathbf{r}') = \frac{H(x; x')}{2\pi l} + \sum_{m=1}^{\infty} \frac{z_+^m + \bar{z}_+^m + z_-^m + \bar{z}_-^m + \zeta_+^m + \bar{\zeta}_+^m + \zeta_-^m + \bar{\zeta}_-^m}{4\pi m(1 - q^m)} \quad (4.46)$$

where

$$H(x; x') = \frac{2}{L} \sum_{n=1}^{\infty} \frac{\cos\left(\frac{\pi n x}{L}\right) \cos\left(\frac{\pi n x'}{L}\right)}{\left(\frac{\pi n}{L}\right)^2} = \frac{L}{12} \left[h\left(\frac{x-x'}{L}\right) + h\left(\frac{x+x'}{L}\right) \right], \quad h(\theta) = 3\theta^2 - 6|\theta| + 2, \quad (4.47)$$

is the one-dimensional Green's function in the x -direction, and $z_{\pm} = e^{r_{\pm}/l}$, $\zeta_{\pm} = e^{\rho_{\pm}/l}$ with

$$r_+ = -|x + x'| + i(y - y'), \quad r_- = -|x - x'| + i(y - y') \quad (4.48)$$

and

$$\rho_+ = |x + x'| - 2L + i(y - y'), \quad \rho_- = |x - x'| - 2L + i(y - y') \quad (4.49)$$

and $\bar{\cdot}$ denotes complex conjugate. Since $q < 1$ we can write $(1 - q^m)^{-1} = \sum_{n=0}^{\infty} (q^m)^n$ for all $m \geq 1$, hence the sum in Equation (4.46) can be written

$$\sum_{m=1}^{\infty} \sum_{n=0}^{\infty} (q^n)^m \frac{z_+^m + \bar{z}_+^m + z_-^m + \bar{z}_-^m + \zeta_+^m + \bar{\zeta}_+^m + \zeta_-^m + \bar{\zeta}_-^m}{4\pi m}. \quad (4.50)$$

Notice that when $z_{\pm} \neq 1$ and $\zeta_{\pm} \neq 1$ (i.e., when $r_{\pm} \neq 0$ and $\rho_{\pm} \neq 0$) this double sum is absolutely convergent, so we can interchange the order of summation in Equation (4.50) and then perform the sum over the index m , yielding

$$\begin{aligned} -\frac{1}{4\pi} \sum_{n=0}^{\infty} (\ln |1 - q^n z_+|^2 + \ln |1 - q^n z_-|^2 + \ln |1 - q^n \zeta_+|^2 + \ln |1 - q^n \zeta_-|^2) \\ = -\frac{1}{2\pi} \ln |1 - z_+| |1 - z_-| |1 - \zeta_+| |1 - \zeta_-| + \mathcal{O}(q). \end{aligned} \quad (4.51)$$

The only singularity exhibited by Equation 4.51 in Ω_0 is at $(x, y) = (x', y')$, in which case $z_- = 1$ and $\ln |1 - z_-|$ diverges. Writing $\ln |1 - z_-| = \ln |r_-| + \ln(|1 - z_-|/|r_-|)$ and noting that $\ln |r_-| = \ln |\mathbf{r} - \mathbf{r}'|$ and $\ln(|1 - z_-|/|r_-|)$ is regular, we find

$$G(\mathbf{r}; \mathbf{r}') = -\frac{1}{2\pi} \ln |\mathbf{r} - \mathbf{r}'| + \mathcal{G}(\mathbf{r}; \mathbf{r}'), \quad (4.52)$$

where the regular part of G is

$$\mathcal{G}(\mathbf{r}; \mathbf{r}') = \frac{H(x; x')}{2\pi l} - \frac{1}{2\pi} \ln \frac{|1 - z_+| |1 - z_-| |1 - \zeta_+| |1 - \zeta_-|}{|r_-|} + \mathcal{O}(q). \quad (4.53)$$

4.3 Comparison of singular perturbation solution with numerical and one-dimensional solutions

In this section we present the steady-state solutions U , U_j , R_j and S_j given in Equations (4.8), (4.9), (4.36) and (4.38). We also compare these with numerical solutions of Equations (4.10)-(4.13) and solutions of the one-dimensional model to be presented in Section 4.5. For the two-dimensional numerical solutions we use the *Partial Differential Equation Toolbox* of Matlab [83]. Because the values of U_j are not known *a priori* and there is no solution method offered by the *Partial Differential Equation Toolbox*

to self-consistently determine them, we use the values of R_j determined by Equations (4.38) and (4.8) when implementing the boundary conditions (4.13). In Figure 4.2A we plot the steady-state concentration U for a cable of length $L = 100\mu m$ and radius $l = (2\pi)^{-1}\mu m$ having 99 identical spines spaced $1\mu m$ apart along a single horizontal of the cable ($y = 0.5\mu m$), and in Figure 4.2B we plot the corresponding values of U_j , R_j and S_j . Here the diffusivity is $D = 0.1\mu m^2 s^{-1}$ [39, 3], the somatic flux is $\sigma_0 = 0.1\mu m^{-1} s^{-1}$, and that all spines are identical with $\epsilon\rho = 0.1\mu m$, $A = 1\mu m$, $\omega = 10^{-3}\mu m^2 s^{-1}$, $k = 10^{-3}\mu m^2 s^{-1}$, $\sigma^{rec} = 10^{-3} s^{-1}$, $s^{deg} = 10^{-4} s^{-1}$, $\delta = 10^{-3} s^{-1}$. While U decays significantly along the length of the cable, it varies very little around the circumference of the cable due to the large aspect ratio of the cable. In Figure 4.2C we show the results of numerically solving the original steady-state system for U described in Equations (4.10)-(4.13). Note that this numerical solution agrees almost perfectly with the perturbation solution. Figure 4.2D plots the concentrations U_j , R_j and S_j from the one-dimensional model. The agreement is exact, illustrating the pseudo-one-dimensional nature of our large aspect ratio system.

We consider the parameter regime of Figure 4.2 physiological in the sense that parameter values were chosen from experimental data [3, 31, 39, 126, 120] in conjunction with previous modeling studies [11, 12]. In Figure 4.3 we consider the effect of the size of ϵ on the solution, so for purposes of illustration we set $L = 2\mu m$, $\omega = k = 1\mu m^2 s^{-1}$ and include only one spine centered at $(x, y) = (1, 0.5)$. In Figures 4.3A-C we show the solution of U when $\epsilon\rho = 0.1, 0.01$ and $0.4\mu m$, respectively. In each case the average value of U on the boundary of the spine neck is $U_1 = 1210\mu m^{-2}$. This is because the $\mathcal{O}(\nu)$ term of U_j in Equation 4.40 is equal to zero in the case of one spine, making U_1 independent of ϵ . On the other hand, from the same equation we see that χ varies as $-\ln(\epsilon\rho)$, hence this background concentration slowly decreases with increasing ϵ , as can be seen in the figures. In Figures 4.3D-F we show corresponding plots for the numerical solutions of U . Notice how the singular perturbation solution approaches the numerical solution as ϵ decreases. In Figure 4.3G we plot the solution from the one-dimensional model. Although this model contains no information about the radius of the spine neck, it agrees well with the two-dimensional solutions.

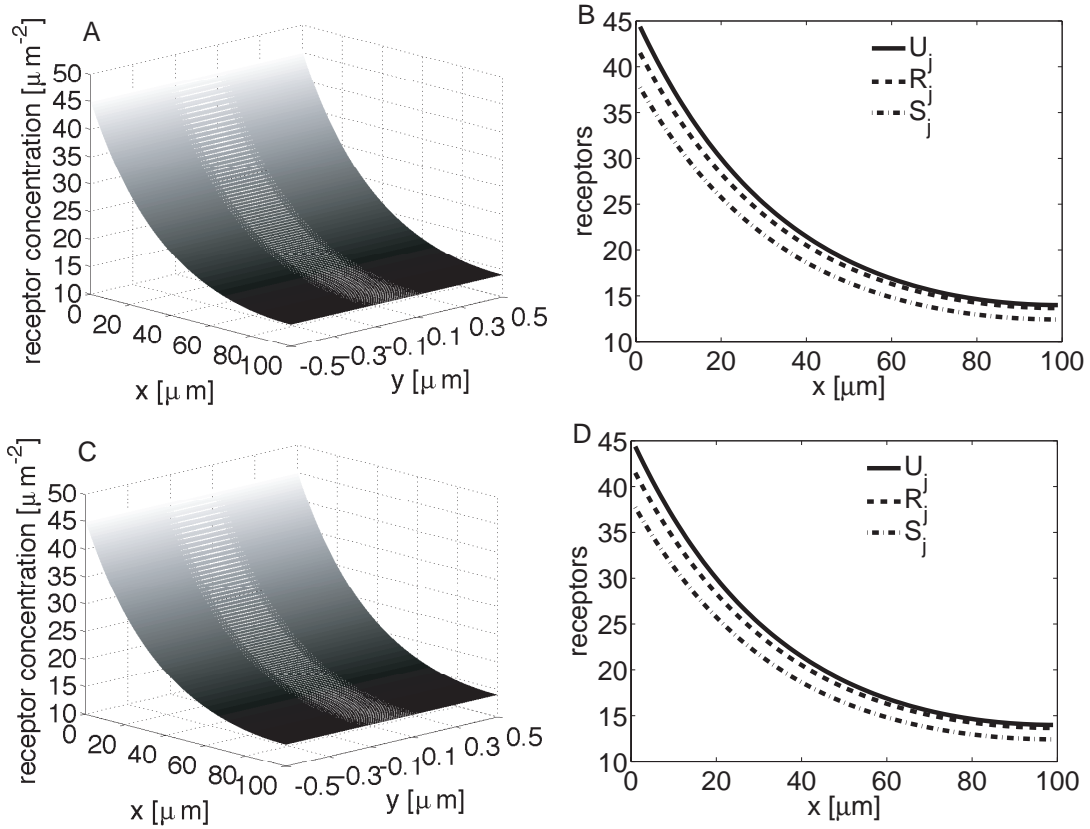


Figure 4.2. Solutions U , U_j , R_j and S_j . Cable and spine parameter values are as given in the text. (A-B) Plot of Equation 4.36 and corresponding plots of U_j , R_j and S_j . (C) Numerical solution of Equations (4.10)-(4.13). (D) Plots of U_j , R_j and S_j from one-dimensional model (see Section 4.5).

4.4 Mean first passage time for a receptor

In this section we calculate the mean first passage time (MFPT) for a single receptor to travel an axial distance X from the soma, $X \leq L$, assuming that the receptor does not undergo degradation. We then use this to determine an effective diffusivity, which takes into account the effects of trapping at spines. We proceed by reinterpreting the dendritic receptor concentration as a probability density and the diffusion equation (4.1) as a Fokker–Planck (FP) equation. The FP equation is defined on a spatial domain Ω_ε^X where

$$\Omega_\varepsilon^X = \Omega_X \setminus \bigcup_{j=1}^{M_X} \Omega_j, \quad \Omega_j = \{\mathbf{r} : |\mathbf{r} - \mathbf{r}_j| \leq \varepsilon\rho\},$$

$\Omega_X = \{(x, y); 0 < x < X, |y| < \pi l\}$ and M_X is the number of spines within the rectangular domain Ω_X . We impose an absorbing boundary condition at $x = X$ so that the receptor

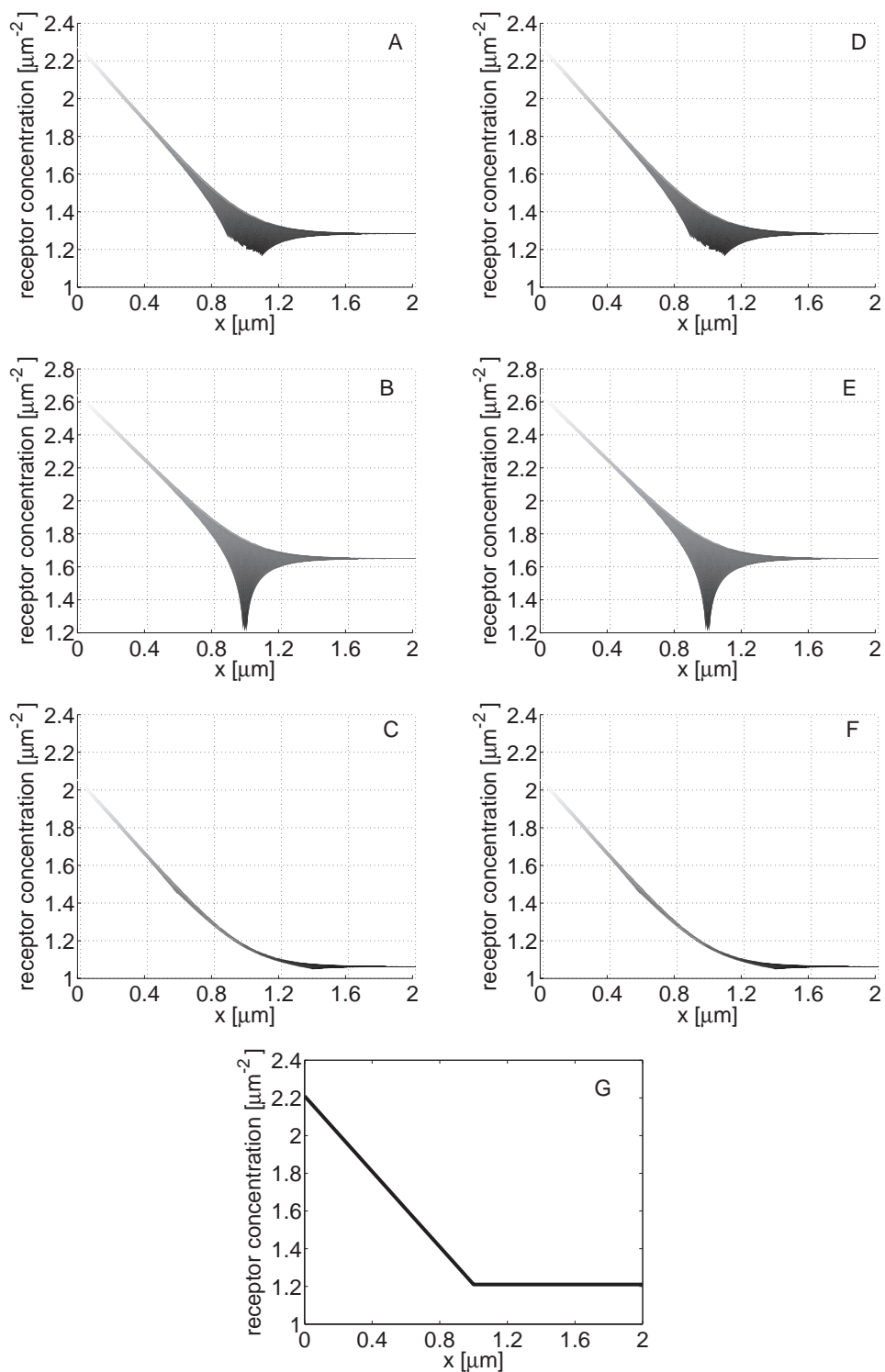


Figure 4.3. Effect of ϵ on the solution U . (A-C) Plots of Equation (4.36) for parameter values as given in the text and $\epsilon\rho = 0.1, 0.01$ and $0.4\mu\text{m}$, respectively. (D-F) Corresponding plots of numerical solutions. (G) Plot of the one-dimensional solution (see Section 4.5).

is immediately removed once it reaches this boundary, i.e., we are only interested in the time it takes for a receptor to first reach $x = X$ from the soma. Let $u(\mathbf{r}, t | \mathbf{r}_0, 0)$ denote the probability density that at time $t \geq 0$ the receptor is located at $\mathbf{r} \in \Omega_\varepsilon^X$, given that it started at the point $\mathbf{r}_0 = (0, y_0)$. The probability density u evolves according to the FP equation

$$\frac{\partial u}{\partial t} = D\nabla^2 u, \quad (\mathbf{r}, t) \in \Omega_\varepsilon^X \times [0, \infty) \quad (4.54)$$

with periodic boundary conditions at the ends $y = \pm\pi l$,

$$u(x, \pi l, t | \mathbf{r}_0, 0) = u(x, -\pi l, t | \mathbf{r}_0, 0), \quad \partial_y u(x, \pi l, t | \mathbf{r}_0, 0) = \partial_y u(x, -\pi l, t | \mathbf{r}_0, 0), \quad (4.55)$$

and

$$\partial_x u(0, y, t | \mathbf{r}_0, 0) = 0, \quad u(X, y, t | \mathbf{r}_0, 0) = 0. \quad (4.56)$$

At each interior boundary $\partial\Omega_j$ we impose the mixed boundary condition

$$\varepsilon \partial_n u(\mathbf{r}, t | \mathbf{r}_0, 0) = -\frac{\omega_j}{2D\pi\rho}(u_j - r_j), \quad \mathbf{r} \in \partial\Omega_j, \quad j = 1, \dots, M_X. \quad (4.57)$$

assuming that $u(\mathbf{r}, t | \mathbf{r}_0, 0) = u_j(t | \mathbf{r}_0, 0) \equiv u(\mathbf{r}_j, t | \mathbf{r}_0, 0)$ for all $\mathbf{r} \in \partial\Omega_j$. Here $A_j r_j(t | \mathbf{r}_0, t)$ denotes the probability that the receptor is located within the j th spine at time t . Defining $s_j(t | \mathbf{r}_0, t)$ to be the corresponding probability that the receptor is located within the j th intracellular pool, we have

$$A_j \frac{dr_j}{dt} = \Omega_j [u_j - r_j] - k_j r_j + \sigma_j^{rec} s_j \quad (4.58)$$

$$\frac{ds_j}{dt} = -\sigma_j^{rec} s_j + k_j r_j \quad (4.59)$$

Since we are assuming that the receptor has not been degraded over the time interval of interest we have set $\sigma_j^{deg} = 0$ for all j . The initial conditions are $u(\mathbf{r}, 0 | \mathbf{r}_0, 0) = \delta(\mathbf{r} - \mathbf{r}_0)$ and $r_j(0 | \mathbf{r}_0, 0) = s_j(0 | \mathbf{r}_0, 0) = 0$ for all j .

Let $\tau(X | \mathbf{r}_0)$ denote the time it takes for a receptor starting at $\mathbf{r}_0 = (0, y_0)$ to first reach the boundary $x = X$. The function

$$F(X, t | \mathbf{r}_0) \equiv \int_{\Omega_\varepsilon^X} u(\mathbf{r}, t | \mathbf{r}_0, 0) d\mathbf{r} + \sum_{j=1}^{M_X} [A_j r_j(t | \mathbf{r}_0, 0) + s_j(t | \mathbf{r}_0, 0)] \quad (4.60)$$

is the probability that $t < \tau(X | \mathbf{r}_0)$; i.e., the probability that a receptor which was initially at the origin has not yet reached $x = X$ in a time t . Notice that $1 - F$ is the cumulative density function for τ , hence

$$\frac{\partial(1 - F)}{\partial t} = -\frac{\partial F}{\partial t} \quad (4.61)$$

is its probability density function. Thus the MFPT T is:

$$T = - \int_0^\infty t \frac{\partial F}{\partial t} dt = \int_0^\infty F dt. \quad (4.62)$$

The last equality in (4.62) follows by integrating the first integral by parts and recalling that F , being an L^1 function in time, decays more rapidly to zero than t^{-1} as t becomes large. Therefore, integrating Equation (4.60) over time gives us the following expression for $T(X|\mathbf{r}_0)$:

$$T(X|\mathbf{r}_0) = \lim_{z \rightarrow 0} \left(\int_{\Omega_\varepsilon^X} \hat{u}(\mathbf{r}, z|\mathbf{r}_0, 0) d\mathbf{r} + \sum_{j=1}^{M_X} [A_j \hat{r}_j(z|\mathbf{r}_0, 0) + \hat{s}_j(z|\mathbf{r}_0, 0)] \right) \quad (4.63)$$

where $\hat{\cdot}$ denotes the Laplace transform,

$$\hat{f}(z) \equiv \int_0^\infty e^{-zt} f(t) dt. \quad (4.64)$$

Laplace transforming Equations (4.54)-(4.59) using the initial conditions, and taking the limit $z \rightarrow 0$ shows that

$$\hat{u}_j(0|\mathbf{r}_0, 0) = \hat{r}_j(0|\mathbf{r}_0, 0) = \frac{\sigma_j^{rec}}{k_j} \hat{s}_j(0|\mathbf{r}_0, 0) \quad (4.65)$$

Hence, setting $\hat{u}(\mathbf{r}; \mathbf{r}_0) = \lim_{z \rightarrow 0} \hat{u}(\mathbf{r}, z|\mathbf{r}_0, 0)$, we obtain the boundary value problem

$$D\nabla^2 \hat{u}(\mathbf{r}; \mathbf{r}_0) = -\delta(\mathbf{r} - \mathbf{r}_0), \quad \mathbf{r} \in \Omega_\varepsilon^X \quad (4.66)$$

with

$$\hat{u}(x, \pi l; \mathbf{r}_0) = \hat{u}(x, -\pi l; \mathbf{r}_0), \quad \partial_y \hat{u}(x, \pi l; \mathbf{r}_0) = \partial_y \hat{u}(x, -\pi l; \mathbf{r}_0), \quad (4.67)$$

$$\partial_x \hat{u}(0, y; \mathbf{r}_0) = 0, \quad \hat{u}(X, y; \mathbf{r}_0) = 0. \quad (4.68)$$

and

$$\partial_n \hat{u}(\mathbf{r}; \mathbf{r}_0, 0) = 0, \quad \mathbf{r} \in \partial\Omega_j, \quad j = 1, \dots, M_X. \quad (4.69)$$

The boundary conditions on the circles $\partial\Omega_j$ are nonsingular, so that we can take the limit $\varepsilon \rightarrow 0$. It follows that to lowest order in ε , $\hat{u}(\mathbf{r}|\mathbf{r}_0) = G_X(\mathbf{r}; \mathbf{r}_0)/D$ where G_X is the Green's function on the rectangular domain Ω_X with periodic boundary conditions at

the ends $y = \pm\pi l$, a reflecting boundary at $x = 0$ and an absorbing boundary at $x = X$. Thus,

$$G_X(\mathbf{r}; \mathbf{r}') = \frac{2}{|\Omega_X|} \sum_{m=-\infty}^{\infty} \sum_{n=0}^{\infty} \frac{\cos\left(\frac{\pi(2n+1)x}{2X}\right) \cos\left(\frac{\pi(2n+1)x'}{2X}\right) e^{im(y-y')/l}}{\left(\frac{\pi(2n+1)}{2X}\right)^2 + \left(\frac{m}{l}\right)^2}. \quad (4.70)$$

Equations (4.63) and (4.65) together with the result $\int_{\Omega_X} G_X(\mathbf{r}; \mathbf{r}_0) d\mathbf{r} = X^2/2$ imply that

$$T(X|\mathbf{r}_0) = \frac{X^2}{2D} + \sum_{j=1}^{M_X} \frac{\eta_j}{D} G_X(\mathbf{r}_j; \mathbf{r}_0), \quad (4.71)$$

where

$$\eta_j = A_j + \frac{k_j}{\sigma_j^{rec}}. \quad (4.72)$$

4.4.1 Evaluation of Green's Function

We wish to evaluate the Green's function G_X in Equation 4.70, and begin by expressing the double sum as

$$G_X(\mathbf{r}; \mathbf{r}') = \frac{2}{|\Omega_X|} \sum_{n=0}^{\infty} \frac{\cos\left(\frac{\pi(2n+1)x}{2X}\right) \cos\left(\frac{\pi(2n+1)x'}{2X}\right)}{\left(\frac{\pi(2n+1)}{2X}\right)^2} + \frac{4}{|\Omega_X|} \sum_{m=1}^{\infty} \sum_{n=0}^{\infty} \frac{\cos\left(\frac{\pi(2n+1)x}{2X}\right) \cos\left(\frac{\pi(2n+1)x'}{2X}\right) \cos\left(\frac{m(y-y')}{l}\right)}{\left(\frac{\pi(2n+1)}{2X}\right)^2 + \left(\frac{m}{l}\right)^2}. \quad (4.73)$$

Using the formula

$$\sum_{k=0}^{\infty} \frac{\cos((2k+1)\theta)}{(2k+1)^2 + b^2} = \frac{\pi}{4b} \left[\frac{\cosh(b(\pi - |\theta|))}{\sinh(\pi b)} - \frac{\cosh(b|\theta|)}{\sinh(\pi b)} \right], \quad |\theta| \leq \pi, \quad (4.74)$$

we can perform the sum over the index n in Equation (4.73), yielding

$$\frac{1}{2\pi} \sum_{m=1}^{\infty} \frac{\cos\left(\frac{m(y-y')}{l}\right) \left[\cosh\left(\frac{m(2X-|x-x'|)}{l}\right) + \cosh\left(\frac{m(2X-|x+x'|)}{l}\right) \right]}{m \sinh\left(\frac{2Xm}{l}\right)}. \quad (4.75)$$

Following arguments similar to those used in section 4.2.3,

$$\frac{\cosh\left(\frac{m(2X-|x-x'|)}{l}\right) + \cosh\left(\frac{m(2X-|x+x'|)}{l}\right)}{\sinh\left(\frac{2Xm}{l}\right)} = (1 - q_X^{2m})^{-1} \left[e^{-m|x-x'|/l} + e^{-m|x+x'|/l} + e^{(m|x-x'|-2X)/l} + e^{(m|x+x'|-2X)/l} \right], \quad (4.76)$$

where $q_X = e^{-2X/l}$. Our calculations are greatly simplified if X is not too small (e.g., by assuming that $X \geq l/2$), in which case we find

$$G_X(\mathbf{r}; \mathbf{r}') = \frac{H_X(x; x')}{2\pi l} - \frac{1}{2\pi} \ln |1 - z_+| |1 - z_-| + \mathcal{O}(q_X) \quad (4.77)$$

where

$$\begin{aligned} H_X(x; x') &= \frac{2}{X} \sum_{n=0}^{\infty} \frac{\cos\left(\frac{\pi(2n+1)x}{2X}\right) \cos\left(\frac{\pi(2n+1)x'}{2X}\right)}{\left(\frac{\pi(2n+1)}{2X}\right)^2} \\ &= \frac{X}{2} \left[h_X\left(\frac{x-x'}{X}\right) + h_X\left(\frac{x+x'}{X}\right) \right], \quad h_X(\theta) = 1 - |\theta|, \end{aligned} \quad (4.78)$$

is the one-dimensional Green's function in the x -direction, and z_{\pm} is as defined in Equation 4.48. Since $T(X|\mathbf{r}_0)$ depends only on $G_X(\mathbf{r}_j; \mathbf{r}_0)$ and $\mathbf{r}_j \neq \mathbf{r}_0$ for all $j = 1, \dots, M_X$, it is not necessary to separate the regular and singular parts of G_X . Also note that since $x_0 = 0$,

$$G_X(\mathbf{r}_j; \mathbf{r}_0) = \frac{X - x_j}{2\pi l} - \frac{1}{2\pi} \ln \left| 1 - e^{-x_j/l} e^{i(y_j - y_0)/l} \right|^2 + \mathcal{O}(q_X). \quad (4.79)$$

Again, if x_j is not too small (e.g., $x_j \geq l/2$) then the contribution of the logarithmic term in Equation 4.79 is of order $q_{x_j} = e^{-2x_j/l}$, hence

$$G_X(\mathbf{r}_j; \mathbf{r}_0) = \frac{X - x_j}{2\pi l} + \mathcal{O}(q_{x_j}). \quad (4.80)$$

Note that we have derived a similar expression in a previous study [12]. In fact, because $\mathcal{O}(q_{x_j})$ is exponentially small for x_j sufficiently large (e.g., $x_j \geq l$), this term can be dropped from Equation 4.80, yielding the one-dimensional Green's function calculated in [12]. The fact that these results are effectively one-dimensional is due to the large aspect ratio of our system.

4.4.2 Effective and anomalous diffusion

Following the discussion of the previous paragraph, we will assume that all x_j are sufficiently large so that $G_X(\mathbf{r}_j; \mathbf{r}_0)$ is well-approximated by $(X - x_j)/(2\pi l)$. Since we are dropping any explicit dependence on y and y_0 , we simply denote the MFPT $T(X|\mathbf{r}_0)$ by T . In the case of a large number of identical spines uniformly distributed along the

length of the cable with spacing d (i.e., $M_X = X/d \gg 1$ and $x_j = jd$ for all j) we can compute an effective diffusivity D_{eff} :

$$\begin{aligned} T &= \frac{X^2}{2D} + \frac{\eta}{2\pi l D} \sum_{j=1}^{M_X} (X - jd) = \frac{X^2}{2D} + \frac{\eta}{2\pi l D} \left(M_X X - \frac{(M_X + 1)M_X d}{2} \right) \\ &\approx \frac{X^2}{2D} + \frac{\eta}{2\pi l D} \left(M_X X - \frac{M_X^2 d}{2} \right) = \frac{X^2}{2D} \left(1 + \frac{\eta}{2\pi l d} \right) = \frac{X^2}{2D_{eff}} \end{aligned} \quad (4.81)$$

where

$$D_{eff} = D \left(1 + \frac{\eta}{2\pi l d} \right)^{-1} = D \left(1 + \frac{A + k/\sigma^{rec}}{2\pi l d} \right)^{-1}. \quad (4.82)$$

As one would expect, the presence of traps reduces the effective diffusivity of a receptor. In particular, the diffusivity is reduced by increasing the ratio k/σ^{rec} of the rates of endocytosis and exocytosis, by increasing the surface area A of a spine, or by decreasing the spine spacing d . Interestingly, D_{eff} does not depend on the hopping rate ω . At first sight this might seem counterintuitive, since a smaller ω implies that a receptor finds it more difficult to exit a spine. However, this is compensated by the fact that it is also more difficult for a receptor to enter a spine in the first place. (For a more detailed analysis of entry/exit times of receptors with respect to spines see [45, 46].)

In Equation 4.81 the MFPT T is proportional to X^2 . This relationship is the hallmark of Brownian diffusion, and here it is due to the fact that the spacing between spines is independent of the index j . Now suppose that the spacing varies with j , say $x_j = d(\ln(j) + 1)$. In this case $M_X = e^{X/d-1}$, hence M_X grows exponentially with X [80]. Therefore,

$$\begin{aligned} T &= \frac{X^2}{2D} + \frac{\eta}{2\pi l D} \sum_{j=1}^{M_X} (X - d(\ln(j) + 1)) = \frac{X^2}{2D} + \frac{\eta}{2\pi l D} (M_X X - d(\ln(M_X!) + M_X)) \\ &\approx \frac{X^2}{2D} + \frac{\eta}{2\pi l D} (M_X X - dM_X \ln(M_X)) = \frac{X^2}{2D} + \frac{\eta d}{2\pi l D} e^{X/d-1} = \frac{X^2}{2D_{eff}(X)}, \end{aligned} \quad (4.83)$$

where

$$D_{eff}(X) = D \left(1 + \frac{A + k/\sigma^{rec}}{2\pi l d} \frac{e^{X/d-1}}{\frac{(X/d)^2}{2}} \right)^{-1}. \quad (4.84)$$

The fact that the effective diffusivity is a function of X indicates anomalous diffusion, which is to say that the relationship $T \propto X^2$ does not hold. Moreover, because $e^{X/d-1}$ grows faster than X^2 , the anomalous diffusion is subdiffusion.

4.5 One-dimensional approximation of outer solution

Figures 4.2 and 4.3 demonstrate two important facts about our multi-spine model of AMPA receptor trafficking: 1) the outer solution (4.36) approximates extremely well the numerical solutions of Equations (4.10)-(4.13), and 2) for long cables these solutions are essentially one-dimensional. In this section we present a model of AMPA receptor trafficking across multiple spines that treats the cable as one-dimensional. Steady-state solutions of this model are essentially the outer solution averaged over circumferences of the cable (i.e., average over the y -coordinate).

Our one-dimensional simplification replaces the partial differential equation (4.1) and boundary conditions (4.4) for U by the following single equation,

$$\frac{\partial U}{\partial t} = D \frac{\partial^2 U}{\partial x^2} - \sum_{j=1}^M \frac{\omega_j}{2\pi l} [U_j - R_j] \delta(x - x_j), \quad (4.85)$$

while the the boundary conditions (4.2) and (4.3) for U and the ordinary differential Equations (4.6) for R and (4.7) for S remain in effect.

Equations (4.8)-(4.9) continue to describe the steady-state values of R_j and S_j , while U_j is determined from the steady-state version of Equation (4.85):

$$0 = D \frac{d^2 U}{dx^2} - \sum_{j=1}^M \frac{\hat{\omega}_j}{2\pi l} (U_j - \hat{R}_j) \delta(x - x_j), \quad (4.86)$$

where $\hat{\omega}_j$ and \hat{R}_j are given in Equation (4.15). Note the similarity of this equation with Equation (4.29). Integrating Equation (4.86) over the interval $0 \leq x \leq L$ leads to the self-consistency condition (4.16). Equation (4.86) is solved in terms of the generalized one-dimensional Green's function $H(x, x')$, which satisfies the equation

$$\frac{d^2 H(x, x')}{dx^2} = -\delta(x - x') + L^{-1}, \quad (4.87)$$

with reflecting boundary conditions at the ends $x = 0, L$. A standard calculation shows that H is given as in Equation (4.47). Hence the dendritic surface receptor concentration has an implicit solution of the form

$$U(x) = \frac{\sigma_0}{D} H(x, 0) - \sum_{j=1}^M \frac{\hat{\omega}_j U_j}{2\pi l D} H(x, x_j) + \xi, \quad (4.88)$$

where the constant ξ is determined from the self-consistency condition (4.16). Note that this formula for U is of the same form as the y -coordinate average of the outer solution

(4.36). However, these two solutions are not equal since the outer solution (4.36) contains information about the radius of spine necks while the solution (4.88) does not.

We can now generate a matrix equation for the concentration of dendritic receptors U_i at the i th spine, $i = 1, \dots, M$, by setting $x = x_i$ in Equation (4.88):

$$U_i = \frac{\sigma_0}{D} H_i - \sum_{j=1}^M \frac{\hat{\omega}_j}{2\pi l D} H_{ij} U_j + \xi, \quad (4.89)$$

where $H_i = H(x_i, 0)$ and $H_{ij} = H(x_i, x_j)$. If the matrix \mathbf{C} with elements $C_{ij} = \hat{\omega}_j H_{ij} / (2\pi l D)$ does not have -1 as an eigenvalue (which is the generic case), then the matrix $\mathbf{I} + \mathbf{C}$, where again \mathbf{I} is the $M \times M$ identity matrix, is invertible and we can solve the system (4.89). That is, setting $\mathbf{N} = (\mathbf{I} + \mathbf{C})^{-1}$, we have

$$U_i = \sum_{j=1}^M N_{ij} \left(\frac{\sigma_0}{D} H_j + \xi \right) \quad (4.90)$$

The self-consistency condition (4.16) then determines ξ :

$$\xi = \sigma_0 \left[\frac{1 - \sum_{k,l} \hat{\omega}_k N_{kl} H_l / D}{\sum_{k,l} \hat{\omega}_k N_{kl}} \right], \quad (4.91)$$

Equations (4.90) and (4.91) determine the dendritic receptor concentration U_j at the discrete site x_j of the j th dendritic spine. Substituting this solution into Equation (4.88) then generates the full receptor concentration profile $U(x)$, which is used to produce the one-dimensional plots in Figures 4.2 and 4.3.

CHAPTER 5

ONE-DIMENSIONAL CONTINUUM APPROXIMATION OF THE MULTISPINE MODEL

In Chapter 4 we saw that, according to Equations (4.52), (4.53), (4.44) and the results of Section (4.3), the steady-state solutions of the multispine model are essentially one-dimensional due to the fact that the length of a dendritic cable is much larger than its radius (i.e., $L \gg l$). The appropriate one-dimensional version of the two-dimensional trafficking model was presented in Section 4.5. Following the formulation of the outer problem (see Section 4.2.1, viz. Equation (4.29)), the population of spines was treated as the sum of delta functions in this one-dimensional model (see Equation (4.86)). In this chapter we will use the formulation of the one-dimensional model of Section 4.5 to calculate the distribution of synaptic receptor numbers across spines, and hence determine how lateral diffusion regulates the strength of a synapse. Because the distribution of spines on the surface of a dendrite is typically dense we will in this chapter approximate the sum of delta functions mentioned above as a continuous density. Treating the spine population of a dendrite as a continuum yields an effective “cable equation” for AMPA receptor trafficking, providing among other things an effective length constant for receptor trafficking. With the solutions of the “cable equation” in hand we investigate the efficacy of lateral diffusion in supplying somatic receptors to distal synapses, and the possible role of lateral diffusion in mediating a form of heterosynaptic plasticity. Our modeling and analysis suggest that 1) lateral membrane diffusion alone is an insufficient synaptic delivery mechanism, 2) local changes in the constitutive recycling of AMPA receptors induce nonlocal changes in synaptic strength, and 3) AMPA receptor trafficking is not likely to mediate heterosynaptic forms of LTP/LTD.

5.1 One-dimensional continuum multi-spine model

As in Chapter 4 we consider a population of excitatory synapses and their associated dendritic spines distributed along a single dendritic cable of length L , see Figure 5.1A. There are typically thousands of spines distributed along a single dendrite with a typical spacing between spines of $\leq 1 \mu\text{m}$, which is several orders of magnitude smaller than L [41]. Therefore, we represent the population of spines in terms of a continuous density (number of spines per unit surface area) $\rho(x)$, $0 < x < L$, where x denotes axial distance along the dendrite from the soma. The density satisfies the normalization condition $\int_0^L \rho(x) dx = M/(2\pi l)$, where M is the total number of spines on the dendrite and l is its radius. For simplicity, we assume throughout that the spine density and intrinsic properties of an individual spine depend only on distance from the soma so that the cable can be treated as a one-dimensional system.

As in previous chapters, let $U(x, t)$ denote the concentration of dendritic AMPA receptors at position x along the cable at time t . Similarly, let $R(x, t)$ denote the concentration of AMPA receptors within the ESM, and let $P(x, t), Q(x, t)$ denote, respectively, the concentration of free and bound AMPA receptors in the PSD of the population of spines at (x, t) . The dendritic AMPA receptor concentration evolves according to the equation

$$\frac{\partial U}{\partial t} = D \frac{\partial^2 U}{\partial x^2} - \rho(x)\omega(x)(U - R). \quad (5.1)$$

The first term on the right-hand side of Equation (5.1) represents the Brownian diffusion of AMPA receptors along the surface of the cable. The second term on the right-hand side determines the number of AMPA receptors per unit time that flow into or out of the spines at x , which is taken to be proportional to the difference in concentrations across the junction between each spine and the dendritic cable with $\omega(x)$ the corresponding hopping rate. Note that Equations 5.1 and 4.86 are equal when the spine distribution $\rho(x) = \sum_{j=1}^M \delta(x - x_j)$. Equation 5.1 is supplemented by the following boundary conditions at the ends of the cable:

$$\partial_x U(0, t) = -\frac{\sigma_0}{2\pi l D}, \quad \partial_x U(L, t) = 0 \quad (5.2)$$

Again σ_0 represents the number of AMPA receptors inserted into the dendrite at the boundary $x = 0$ (adjacent to the soma) arising from somatic exocytosis [2], and the distal end of the cable at $x = L$ is taken to be closed.

The receptor concentrations and numbers at each spine satisfy the following equations:

$$\frac{dR}{dt} = \frac{\omega}{A}(U - R) - \frac{k}{A}R - \frac{h}{A}(R - P), \quad (5.3)$$

$$\frac{dP}{dt} = \frac{h}{a}(R - P) - \alpha(Z - Q)P + \beta Q + \frac{\sigma^{rec}}{a}(1 - f)S, \quad (5.4)$$

$$\frac{dQ}{dt} = \alpha(Z - Q)P - \beta Q, \quad (5.5)$$

$$\frac{dS}{dt} = -\sigma^{rec}(1 - f)S - \sigma^{deg}fS + kR + \delta \quad (5.6)$$

where it is assumed that all single-spine parameters may themselves depend on x (not shown for notational convenience). Note that we are again treating a spine as being composed of two compartments. These equations for AMPA receptor trafficking within a spine correspond to those proposed for GluR2/3 heteromers in Chapter 3 (see Equations (3.1)-(3.7), also see Figure 5.1B). As before, the first term on the right-hand side of Equation (5.3) represents the exchange of AMPA receptors in the ESM with AMPA receptors on the dendritic surface. Since $\omega(U - R)$ represents the number of AMPA receptors per unit time flowing across the junction between the dendritic cable and ESM, it is necessary to divide through by the surface area A of the ESM in order to properly conserve AMPA receptor numbers. The second term in Equation (5.3) and the third term of Equation (5.6) represent endocytosis from the ESM into the intracellular pool at a rate of k receptors per unit time. If endocytosis occurs uniformly throughout the ESM then k scales with the area A . However, there is some evidence that endocytosis is concentrated at certain hotspots close to the border with the PSD [6], in which case k could be independent of A . The last term in Equation (5.3) and the first term in Equation (5.4) represents the exchange of AMPA receptors in the ESM with free PSD receptors. Similar to the dendrite-spine exchange, $h(R - P)$ represents the number of AMPA receptors per unit time flowing across the PSD-ESM junction with hopping rate h , and we must divide by the appropriate surface area in order to conserve AMPA receptor numbers. Here a denotes the surface area of the PSD of a synapse, so that $A + a$ denotes the surface area of the entire spine. The second term in Equation (5.4) and the first term in Equation (5.5) represent the binding of free PSD AMPA receptors at a rate $Z - Q$, where Z is the concentration of scaffolding protein, $Z - Q$ is the concentration of free scaffolding protein, and α is the binding rate per free binding site. The third term of Equation (5.4) and the last term of Equation (5.5) represent the unbinding of bound PSD AMPA receptors at a rate β . The last term of Equation (5.4) and the first term of

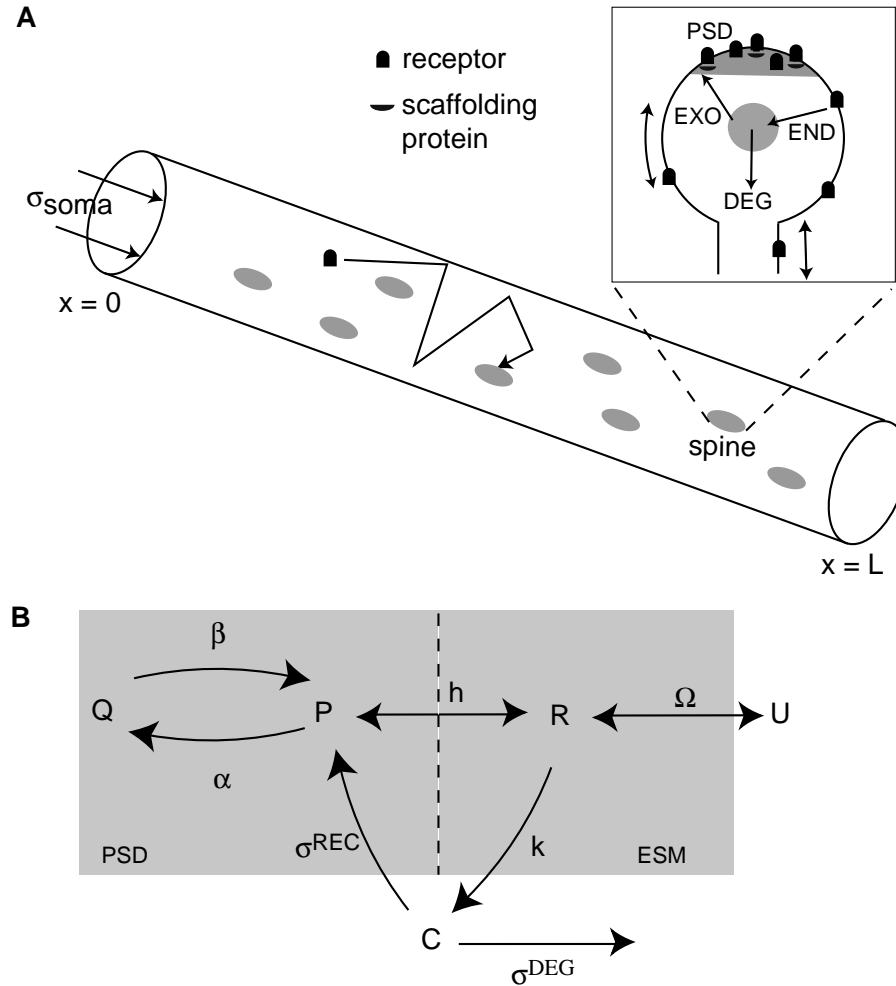


Figure 5.1. One-dimensional continuum model of AMPA receptor trafficking across multiple dendritic spines. (A) One-dimensional dendritic cable of circumference l and length L . An AMPA receptor diffuses freely on the surface of the cable with diffusivity D until it encounters a spine where it may be immobilized through interactions with scaffolding proteins within the postsynaptic density (PSD). Surface receptors are internalized via endocytosis (END), and then either recycled to the surface via exocytosis (EXO) or degraded (DEG), see inset. Fast exocytosis from the soma generates a surface flux σ_0 at one end of the cable. (B) Simplified two-compartment model of a dendritic spine (see Chapter 3). Free AMPA receptors (concentration P) bind to scaffolding proteins within the PSD to form bound AMPA receptors (concentration Q) at a rate α (multiplied by the concentration of free binding sites) and unbind at a rate β . Free AMPA receptors flow between the PSD and ESM at a hopping rate h , and flow between the ESM (concentration R) and surface of the dendritic cable (concentration U) at a rate ω . Free AMPA receptors within the ESM are internalized at a rate k . Receptors are inserted into the PSD from an intracellular pool of S receptors at a rate $\sigma^{rec}(1-f)$ where f is the fraction of intracellular receptors that are sorted for degradation at a rate σ^{deg} .

Equation (5.6) represents the exocytosis of AMPA receptors from the intracellular pool into the PSD, with σ^{rec} the rate of receptors entering the PSD per unit time and $1 - f$ the fraction of intracellular receptors sorted for recycling. The second and fourth term of Equation (5.6) represent, respectively, the local degradation and production of receptors stored in intracellular pools. Finally, we again assume that the strength of a synapse is identified with the total number of PSD AMPA receptors, $N = a(P + Q)$ (but see Section 3.4).

5.1.1 Model extensions during LTP and LTD

In Chapter 3 we considered various experimentally-motivated mechanisms for the regulation of receptor trafficking induced by LTP/LTD stimulus protocols. Here we describe extensions of these mechanisms that take into account lateral diffusion of receptors between multiple spines. (See Figure 5.2 for a schematic illustration of how we model changes in receptor trafficking within a spine during LTP/LTD). Following the “slot” protein hypothesis of Shi et al (2001), we assume that there exists a second intracellular pool of AMPA receptors (corresponding to GluR1/2 heteromers) that is activated during LTP, see Figure 5.2A. Induction of LTP leads to the rapid insertion of these receptors into the ESM at a rate σ_c , which is taken to be faster than the rate of constitutive recycling. At some point before or during the process of exocytosis, the receptors are further assumed to form a receptor-scaffolding protein complex, perhaps mediated by TARPs (transmembrane AMPA receptor regulatory proteins) such as stargazin [10]. Following surface insertion, a receptor-scaffolding protein complex either diffuses into the PSD, where the scaffolding protein can associate with the PSD and create a new “slot” for AMPA receptors, or diffuses out of the spine head and into the surface of the dendrite, where it may encounter and enter other spines, see Figure 5.2B. It is assumed that the surface complexes are transported in a similar fashion to baseline AMPA receptors except for the following modifications: 1) The hopping rate h_c of the complexes between the ESM and PSD is increased relative to baseline in order to simulate the complex’s preference for PSDs, 2) the rate at which the complexes associate with the PSD is taken to be $\alpha_c(Z_c - Z)$, where Z_c is the maximum scaffolding protein concentration for which a PSD has capacity and α_c is the association rate per unused capacity, and 3) newly inserted free surface complexes cannot be re-endocytosed nor can the complex break up into its constituent proteins (at least during some latency period). However, once a complex

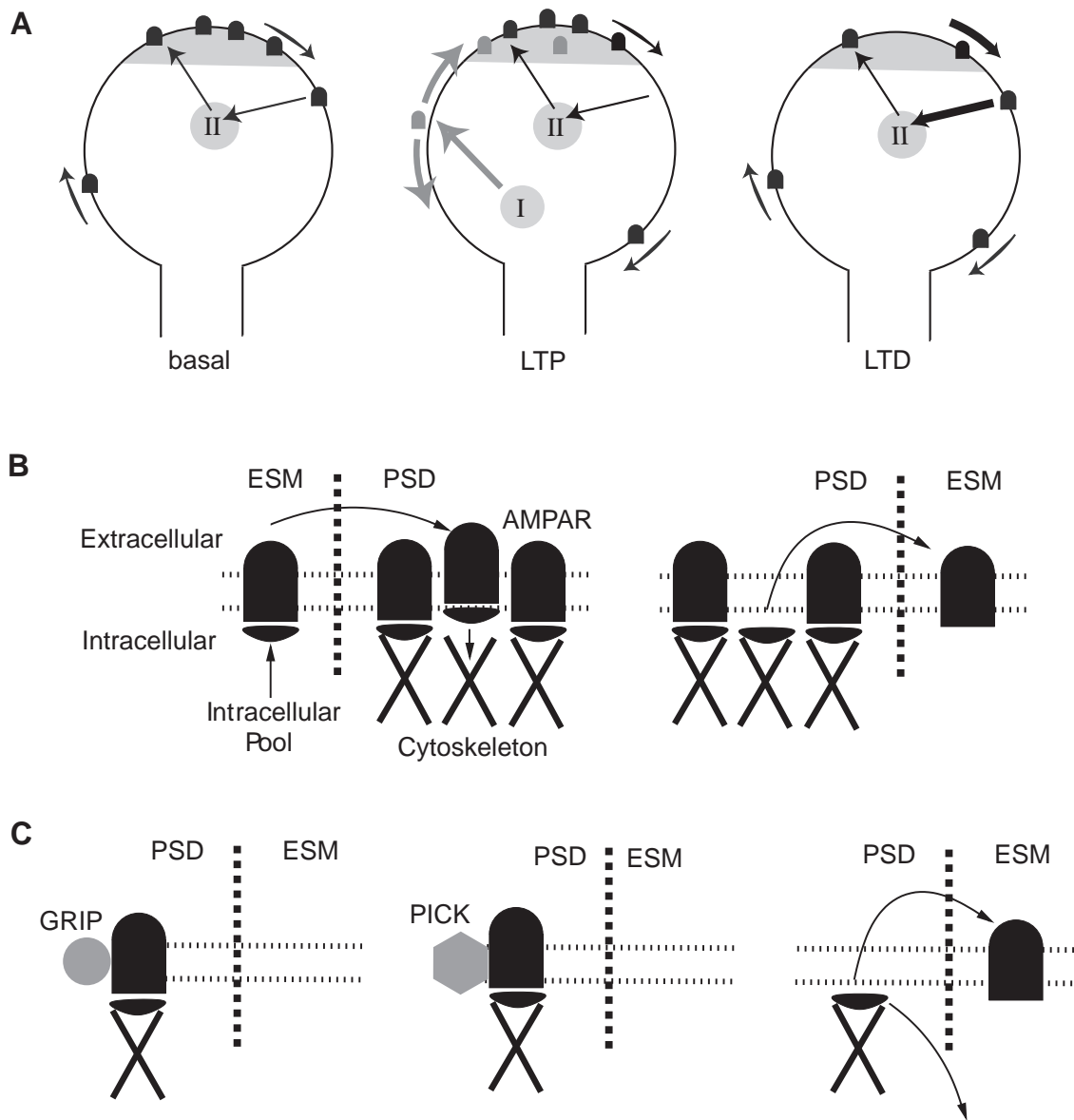


Figure 5.2. Trafficking during LTP/LTD. (A) Trafficking following LTP/LTD induction. During LTP receptors (I) are rapidly inserted into the ESM and either enter the PSD or diffuse to other spines. New slot proteins are transported with newly-inserted receptors. During LTD, the conversion from GRIP to PICK leads to an increased escape from the PSD and subsequent endocytosis (thick arrows) and slots are removed. (B) Increase of slots during LTP. A receptor-scaffold complex is inserted and subsequently enters the PSD where it crosslinks to the cytoskeleton. The bound receptor can then unbind from the scaffolding protein and undergo constitutive recycling. (C) Decrease of slots during LTD. During LTD GRIP-associated receptors change association to PICK. The latter unbind from scaffolding proteins, exit the PSD and are endocytosed. Unoccupied slots are degraded.

becomes associated with the PSD to form a new “slot” the corresponding bound receptor can subsequently unbind from the scaffolding protein and be internalized.

Let U_c , R_c and P_c denote, respectively, the concentration of free complexes in the dendrite, ESM and PSD and let S_c denote the number of receptor complexes within the intracellular pool. Prior to the induction of LTP, we take $U_c = P_c = R_c = 0$ and set S_c to be some fixed constant. Following the application of an LTP stimulus, the surface insertion and trafficking of receptor-scaffolding protein complexes is initiated according to the system of equations

$$\frac{\partial U_c}{\partial t} = D \frac{\partial^2 U_c}{\partial x^2} - \rho(x)\omega(x)(U_c - R_c) \quad (5.7)$$

$$\frac{dR_c}{dt} = \frac{\omega}{A}(U_c - R_c) - \frac{h_c}{A}(R_c - P_c) + \frac{\sigma_c}{A}S_c \quad (5.8)$$

$$\frac{dP_c}{dt} = \frac{h_c}{a}(R_c - P_c) - \alpha_c(Z_c - Z)P_c \quad (5.9)$$

$$\frac{dS_c}{dt} = -\sigma_c S_c \quad (5.10)$$

$$\frac{dZ_c}{dt} = \alpha_c(Z_c - Z)P_c \quad (5.11)$$

Assuming that the baseline population of free receptors still evolves according to Equations (5.1)-(5.4), it follows that the total concentration of bound AMPA receptors within the PSD evolves according to

$$\frac{dQ}{dt} = \alpha(Z - Q)P - \beta Q + \alpha_c(Z_c - Z)P_c \quad (5.12)$$

Note that we considered a much simpler model of LTP in Chapter 3, where slot proteins were inserted directly into the PSD and fixed there.

Our model of receptor trafficking during LTD combines lateral membrane diffusion with our previous model of LTD in a single spine (see Chapter 3). Both free and bound (GluR2/3) receptors in the PSD are now assumed to be in two distinct phosphorylation states that are labeled by a and b , see Figure 5.2C. These correspond to association with the proteins GRIP/ABP and PICK1, respectively [20, 101, 72]. Receptors in the a state behave as in the baseline model, whereas those in the b state are assumed to have a faster unbinding rate β^* and zero binding rate ($\alpha^* = 0$). Decomposing the free and bound GluR2/3 receptor concentrations according to $P = P_a + P_b$ and $Q = Q_a + Q_b$, we have the following modified system of equations for the dynamics of GluR2/3 receptor concentrations within the PSD:

$$\frac{dP_a}{dt} = -\alpha(Z - Q_a)P_a + \beta Q_a - \frac{h}{a}(P_a - R) + \frac{\sigma}{a} - \mu P_a + \nu P_b, \quad (5.13)$$

$$\frac{dP_b}{dt} = \beta^* Q_b - \frac{h^*}{a} P_b + \mu P_a - \nu P_b, \quad (5.14)$$

and

$$\frac{dQ_a}{dt} = \alpha(Z - Q)P_a - \beta Q_a - \mu Q_a + \nu Q_b, \quad (5.15)$$

$$\frac{dQ_b}{dt} = -\beta^* Q_b + \mu Q_a - \nu Q_b. \quad (5.16)$$

Here μ and ν denote the transition rates between the a and b states, which for simplicity are taken to be the same for free and bound receptors. We assume that within the ESM receptors in the b state are rapidly endocytosed and are not recycled, so that $R = R_a$ and the dynamics for R is the same as in Equation (5.3). Finally, in order to have a persistent reduction in synaptic receptor numbers, we assume that as PICK-associated AMPA receptors untether from binding sites, these sites are removed at some rate γ :

$$\frac{dZ}{dt} = \gamma(Z - Q) \quad (5.17)$$

Prior to induction of LTD, we assume that $\mu = \gamma = 0$ so that $P = P_a$ and $Q = Q_a$ and the system behaves as the baseline model. During the application of an LTD stimulus, μ and γ are temporarily increased so that GRIP-associated receptors are converted to PICK-associated receptors as described by the system of Equations (5.13)-(5.17). Since PICK-associated receptors are more likely to unbind from scaffolding proteins we find that Q , and hence Z , decreases. Once the LTD stimulus is removed, μ and γ are reset to zero so that all receptors convert back to the GRIP-associated state and all the remaining binding sites become reoccupied.

5.2 Steady-state analysis

It follows from Equation (5.6) that the steady-state rate of exocytosis is given by

$$\sigma \equiv \sigma^{rec}(1 - f)S = \lambda(kR + \delta), \quad \lambda = \frac{\sigma^{rec}(1 - f)}{\sigma^{rec}(1 - f) + \sigma^{deg}f}. \quad (5.18)$$

Equations (5.3)-(5.5) then imply that the steady-state concentrations of bound and unbound receptors within the PSD are given by

$$P = R + \frac{\sigma}{h}, \quad Q = \frac{\alpha P}{\alpha P + \beta} Z \quad (5.19)$$

and the corresponding steady-state receptor concentration in the ESM is

$$R = \frac{\omega U + \lambda \delta}{\omega + k(1 - \lambda)} \quad (5.20)$$

If the dendritic receptor concentration U were fixed then Equations (5.19) and (5.20) would independently hold for each x (as assumed in our single-spine model, see Chapter (3)). However, U now has to be determined self-consistently by substituting Equation (5.20) into the steady-state version of the diffusion Equation (5.1):

$$D \frac{d^2 U}{dx^2} - \rho(x) \widehat{\omega}(x) U = -\rho(x) \widehat{\omega}(x) \widehat{R}(x) \quad (5.21)$$

with the effective hopping rate $\widehat{\omega}$ and ESM receptor concentration \widehat{R} defined as in Equation (4.15).

5.2.1 Uniform background concentration

Let us first consider a uniform cable with zero somatic flux ($\sigma_0 = 0$). Furthermore, suppose that all trafficking parameters associated with the intracellular pools are independent of dendritic location x . That is, we set $k(x) = k_0$, $\sigma^{rec}(x) = \sigma_0^{rec}$, $\sigma^{deg}(x) = \sigma_0^{deg}$, $f(x) = f_0$, and $\delta(x) = \delta_0$. It then follows that the receptor concentrations U and R are also x -independent and each spine becomes an isolated unit, since there is no net diffusive flux of receptors between the spines and dendrite. In particular, the solution of Equations (5.20) and (5.21) reduces to $U(x) = R(x) = \widehat{R}_0 = \lambda_0 \delta_0 / (k_0 [1 - \lambda_0])$. Note that the receptor concentrations U and R can be spatially uniform even though the number of synaptic receptors may vary due to local variations in the properties of the PSD. That is, the area a of the PSD, the binding rate α , the unbinding rate β , the concentration of scaffolding proteins Z , and the hopping rate h can all be x -dependent.

5.2.2 Nonuniform background concentration

In the case of a uniform cable with a nonzero somatic flux ($\sigma_0 > 0$) or a nonuniform cable, the concentration of receptors along the dendrite is spatially varying. This implies that there will be a net diffusive flux flowing between the dendrite and spines. For simplicity, we consider a uniform spine density, $\rho(x) = \rho_0$ and a uniform spine neck hopping rate, $\omega = \omega_0$. However, in contrast to the previous example, we allow the rate of local intracellular production δ to vary with x . Equation (5.21) then reduces to

$$D \frac{d^2 U}{dx^2} - \Lambda_0^2(x) U = -\Lambda_0^2(x) \widehat{R}(x) \quad (5.22)$$

where

$$\Lambda_0 = \sqrt{\frac{\rho_0 \widehat{\omega}_0}{D}}, \quad \widehat{\omega}_0 = \frac{\omega_0 k_0 (1 - \lambda_0)}{\omega_0 + k_0 (1 - \lambda_0)} \quad (5.23)$$

Integrating Equation (5.22) with respect to x and using the boundary conditions (5.2) yields the conservation equation

$$\sigma_0 = M \widehat{\omega}_0 (\overline{U} - \overline{\widehat{R}}) \quad (5.24)$$

where

$$\overline{U} = \frac{1}{L} \int_0^L U dx, \quad \overline{\widehat{R}} = \frac{1}{L} \int_0^L \widehat{R} dx \quad (5.25)$$

are the average values of U and \widehat{R} , respectively. This implies that the total number of receptors entering the dendrite from the soma is equal to the total number of receptors hopping from the dendrite into the M spines and being degraded. Note that if there were no degradation of receptors in the local intracellular pools ($\sigma_0^{deg} = 0, \lambda_0 = 1$) then $\widehat{\omega}_0 = 0$ and it would be impossible to satisfy the conservation equation (5.24); the number of receptors in the dendrite would grow without bounds.

The steady-state diffusion Equation (5.22) can be solved using Green's function methods along similar lines to the standard cable equation describing electrical current flow in passive dendrites [106, 140, 25] with Λ_0 an effective space constant for surface receptor diffusion and transport. Given the boundary conditions (5.2), the resulting solution for the dendritic receptor concentration can be written in the form

$$U(x) = \frac{\sigma_0}{D} G(x, 0) + \Lambda_0^2 \int_0^L G(x, x') \widehat{R}(x') dx' \quad (5.26)$$

where G is the one-dimensional Green's function for a uniform cable of length L with closed ends at $x = 0, L$:

$$G(x, x') = \frac{\cosh(\Lambda_0[|x - x'| - L]) + \cosh(\Lambda_0[x + x - L])}{2\Lambda_0 \sinh(\Lambda_0 L)}. \quad (5.27)$$

Having determined the dendritic receptor concentration U , the corresponding spatial variation in the number of synaptic receptors along the cable can be obtained from Equations (5.18)-(5.20). Substitution of Equation (5.27) into (5.26) shows that if $\widehat{R}(x) = \widehat{R}_0$ then

$$U(x) = \frac{\sigma_0}{D} \frac{\cosh(\Lambda_0[x - L])}{\Lambda_0 \sinh(\Lambda_0 L)} + \widehat{R}_0 \quad (5.28)$$

Assuming $\Lambda_0 L \ll 1$, we see that the dendritic receptor concentration is an exponentially decaying function of distance from the soma x , asymptotically approaching the uniform

background concentration \widehat{R}_0 at a rate Λ_0 . In the more general case of a spatially varying distribution \widehat{R} , Equation (5.26) implies that the receptor concentration at x depends nonlocally on the properties of spines at other locations x' on the dendrite as specified by $\widehat{R}(x')$. This illustrates the possible role of lateral diffusion in mediating a form of heterosynaptic plasticity. That is, local changes in the rate of synthesis can induce non-local changes in dendritic and synaptic receptor concentrations. A similar conclusion holds for local changes in the rate of constitutive recycling and degradation (see Section 5.4), although Equation (5.22) now has to be solved numerically since $\widehat{\omega}$ is x -dependent.

5.3 Delivery of synaptic AMPA receptors from the soma via lateral diffusion

There is currently some controversy regarding the major mechanism whereby AMPA receptors are trafficked to dendritic spines. A number of studies propose a local mechanism that combines fast exocytosis of intracellular AMPA receptors into dendritic membrane near synapses with lateral diffusion within the spine surface to synapses [31, 68, 100, 10]. The intracellular receptor pools are then replenished by the constitutive recycling of synaptic receptors and the delivery of new AMPA receptors via microtubule-based vesicular trafficking [117, 18]. However, this has recently been questioned by the photoinactivation studies of Adesnik et al. (2005), which found that while exocytosis at the soma is still fast, recycling of AMPA receptors at synapses is much slower, suggesting that the major source of synaptic receptors arises from their lateral diffusion from the soma to the synapse. One of the potential limitations of the latter mechanism is that diffusion is slow. That is, an estimate for the mean time a receptor takes to travel a distance x from the soma via free diffusion within the membrane of a uniform dendritic cable is $\tau = x^2/2D$, where D is the membrane diffusivity. Experimental estimates of D vary from 0.01 to 0.5 $\mu\text{m}^2 \text{s}^{-1}$ [9, 132, 39, 2, 3]. Taking a value of D at the upper end of this range shows that the mean time to reach a proximal synapse at 100 μm from the soma is of the order 3 hrs, whereas the time to reach a distal dendrite at 1 mm from the soma is of the order 300 hrs. The latter is much longer than the average lifetime of an AMPA receptor, which is approximately 1 day [44]. These simple calculations actually underestimate the mean travel time of a receptor along a dendrite, since they do not take into account the fact that dendritic spines can trap receptors, thus further slowing their progress along a dendrite (see Section 4.4).

Perhaps one could argue that the relatively slow local constitutive recycling of receptors found by Adesnik et al. (2005) provides a mechanism for allowing viable receptors to eventually reach distal synapses. Therefore, irrespective of the rate of constitutive recycling, let us assume that sufficient time has occurred for the receptor concentrations along the dendrite and within the dendritic spines to reach a steady state. For simplicity, consider a uniform dendritic cable of length $L = 1$ mm and circumference $l = 1\mu\text{m}$, containing $M = 1000$ identical spines distributed uniformly along the cable with density $\rho = 1\mu\text{m}^{-2}$. Using Equations (5.18)-(5.20) and (5.28) we can then determine how the steady-state number of synaptic receptors varies as a function of distance from the soma for various choices of model parameters, including those corresponding to the cases of fast and slow recycling. In Figure 5.3A we plot the steady-state distribution of receptors for spines with the baseline parameters values given in Table 5.1. These values correspond to the case of fast constitutive recycling, having a time constant of approximately 16 min [31, 68, 100]. We also take the somatic flux to be $\sigma_0 = 0.1\mu\text{m}^{-1}\text{s}^{-1}$ and the AMPA receptor diffusivity in the cable to be $D = 0.1\mu\text{m}^2\text{s}^{-1}$. It can be seen that the dendritic receptor concentration decays exponentially from the soma at a rate $\Lambda_0 \approx 0.01\mu\text{m}^{-1}$, reaching an asymptotic value of $\hat{R} \approx 90$ receptors μm^{-2} near the half-length of the cable (at $x = 500\mu\text{m}$). This asymptotic level is what would be observed uniformly if the somatic flux were set to zero (i.e., $\sigma_0 = 0$). The values of \hat{R} and Λ_0 are consistent with Equations (4.15) and (5.23), respectively. The number of synaptic receptors also decreases exponentially from the soma reaching an asymptotic value of around 40 receptors. Note

Table 5.1. Basal parameter values for dendritic spines

Parameter	Symbol	Value	Units	Reference
Area of PSD	a	0.1	μm^2	[126]
Area of ESM	A	1	μm^2	[126]
Concentration of scaffolding proteins	Z	200	μm^{-2}	This chapter
Binding rate	α	10^{-4}	$\mu\text{m}^2\text{s}^{-1}$	This chapter
Unbinding rate	β	10^{-4}	s^{-1}	This chapter
PSD-ESM hopping rate	h	10^{-3}	$\mu\text{m}^2\text{s}^{-1}$	This chapter
ESM-dendrite hopping rate	ω	10^{-3}	$\mu\text{m}^2\text{s}^{-1}$	This chapter
Rate of endocytosis	k	10^{-3}	$\mu\text{m}^2\text{s}^{-1}$	[31]
Rate of recycling	σ^{rec}	10^{-3}	s^{-1}	[118]
Rate of degradation	σ^{deg}	10^{-5}	s^{-1}	This chapter
Rate of production	δ	10^{-3}	s^{-1}	This chapter
Fraction sorted for degradation	f	0.1	none	This chapter

that for the given choice of parameters, AMPA receptors occupy the 20 binding sites provided by scaffolding proteins within each PSD and, except for synapses located within the first 100 μm of the cable, this represents approximately half of the AMPA receptors found within the PSD. This division of synaptic AMPA receptors into roughly equal proportions of mobile and immobile receptors agrees with data from both single-particle tracking and FRAP experiments [39, 3]. Also shown in Figure 5.3A are the receptor profiles for a somatic flux $\sigma_0 = 1 \text{ s}^{-1}$ (thin solid curves), which corresponds to a receptor entering the cable from the soma every second. This gives rise to synaptic receptor numbers of approximately 200 near the soma, which is at the high end of experimental observations [94, 23, 131]. However, since the space constant Λ_0 and the asymptotic background concentration are both independent of somatic flux σ_0 , receptor numbers approach the same asymptotic value at the same rate. Thus taking σ_0 to be too large strongly biases the strength of proximal synapses.

In Figure 5.3B we present corresponding receptor profiles in the case of faster diffusivity ($D = 0.45 \mu\text{m}^2 \text{s}^{-1}$) and slower constitutive recycling, as suggested by Adesnik et al (2005). We simulate the latter by introducing a 10-fold reduction in the rates of endocytosis and recycling so that $k = 10^{-4} \mu\text{m}^2 \text{s}^{-1}$ and $\sigma^{rec} = 10^{-4} \text{ s}^{-1}$. In this case, recycling has a time constant of approximately 3 hr. The baseline effective degradation rate $f\sigma^{deg} = 10^{-5} \text{ s}^{-1}$ is not changed, however, since a degradation time constant of around 1 day is comparable to the observed half-life of an AMPA receptor [95, 44], reducing σ^{deg} further would allow for non-viable AMPA receptors to be included in our simulations. The profiles in Figure 5.3B are similar to those in Figure 5.3A, except that now the rate of exponential decay is slower and the asymptotic number of receptors in the PSD is 30, a 21% reduction in the number of synaptic receptors due to a 44% loss of mobile receptors. The reason for this reduction is that a decrease in the rate of constitutive recycling leads to a decrease in the net rate of exocytosis of receptors into the PSD, see Equations (5.18) and (5.19). In Figure 5.3C,D we show how the space constant Λ_0 and the asymptotic number of synaptic receptors varies with the rate of constitutive recycling and other biophysical parameters. Note, in particular, that Λ_0 depends weakly on the rate of constitutive recycling, indicating that the latter does not play a significant role in determining how effectively receptors diffuse from the soma to distal dendrites. The studies of Adesnik et al. (2005) suggest that neither synthesis nor microtubule-based vesicular trafficking of AMPA receptors contribute significantly

to synaptic receptor numbers, as the incubation of their cultures in either the protein synthesis inhibitor cycloheximide or the microtubule polymerization inhibitor colchicine did not affect their results. We simulate this in Figure 5.3E,F by setting the intracellular rate of receptor production $\delta = 0 \text{ s}^{-1}$ with all other parameters as in Figure 5.3A,B respectively. Since Λ_0 is only weakly dependent on the rate of constitutive recycling, we find that diffusion can only supply distal synapses if the diffusivity D is sufficiently fast as in Figure 5.3F. However, the required value of D is at the extreme end of experimentally measured values. Moreover most synapses now have negligible free receptors, which is inconsistent with single-particle tracking and FRAP experiments [39, 3]. It should also be noted that we are taking a relatively low density of spines along the dendrite [93]; increasing ρ would increase Λ_0 and thus make the delivery of receptors to distal synapses even more difficult.

Combining these steady-state results with our previous argument regarding the amount of time required for receptors to diffuse to distal synapses, suggests that the combination of somatic synthesis and lateral diffusion proposed by Adesnik et al. (2005) is insufficient to supply receptors to distal synapses, unless one takes unrealistically large values of the diffusivity. Another conclusion that can be drawn from our steady-state analysis is that the steady-state dendritic receptor concentration is relatively insensitive to the rate of constitutive recycling. On the other hand, the rate of constitutive recycling does have a significant affect on the steady-state number of receptors within the PSD, see Figure 5.3D. We find that in our model fast constitutive recycling produces synaptic receptor numbers more consistent with experimental observations [94, 23, 131]. Hence, for the remainder of this chapter we will use dendritic spine parameter values corresponding to fast constitutive recycling and a nonzero local intracellular production rate as given in Table 5.1. We also set $\sigma_0 = 0 \text{ s}^{-1}$ and take the diffusivity of AMPA receptors in the cable to be $D = 0.1 \mu\text{m}^2\text{s}^{-1}$. Note, however, that the results presented below still hold (at least qualitatively) in the case of slow constitutive recycling.

5.4 Nonlocal effects of constitutive recycling mediated by lateral diffusion

In Figure 5.3 we assumed that all spines are identical and are uniformly distributed along the cable. However, there is a considerable amount of heterogeneity in the properties of spines within a single neuron (reviewed in [93]). Spine morphology ranges from small

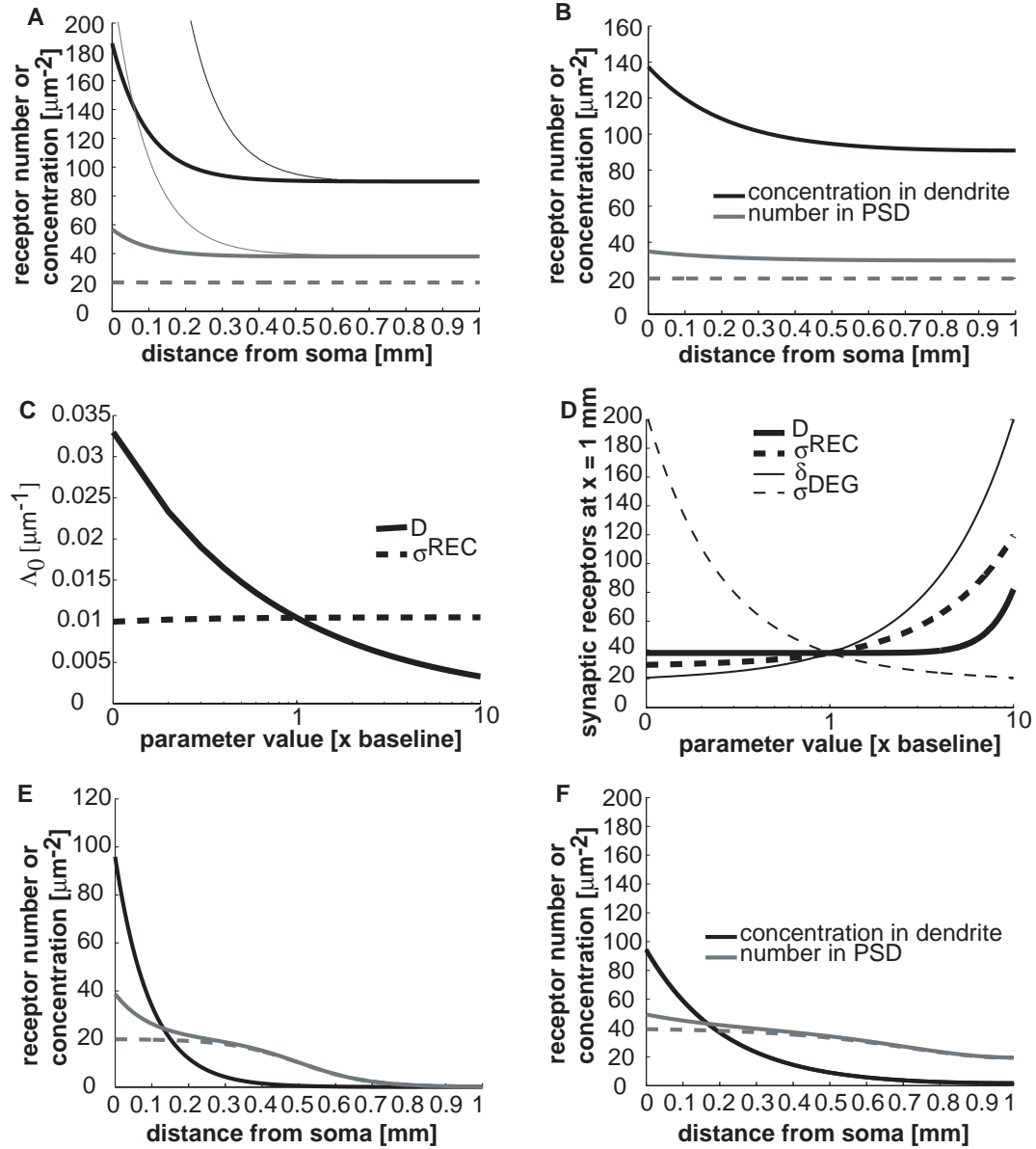


Figure 5.3. Steady-state distribution of AMPA receptors. Length and circumference of cable are $L = 1$ mm and $l = 1 \mu\text{m}$. $M = 1,000$ identical spines are distributed uniformly along cable with density $\rho = 1 \mu\text{m}^{-2}$. Unless specified otherwise, spine parameters have baseline values in Table 5.1. Somatic flux is $\sigma_0 = 0.1 \mu\text{m}^{-1}\text{s}^{-1}$. (A) Receptor profiles for fast constitutive recycling ($\sigma^{rec} = 10^{-3} \text{ s}^{-1}$ and $k = 10^{-3} \mu\text{m}^2\text{s}^{-1}$) and diffusivity $D = 0.1 \mu\text{m}^2\text{s}^{-1}$. The dendritic receptor concentration (solid black) and synaptic receptor number (solid gray) decrease exponentially from soma. Profiles for $\sigma_0 = 1 \mu\text{m}^{-1}\text{s}^{-1}$ are shown as thin curves. Number of bound PSD receptors are also shown (dashed gray). (B) Receptor profiles for slow constitutive recycling ($\sigma^{rec} = 10^{-4} \text{ s}^{-1}$ and $k = 10^{-4} \mu\text{m}^2\text{s}^{-1}$) and fast diffusivity $D = 0.45 \mu\text{m}^2\text{s}^{-1}$. Profiles are similar to A except decay rate is slower and receptor numbers are reduced. (C) Rate of decay Λ_0 as function of constitutive recycling rate σ^{rec} and diffusivity D . (D) Synaptic receptor number at distal synapses as function of parameters. (E, F) Same as A, B without production ($\delta = 0$).

filopodial protrusions to large mushroom-like bulbs, and properties such as the surface area of a spine and spine density tend to vary systematically along the dendrite [61]. One of the basic assumptions of our continuum model is that populations of spines at a particular location on the dendritic cable have similar properties. This is reasonable given that local populations of synapses are likely to receive similar inputs. Under this assumption, we can investigate how the steady-state distribution of synaptic receptors depends on variations in spine properties with distance from the soma. One of the basic results that emerges from our steady-state analysis (see Section 5.2) is that the number of receptors at a given synapse depends nonlocally on the spatial distribution of certain spine properties along the dendritic cable. Nonlocal effects are mediated by lateral membrane diffusion within the dendrite, so that such properties correspond to parameters that appear in the steady-state diffusion Equation (5.21). These include the spine density ρ , the hopping rate through the spine neck ω and the various parameters associated with constitutive recycling: the local rates of exo/endocytosis σ^{rec} and k , degradation σ^{deg} and production δ . On the other hand, parameters that specify properties of the PSD are purely local, including the area a of the PSD, the rates at which receptors bind to and unbind from scaffolding proteins α and β , respectively, and the concentration of scaffolding proteins Z .

It follows from the above that the lateral diffusion of AMPA receptors within the surface of the dendritic cable mediates a nonlocal interaction between synapses. This is illustrated in Figure 5.4 where we plot receptor profiles for localized variations away from baseline of the rates of constitutive recycling or degradation/synthesis. For simplicity we assume that the length of the cable is $L = 200 \mu\text{m}$, that the spine density is again uniform with $\rho = 1 \mu\text{m}^{-2}$, and that there is no somatic flux of receptors ($\sigma_0 = 0$). All spines are assumed to be identical with baseline parameters as in Table 5.1 except those located 90 to 110 μm from the soma, which employ all baseline parameters except those being perturbed. We first consider the effect of the exocytic rate σ^{rec} . While increasing σ^{rec} slightly potentiates the number of synaptic receptors of the perturbed and neighboring spines, decreasing σ^{rec} to 10^{-4} s^{-1} (0.1x baseline) causes a large depression in the number of synaptic receptors at all spines, from 38 to 27 (29% decrease) receptors within the perturbed spines and to 32 (16% decrease) receptors within spines at the ends of cable located 90 μm from the border of the perturbed region (see Figure 5.4A). In both cases the number of intracellular receptors within the perturbed region is dramatically different

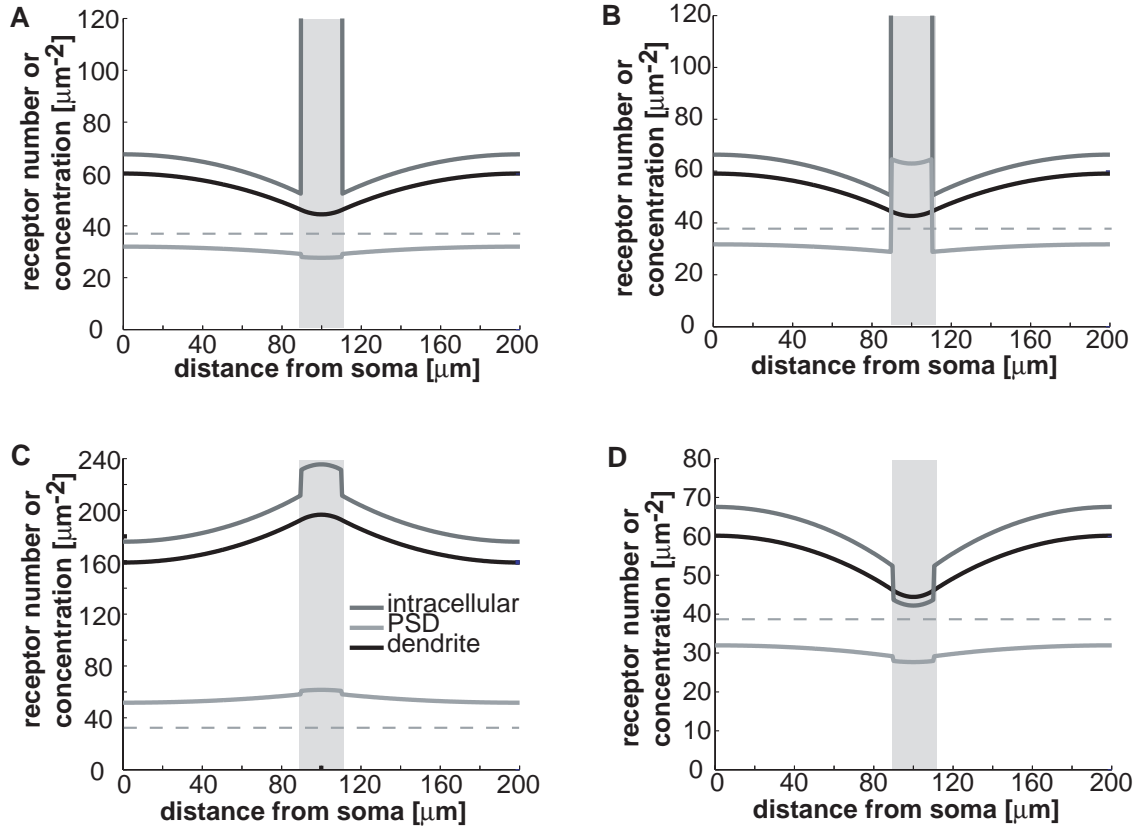


Figure 5.4. Nonlocal effects of variations in constitutive recycling. A dendritic cable of length $L = 200\mu\text{m}$, circumference $l = 1\mu\text{m}$ and diffusivity $D = 0.1\mu\text{m}^2\text{s}^{-1}$ has a uniform distribution of spines with density $\rho_0 = 1\mu\text{m}^{-2}$. All spines are identical, with baseline parameters as in Table 5.1, except those located 90 to 110 μm from the soma (shaded gray region), for which one of the parameters associated with constitutive recycling (σ^{rec} , k , σ^{deg} , δ) is perturbed. Before perturbation all synapses have 38 receptors (dashed light gray). After perturbation, the resulting steady-state dendritic receptor concentration (black), the number of intracellular receptors (gray) and the total number of receptors in the PSD (solid light gray) are plotted as functions of distance x from the soma. (A) Receptor profiles in response to a local reduction in the rate of recycling σ^{rec} (0.1 x baseline). (B) Receptor profiles in response to a local increase in the rate of endocytosis k (10 x baseline). (C) Receptor profiles in response to a local increase in the rate of synthesis δ (10 x baseline). (D) Receptor profiles in response to a local increase in the rate of degradation σ^{deg} (10 x baseline).

from baseline values, showing the strong dependence of this receptor population on the recycling rate σ^{rec} .

Increasing the rate of endocytosis k to $10^{-2}\mu\text{m}^2\text{s}^{-1}$ (10x baseline) causes synaptic receptor numbers to increase by 65% from 38 to 63, yet all other synapses are depressed, to 29 (24% decrease) in neighboring spines and to 32 (16% decrease) in spines at the cable ends (see Figure 5.4B). That an increase in endocytosis leads to an increase in the number of receptors found within the PSD may seem counterintuitive at first sight. However, recall that receptors are not endocytosed from the PSD but from the extrasynaptic region of the spine head. This increases the number of the receptors in the local intracellular pool available to be exocytosed into the PSD, accounting for the increase in synaptic receptors. By decreasing k , synaptic receptor numbers are depressed from 38 to 31 (18% decrease) receptors in the perturbed region while all other synapses experience a slight increase to 40 (5% increase). Again, the intracellular pools depend strongly on the endocytic rate k .

Although there is very little change in receptor numbers when the rate of production δ is reduced, all synapses are potentiated when δ is increased to 10^{-2} s^{-1} (10x baseline), from 38 to 61 (60% increase) synaptic receptors in the perturbed region, to 58 (53% increase) just outside the perturbed region and to 51 (34% increase) at the cable ends (see Figure 5.4C). Intracellular receptors have also increased approximately 2-fold across all spines. While decreasing σ^{deg} slightly potentiates all synapses, increasing σ^{deg} to 10^{-3} s^{-1} (10x baseline) depresses all synapses, from 38 to 28 (26% decrease) synaptic receptors in the perturbed region, to 29 (24% decrease) just outside the perturbed region and to 32 (16% decrease) at the cable ends (see Figure 5.4D). In contrast to increased δ , intracellular receptors have now decreased approximately 2-fold across all spines.

5.5 Lateral diffusion of AMPA receptors unlikely to mediate heterosynaptic LTP/LTD

Our multispine model shown in Figure 5.1 relies heavily on our model of AMPA receptor trafficking at a single spine (see Chapter 3). In our study of the single-spine model we showed that both LTP and LTD could be reproduced by affecting changes in trafficking parameters that are likely targets of the second-messenger pathways activated by experimental LTP/LTD protocols [119, 125, 10, 75, 22, 56]. However, because our model contained only the dynamics of receptor trafficking at a single dendritic spine, we were unable to consistently determine the concentration of AMPA receptors in the dendritic membrane just outside the spine. Instead, we assumed that this “background”

concentration was approximately constant for the duration of our simulations. An advantage of our multispine model is that this background receptor concentration is determined self-consistently given receptor concentrations and dynamics at all other locations of the cable, providing both a more accurate representation of the single-spine trafficking of AMPA receptors and a more appropriate setting in which to study LTP/LTD. In addition, our multispine model allows us to examine whether or not lateral diffusion mediates a form of heterosynaptic LTP/LTD. Various experiments have shown that inducing LTP locally can lead to the spread of LTP [115, 35] or LTD [112, 107] to nearby synapses, and that inducing LTD can lead to a similar spread of LTP [107] or LTD [37]. Such heterosynaptic effects are thought to be mediated by a number of processes, including the spillover and uptake of glutamate, retrograde signaling of extracellular messengers and postsynaptic signaling of intracellular messengers (see [92] for a review). Notably, AMPA receptor trafficking is not among the offered explanations. Here we show that the regulation of AMPA receptor trafficking within dendritic spines combined with lateral membrane diffusion provides a mechanism for the expression of homosynaptic but not heterosynaptic LTP/LTD. In each case, we assume that prior to an LTP or LTD stimulus, the spines are in steady-state with baseline parameter values as summarized in Table 5.1. An LTP or LTD inducing stimulus then switches on a modification in receptor trafficking as represented schematically in Figure 5.2 and described mathematically by Equations (5.7)-(5.12) for LTP and Equations (5.13)-(5.17) for LTD (see Materials and Methods). The various LTP/LTD model parameters are listed in Tables 5.2 and 5.3.

5.5.1 Long-term potentiation

We assume that the induction of LTP at a synapse is expressed when, at time $t = 0$ s, a pool of AMPA receptor-scaffolding protein complexes is rapidly inserted into the ESM compartment of the spine containing the synapse. These receptor-scaffolding complexes can either diffuse into the PSD, where the scaffolding protein can associate with the

Table 5.2. Parameters during LTP

Parameter	Symbol	Value	Units	Reference
Scaffolding capacity of PSD	Z_c	600	μm^{-2}	This chapter
Binding rate	α_c	10^{-2}	$\mu\text{m}^2\text{s}^{-1}$	This chapter
PSD-ESM hopping rate	h_c	10^{-2}	$\mu\text{m}^2\text{s}^{-1}$	This chapter
Rate of exocytosis	σ_c	0.1	s^{-1}	This chapter

Table 5.3. Parameters during LTD

Parameter	Symbol	Value	Units	Reference
Unbinding rate	β^*	10^{-2}	s^{-1}	This chapter
Association rate with PICK	μ	10^{-2}	s^{-1}	This chapter
Association rate with GRIP	ν	10^{-2}	s^{-1}	This chapter
Rate of scaffolding removal	γ	5×10^{-3}	$\mu m^{-2} s^{-1}$	This chapter

PSD and create a new “slot” for free AMPA receptors, see Figure 5.2B, or diffuse out of the spine head and into the surface of the dendrite, where it may encounter and enter another spine. The dynamics of the receptor-scaffolding protein complexes is described by Equations (5.8)-(5.12). In Figure 5.5A-E we show the results of inducing LTP at synapses in a $30 \mu m$ wide region of the cable located $85-115 \mu m$ from the soma. As in Figure 5.4, we assume that the length of the cable is $L = 200 \mu m$, the spine density is $\rho = 1 \mu m^{-2}$, the somatic flux is $\sigma_0 = 0$, and all spines are initially identical with parameters as in Table 5.1. The plots of Figure 5.5 were obtained by numerically solving Equations 5.3-5.6 supplemented by Equations 5.7-5.11. Note that a total of 100 complexes are inserted at a rate of $\sigma^{rec} = 0.1 s^{-1}$. Figure 5.5A shows the receptor profiles 6 hrs after induction. Synapses within the region of induction have 78 synaptic receptors, approximately double the number they possessed initially. This rise in synaptic receptor number occurs in approximately 1 min (Figure 5.5D), consistent with most electrophysiological data on LTP [7, 40]. There is a corresponding transient increase in the ESM receptor concentration due to the surface insertion of receptor-scaffolding complexes, which then decays back to baseline levels (Figure 5.5B). The time course of the decrease in the ESM concentration has a fast component due to complexes entering the PSD and a slow component due to complexes entering the dendrite. Interestingly, synapses located within $15 \mu m$ of either side of the induction region contain just as many receptors, although the rise time of receptor numbers at these synapses is much slower, taking around 6 hrs at synapses located 70 and $130 \mu m$ from the soma (Figure 5.5E). There is an insignificant change in the ESM and dendritic concentrations (Figure 5.5C).

Thus the induction of LTP in a $30 \mu m$ wide region potentiates synapses not only in the region of induction, but in another $30 \mu m$ of the cable as well. The cause of this heterosynaptic spread of LTP is the spillover of unused receptor-scaffolding complexes. Each PSD is assumed to have capacity for 40 additional scaffolding proteins, leaving 60 complexes unable to associate with the PSD of the spine in which they were inserted.

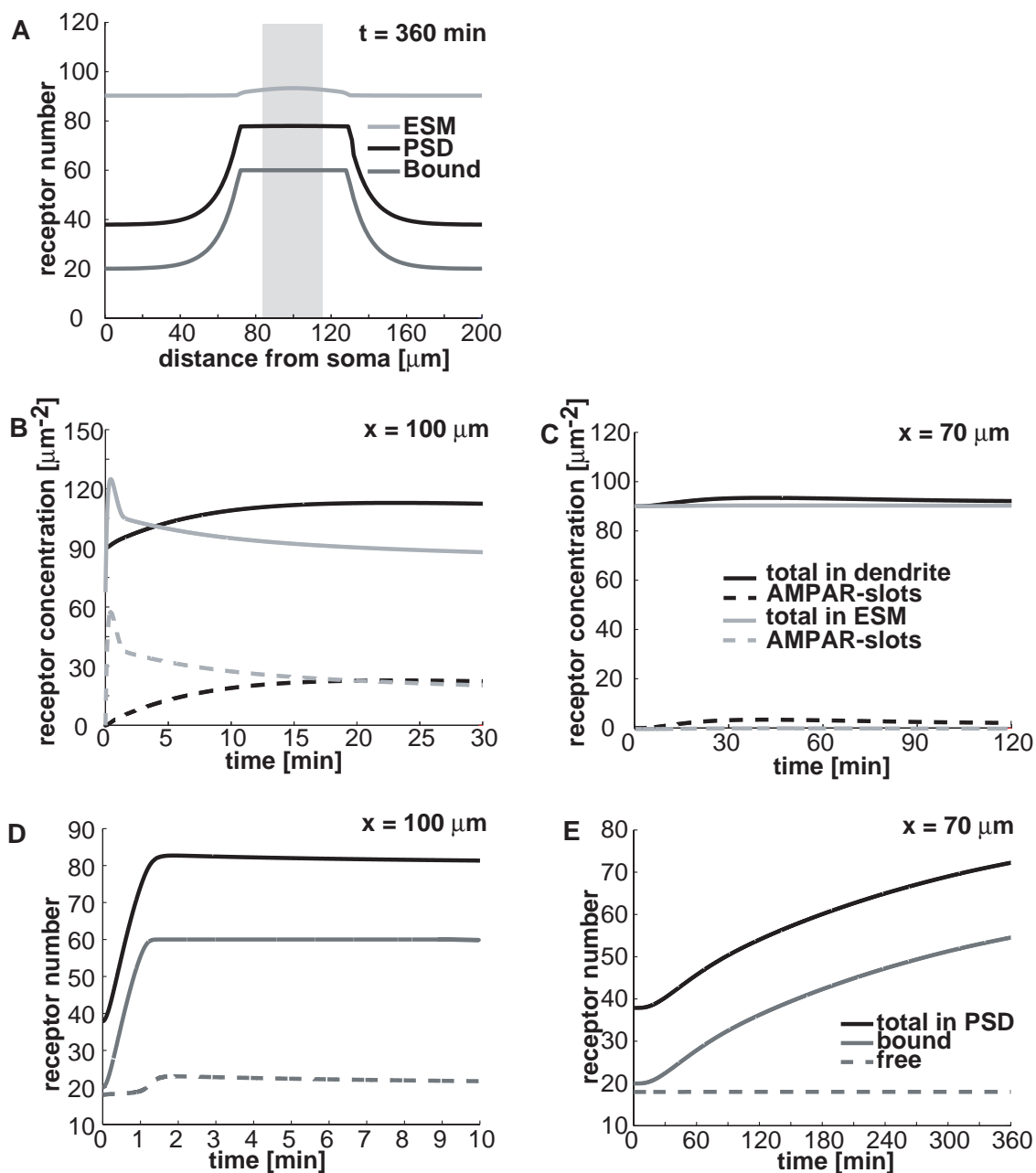


Figure 5.5. Time course of AMPA receptor trafficking during LTP. LTP is induced at time $t = 0$ s from steady-state by inserting 100 receptor-scaffolding complexes into ESMs of spines 85-115 μm from soma (gray region in A). Spine parameters are as in Tables 5.1 and 5.2, other parameters as in Figure 5.4. (A) Profiles 6 hrs after induction. PSD receptor numbers (black) have doubled, both in induction region and at synapses $\leq 15 \mu\text{m}$ away, due to increased bound receptor numbers (dark gray). (B,C) Time course of dendritic (black) and ESM (gray) concentrations within ($x = 100 \mu\text{m}$) and without ($x = 70 \mu\text{m}$) the induction region. (D,E) Time course of total (black), free (solid gray) and bound (dashed gray) PSD receptor numbers for spines shown in B,C respectively.

These complexes diffuse out of the spine and into the surface of the cable and eventually associate with the PSD of another synapse which has not yet reached its capacity for scaffolding proteins. If we were instead to insert 40 complexes upon induction of LTP, all would associate with the PSD of the spine in which they were inserted and hence there would be no heterosynaptic spread of LTP. Due to this strong dependence on the number of inserted complexes and the relatively short range of heterosynaptic spread, it seems unlikely that the spillover of AMPA receptors can account for the heterosynaptic LTP observed by, say, Engert and Bonhoeffer (1997), where in the CA1 region of rat hippocampus they found that LTP can spread as far as $70 \mu\text{m}$ with the heterosynaptic LTP occurring within minutes of the homosynaptic LTP induction. Moreover, Royer and Pare (2003) observed that the induction of LTP in a very small region of guinea pig amygdala can induce very rapid but short-range heterosynaptic LTD. Our simulations do not predict LTD anywhere in the cable. We therefore conclude that AMPA receptor trafficking is unlikely to be the mechanism whereby these heterosynaptic changes during LTP occur.

As we have already discussed, there is some controversy regarding the role of lateral membrane diffusion in supplying spines with receptors (see Adesnik et al. (2005)). This raises the interesting question as to whether or not the increase in synaptic receptor numbers observed during LTP could be due to the influx of surface receptors from the dendrite rather than from the insertion of additional receptors from intracellular pools. We can investigate this issue using our baseline model by supposing that additional slot proteins are inserted directly into the PSD of spines at time $t = 0$, following LTP induction, and seeing how receptors subsequently redistribute according to Equations (5.1)-(5.6). LTP is induced in spines occupying the same region of dendrite as considered in Figure 5.5. The results are shown in Figure 5.6A-E, which are the direct analogs of Figure 5.5A-E. In the region of induction, receptors in the ESM quickly enter the PSD in response to the increased scaffolding concentration, while receptors from the dendrite and intracellular pool slowly replenish the diminishing ESM population (see Figure 5.6B,D). Note that the rise time of synaptic receptor numbers is now approximately 10 min rather than 1 min. Outside the induction region there is a slow reduction in the number of ESM and intracellular receptors in response to the drop in dendritic receptor concentration, and there is a slight drop in the number of synaptic receptors (see Figure 5.6C,E). We conclude that lateral diffusion does provide a mechanism for supplying synapses with

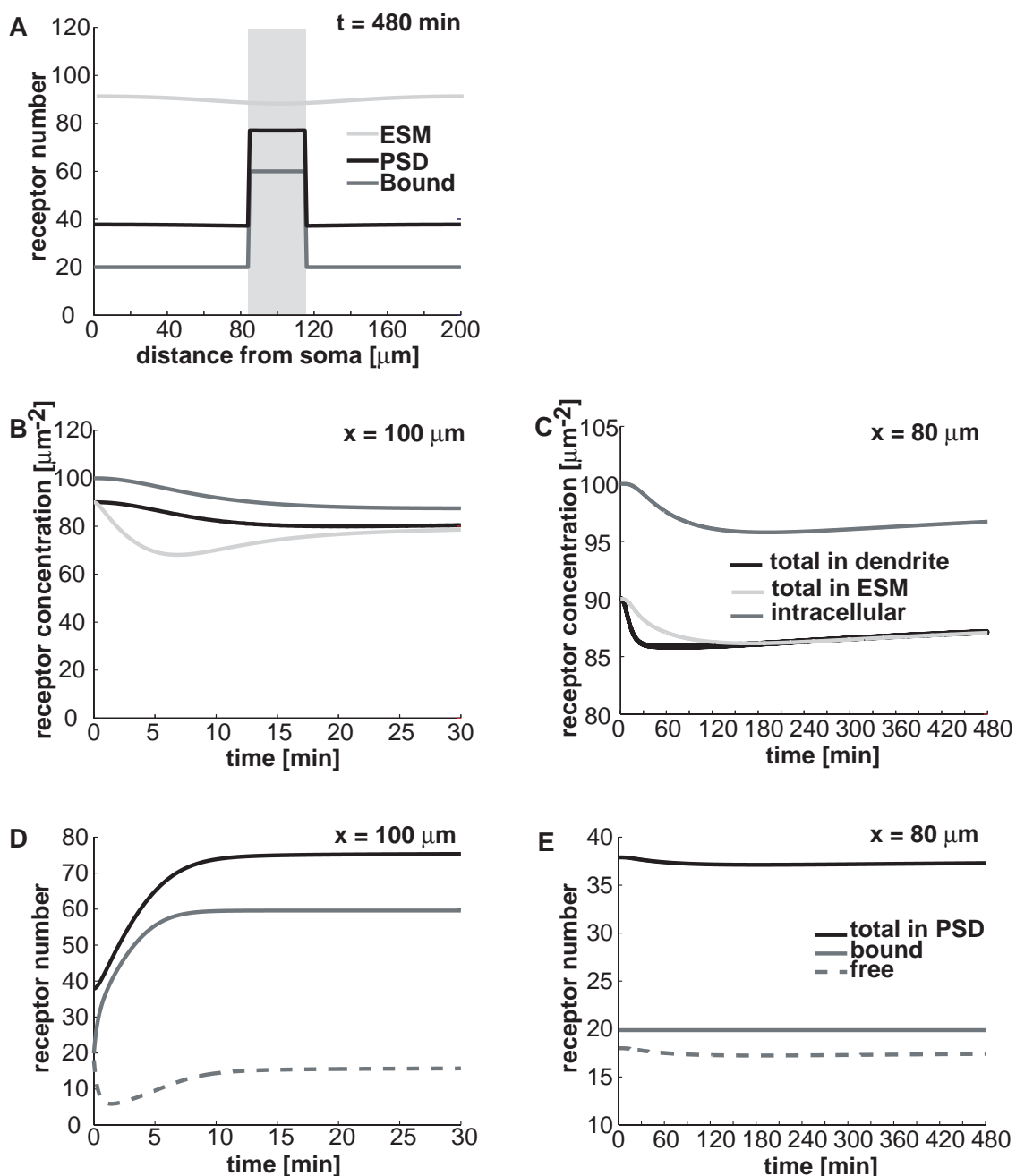


Figure 5.6. Time course of AMPA receptor trafficking during LTP. LTP is induced at time $t = 0$ from steady-state by inserting 40 scaffolding proteins into PSDs of spines located $85\text{--}115 \mu\text{m}$ from the soma (gray region in A). Spine parameters are as in Table 5.1, other parameters as in Figure 5.4. (A) Profiles 8 hrs after induction. PSD receptor numbers (black) doubled in induction region only. (B,C) Time course of dendritic (black), ESM (light gray), and intracellular (dark gray) receptors within ($x = 100 \mu\text{m}$) and outside ($x = 80 \mu\text{m}$) induction region. (D,E) Time course of total (black), free (solid gray) and bound (dashed gray) PSD receptor numbers for spines shown in B,C respectively.

additional receptors during LTP, but it tends to be slower than one based on exocytosis from intracellular pools, as can be seen by comparing Figure 5.6D with Figure 5.5D. The latter mechanism is more consistent with experimental findings [7, 40].

5.5.2 Long-term depression

At time $t = 0$ s we assume that the induction of LTD causes AMPA receptors in the PSD to begin changing their association from the stabilizing GRIP protein to the destabilizing PICK protein, as described by Equations (5.13)-(5.17), shown schematically in Figure 5.2C. The receptor-PICK complexes then unbind from scaffolding proteins, diffuse out of the PSD and are endocytosed; unoccupied scaffolding proteins are also removed from the PSD. The induction of LTD lasts 15 min, at the end of which receptors reassociate with GRIP and are stabilized in the PSD once again. The results of inducing LTD in a $30 \mu\text{m}$ wide region are shown in Figure 5.7, which was obtained by numerically solving Equations 5.1, 5.2, 5.6 and 5.13-5.17. In Figure 5.7A we plot receptor distributions 6 hrs after the induction of LTD. Noticeably, only those synapses in the induction region have been depressed, where a loss of 12 (32%) synaptic receptors is due to the loss of 12 (60%) scaffolding proteins. The time course of this depression is relatively fast, as is shown in Figure 5.7B,D. At the end of 15 min, AMPA receptors reassociate with GRIP and the number of synaptic receptors recovers during the next 10 min as these receptor-GRIP complexes bind to unoccupied scaffolding proteins in the PSD. However, there is not a full recovery of the baseline number of synaptic receptors due to the loss of some scaffolding proteins. Note that at synapses located $x = 84 \mu\text{m}$, which is only $1 \mu\text{m}$ outside the induction region, receptor numbers have hardly been affected (see Figure 5.7C,E). The lack of heterosynaptic effect is due to the fact that our method of LTD simulation does not include means whereby scaffolding protein numbers are altered outside the region of induction.

5.6 Discussion

In this chapter we presented a simplification of our multispine model of Chapter 4. This simplified multispine model allowed us to study how and to what extent the surface diffusion of AMPA receptors between synapses mediates non-local changes in synaptic AMPA receptor numbers. Indeed, we found that local changes in the constitutive recycling of AMPA receptors (i.e., changes in the rates of exo/endocytosis, intracellular production and degradation) can significantly alter the number of receptors

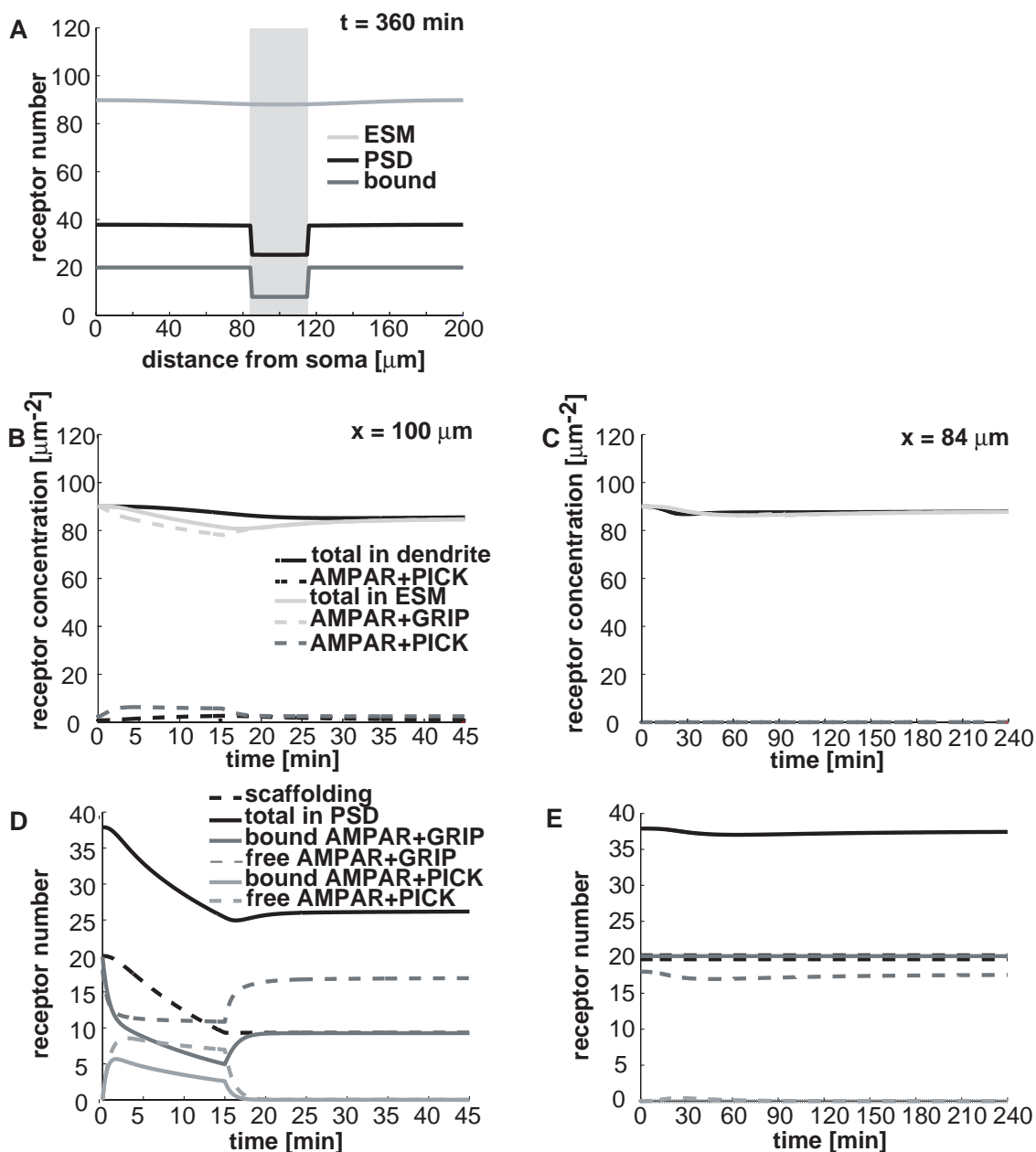


Figure 5.7. Time course of AMPA receptor trafficking during LTD. LTD is induced at time $t = 0$ from steady-state by increasing from zero the transition rate μ from GRIP-association to PICK-association within the PSD of spines located $85\text{--}115 \mu\text{m}$ from the soma (gray region in A), maintained for 15 min. The PICK complexes unbind from scaffolding and are internalized. Unoccupied scaffolding is also degraded during this period. Spine parameters are as in Tables 5.1 and 5.3; other parameter values as in Figure 5.4. (A) Profiles in PSD (black) and ESM (light gray) 6 hrs after induction. (B,C) Time course of dendritic (black) and extrasynaptic (gray) concentrations within ($x = 100 \mu\text{m}$) and outside ($x = 84 \mu\text{m}$) induction region. (D,E) Time course of synaptic receptors and scaffolding numbers for spines shown in B,C respectively.

at synapses many tens of micrometers away (see Figure 5.4). In contrast, changes in the binding/unbinding of AMPA receptors to/from PSD scaffolding proteins (i.e., changes in the binding/unbinding rates, scaffolding protein concentration and PSD surface area) have only a local effect. It is interesting to note that the long-lasting, activity-dependent changes associated with LTP/LTD at excitatory synapses are thought not to involve changes in constitutive recycling, but structural changes in the size of the spine and composition of the PSD (reviewed in [75]). Thus the contribution of AMPA receptor trafficking to LTP/LTD should be localized, as was confirmed in our simulations (see Figures 5.5-5.7). We also analyzed the claims of Adesnik et al. (2005) that, contrary to the prevailing view, 1) the delivery of synaptic AMPA receptors is only through the lateral diffusion of AMPA receptors exocytosed at the soma and 2) constitutive recycling is slow (see Figure 5.3). We found that while changes in the rate of recycling have a relatively small effect on the distribution of synaptic receptors, the passive transport of AMPA receptors from the soma via lateral diffusion insufficiently supplies distal synapses with receptors and requires far more time than the half-life of an AMPA receptor. Thus the local intracellular production of AMPA receptors, whether by microtubule-based vesicular transport or local synthesis, is crucial in delivering and maintaining sufficient synaptic receptor numbers.

We note that there are a number of other biophysical models of AMPA receptor regulation and its role in synaptic plasticity [16, 124, 123, 43, 122, 47, 150, 46]). These models have considered modifications in single channel conductances as well as changes in receptor number, but have tended to focus on single synapses or spines. None have considered the consequences of lateral diffusion between spines on synaptic AMPA receptor numbers. One of the interesting features of our multispine model is that the effects of lateral diffusion can be described mathematically in terms of an effective “cable” equation for receptor trafficking. This means that many of the mathematical and numerical techniques previously developed for studying the passive electrical properties of dendrites (see eg. [140, 25] can be applied to receptor trafficking, including the effects of branching and spatial inhomogeneities.

5.6.1 Maintenance of LTP/LTD

A prediction of both our single- and multispine models is that LTP/LTD can only persist if the scaffolding protein concentration is increased/decreased, otherwise the tran-

sient change in synaptic receptor numbers due to the induction of LTP/LTD cannot be maintained (see Earnshaw and Bressloff, 2006 and Figures 5.5-5.7). Indeed, our models support the “slot” protein hypothesis [121, 21, 75], which claims that a change in the number of “slots” (i.e., AMPA receptor binding sites) provided by PSD scaffolding proteins is essential for maintaining transient changes in synaptic receptor numbers. This is particularly true for LTP, where it is thought that a rise in the number of “slots” contributes to the transition from early- (<1 hr) to late-phase LTP (reviewed in [26]). Other known contributors to late-phase LTP are 1) new gene transcription and synthesis of PSD-related proteins such as receptor subunits and cytoskeletal proteins, 2) changes in the morphology of existing spines including increases in volume, surface area and the number of perforated synapses, and 3) the growth of new dendritic spines (reviewed in [62]). It is possible that the combination of enlarged spine and increased protein concentration is meant to maintain the increased number of “slot” proteins, thus ensuring the transition from early- to late-phase LTP [75]. In fact, it is possible that spine enlargement itself is the mechanism whereby synaptic AMPA receptor numbers are increased and maintained. For example, Matsuzaki et al. (2004) observed that the volume of spines, after being stimulated by the two-photon uncaging of a glutamate compound, follows a time-course typical of electrophysiological LTP recordings – a fast initial rise of volume to 300% of baseline, followed by a slower relaxation to 150-200% of the baseline volume. For simplicity our simulations of LTP/LTD do not include the dynamics of spine morphology nor of protein synthesis, nor do they take into account their role in maintaining scaffolding protein levels. This should not affect the validity of our results during the first 30-60 min of simulation, as most late-phase mechanisms are not evident during this time. For times longer than 1 hr, however, our simulations may not be accurate.

5.6.2 Sharing endosomes

Another simplification of our model is to assume that spines do not share intracellular stores of AMPA receptors. However, Cooney et al. (2002) found that endosomes, the intracellular compartments responsible for the sorting of receptors for recycling or degradation, can be shared by up to 20 spines. Including endosomal sharing in our model would create a potential source of heterosynaptic interaction that could affect our results on AMPA receptor trafficking. However, since the range of heterosynaptic

interactions arising from endosomal sharing ($\sim 10\text{-}20\ \mu\text{m}$) is relatively small compared to the interaction range of lateral AMPA receptor diffusion (entire length of dendritic cable), we expect its effects to be minimal in comparison. Nevertheless, it would be interesting to include endosomal sharing in a future model.

5.6.3 Spine morphology

As was mentioned earlier, spine morphology ranges a great deal, from mature spines with large bulbous heads and narrow necks to short stubby stalks and thin filopodial protrusions. In our model we have only included mature spines since these contain most excitatory synapses. Choosing our model in this way has implications for the heterosynaptic trafficking of AMPA receptors by lateral diffusion, since mature spines have narrow necks that serve to isolate their spine head and PSD from the background trafficking of AMPA receptors in the parent dendrite. In our model the parameter ω determines the rate at which receptors cross spine necks, and a preliminary calculation (see Section 6.1) yields

$$\omega \approx \frac{2\pi r_n D_n}{L_n}$$

where L_n and r_n are the average length and radius of the spine neck, respectively, and D_n is the diffusivity of AMPA receptors in the spine neck. In Section 3.4 we noted that for typical spine lengths and radii, $\omega \approx 7 \times 10^{-3} \mu\text{m}^2\text{s}^{-1}$. Thus on average it might take approximately 3 min for a receptor to cross the neck of a mature spine. A stubby spine might have a neck only a tenth as long and a radius twice as long, in which case a receptor would require only a few seconds to cross it. It is clear then that a population of stubby spines is much more susceptible to the heterosynaptic effects of lateral AMPA receptor diffusion than the populations of mature spines used in our simulations.

5.6.4 Homeostatic synaptic scaling

Experimental studies find that a chronic increase/decrease in average cortical activity induces a global and multiplicative scaling of synaptic AMPA receptor-mediated mEPSCs in the opposite direction, which can be attributed in part to a global modulation of synaptic AMPA receptor constitutive recycling [141, 95, 142, 24]. However, an examination of Equations (5.18)-(5.20) suggests that the steady-state number of synaptic AMPA receptors $N = a(P + Q)$ depends nonlinearly on all the parameters associated with constitutive recycling: the endocytic rate k , the production rate δ , and the rates

of recycling σ^{rec} and degradation σ^{deg} . If all spines are identical, globally scaling any of these parameters will affect the same change of N at all synapses, no matter how nonlinear its dependence. If, however, the spines are not identical, then globally scaling that parameter will not affect a proportionate change to N at all synapses and therefore will not appear to scale multiplicatively. Since spine properties are likely to vary a great deal across a dendrite, it seems unlikely that the observed global multiplicative scaling of AMPA receptor-mediated mEPSPs arises only from the simple up or down regulation of constitutive recycling.

CHAPTER 6

FUTURE DIRECTIONS

In this chapter we propose a number of directions our research on AMPA receptor trafficking could take. In each case the proposed research can be conducted either with the models presented in this thesis or after providing extensions to our current models.

6.1 Extension of spatial single-spine model

In Section 3.3 we presented a spatial model of AMPA receptor trafficking that treated the spine head as a uniform cylinder. The spatial extension of the spine neck was ignored, summarizing its effect on receptor diffusion by a spatial hopping rate ω . It would be interesting to analyze an extension of this spatial model that takes into account the curved geometry of the full spine, including the spine neck. Such a model would allow us to determine ω from first principles, which we now outline. For purposes of illustration let us assume that the spine neck is a uniform cylinder of length L_n and radius r_n . A reasonable estimate for ω is $j_n/U_n(0)$, where j_n is the steady-state flux of AMPA receptors through the junction of the spine neck and dendrite (or spine neck and head, the two should be the same in steady state), and $U_n(s)$ is the AMPA receptor concentration at $s \in [0, L_n]$. Here we are assuming that the junction of interest is at $s = L_n$. This estimate measures the steady-state rate at which the AMPA receptor concentration at the one end of the spine neck traverses the length of the spine neck per unit concentration. The AMPA receptor concentration U_n in the spine neck obeys the diffusion equation

$$\frac{\partial U_n}{\partial t} = D_n \frac{\partial^2 U_n}{\partial s^2}, \quad s \in (0, L_n). \quad (6.1)$$

where D_n is the diffusivity of receptors in the spine neck. We calculate j_n and U_n from the steady-state version of Equation 6.1 (i.e., with $\partial U_n/\partial t = 0$) with the boundary condition $U(L_n) = 0$. This absorbing boundary condition represents the fact that we are interested only in the rate at which AMPA receptors reach the junction. Integrating the steady-state version of Equation 6.1 twice we have

$$U_n(s) = \frac{j_n(L_n - s)}{2\pi r_n D_n} \quad (6.2)$$

and therefore

$$\omega = \frac{2\pi r_n D_n}{L_n}. \quad (6.3)$$

Using $L_n = 0.45$ and $r_n = 0.075\mu\text{m}$ [41] and $D_n = 6.7 \times 10^{-3}\mu\text{m}^2\text{s}^{-1}$ [3], we find that $\omega \approx 7 \times 10^{-3}\mu\text{m}^2\text{s}^{-1}$, which is 7x our baseline value.

6.2 Anomalous lateral diffusion of AMPA receptors at synapses

In Section 2.3 we noted that recent single-particle tracking experiments [132, 39] show the movement of AMPA receptors within the PSD to be subdiffusive. We can begin to think about the causes of this anomalous behavior by calculating the mean first passage time (MFPT) T for a single receptor to escape from a region Ω of the PSD. We derive T starting from the following system of Fokker-Planck equations

$$\frac{\partial p}{\partial t} = D\nabla^2 p + \nu\nabla \cdot (p\nabla\phi) - \alpha Zp + \beta q, \quad (6.4)$$

$$\frac{\partial q}{\partial t} = \alpha Zp - \beta q, \quad (6.5)$$

Here $p(\mathbf{r}, t|\mathbf{r}_0)$ and $q(\mathbf{r}, t|\mathbf{r}_0)$ denote the probability density for finding a single receptor in the free and bound state, respectively, at $(\mathbf{r}, t) \in \Omega \times [0, \infty)$ given that it was initially in the free state at \mathbf{r}_0 ; i.e., $p(\mathbf{r}, 0|\mathbf{r}_0) = \delta(\mathbf{r} - \mathbf{r}_0)$ and $q(\mathbf{r}, 0|\mathbf{r}_0) = 0$, where δ is the Dirac delta functional. A free receptor diffuses in Ω with diffusivity D , and can bind to and unbind from scaffolding proteins at rates α and β , respectively. We assume that the distribution of free scaffolding proteins can be described by a density function Z , and that the effect of trans- and submembranous obstacles can be summarized by a time-independent potential ϕ which imposes the advective velocity $-\nu\nabla\phi$ on free receptors (here ν is a constant with appropriate units). Note that all spatial derivatives are taken with respect to \mathbf{r} and not \mathbf{r}_0 . We take zero Dirichlet conditions on the boundary of Ω ; i.e., $p(\mathbf{r}, t|\mathbf{r}_0) = q(\mathbf{r}, t|\mathbf{r}_0) = 0$ for all $\mathbf{r} \in \partial\Omega$ and $t \geq 0$. Thus a receptor is removed from Ω upon reaching $\partial\Omega$, which represents the fact that we are only interested in the first time a receptor reaches this boundary.

Since the function

$$F(t|\mathbf{r}_0) = \int_{\Omega} [p(\mathbf{r}, t|\mathbf{r}_0) + q(\mathbf{r}, t|\mathbf{r}_0)] d\mathbf{r} \quad (6.6)$$

is the cumulative probability that a receptor is still in Ω at time $t \geq 0$, the function $-\partial F/\partial t$ is the probability density function for the time required to first reach $\partial\Omega$. Therefore, letting T depend on the initial position \mathbf{r}_0 , we have

$$T(\mathbf{r}_0) = - \int_0^\infty t \frac{\partial F(t|\mathbf{r}_0)}{\partial t} dt = \int_0^\infty F(t|\mathbf{r}_0) dt = \int_\Omega [\hat{p}(\mathbf{r}|\mathbf{r}_0) + \hat{q}(\mathbf{r}|\mathbf{r}_0)] d\mathbf{r}, \quad (6.7)$$

where $\hat{\cdot}$ denotes integration of t over the interval $[0, \infty)$. The integration by parts in the first line of Equation 6.7 and the change of the order of integration in the second line of the same equation are allowed because both p and q , being probability density functions, are L^1 functions in both time and space. Integrating Equations 6.4 and 6.5 we find

$$-\delta(\mathbf{r} - \mathbf{r}_0) = D\nabla^2 \hat{p} + \nu \nabla \cdot (\hat{p} \nabla \phi) - \alpha Z \hat{p} + \beta \hat{q}, \quad (6.8)$$

$$0 = \alpha Z \hat{p} - \beta \hat{q}. \quad (6.9)$$

By adding Equations 6.8 and 6.9 together and integrating the boundary condition $p(\mathbf{r}, t|\mathbf{r}_0) = 0$ we derive a stationary partial differential equation for \hat{p} :

$$-\delta(\mathbf{r} - \mathbf{r}_0) = D\nabla^2 \hat{p} + \nu \nabla \cdot (\hat{p} \nabla \phi), \quad \mathbf{r} \in \Omega \quad (6.10)$$

$$\hat{p}(\mathbf{r}|\mathbf{r}_0) = 0, \quad \mathbf{r} \in \partial\Omega. \quad (6.11)$$

Note that \hat{p} is the Green's function for the linear operator described in Equations 6.10 and 6.11. Having solved these equations for \hat{p} we calculate \hat{q} from Equation 6.9:

$$\hat{q} = \frac{\alpha Z}{\beta} \hat{p}. \quad (6.12)$$

Therefore

$$T(\mathbf{r}_0) = \int_\Omega \left(1 + \frac{\alpha Z}{\beta}\right) \hat{p}(\mathbf{r}|\mathbf{r}_0) d\mathbf{r}. \quad (6.13)$$

If the potential ϕ is constant, the first integral yields a term proportional to the mean squared displacement of the receptor, indicating Brownian diffusion. However, the second integral may provide an anomalous term since $\alpha Z/\beta$ need not be constant. In the case that the potential ϕ is not constant, both integrals may generate anomalous terms.

As an example of how to generate subdiffusive behavior within this model, assume for the moment that the potential ϕ is constant so that \hat{p} is the Green's function of Laplace's equation with zero Dirichlet boundary conditions. Because the PSD is roughly planar we assume that Ω is an open disc of radius L . We wish to calculate the MFPT for a receptor initially at the center of this disc, but due to the logarithmic singularity of the Green's

function at this point we cannot directly solve Equation 6.10. Instead we first solve the related problem

$$\frac{D}{r} \frac{\partial}{\partial r} \left(r \frac{\partial \hat{p}}{\partial r} \right) = -\frac{\delta(r-r_0)}{2\pi r_0}, \quad r, r_0 \in (0, L) \quad (6.14)$$

$$\hat{p}(L|r_0) = 0, \quad (6.15)$$

and then take the limit $r_0 \rightarrow 0$. Here we have modified the initial condition so that the receptor is initially a distance r_0 from the center of Ω with uniform probability. Supplementing Equations 6.14 and 6.15 with the natural condition that \hat{p} is finite at $r = 0$, we find

$$\hat{p}(r|r_0) = \frac{1}{2\pi D} \begin{cases} \ln(L/r_0), & r < r_0, \\ \ln(L/r), & r \geq r_0. \end{cases} \quad (6.16)$$

If $\alpha Z/\beta$ is constant, then

$$T(0) = \lim_{r_0 \rightarrow 0} \left(1 + \frac{\alpha Z}{\beta} \right) 2\pi \int_0^L r \hat{p}(r|r_0) dr = \left(1 + \frac{\alpha Z}{\beta} \right) \frac{L^2}{4D} = \frac{L^2}{4D_{eff}} \quad (6.17)$$

where

$$D_{eff} = \frac{D}{1 + \alpha Z/\beta}. \quad (6.18)$$

As expected, the presence of scaffolding proteins reduces the diffusivity of receptors. However, the relationship $T \propto L^2$ still holds and we conclude that a uniform distribution of scaffolding proteins produces effective Brownian diffusion. Now suppose that the scaffolding protein concentration increases from the center of Ω , say $Z(\mathbf{r}) = Z_0 r^a$ with $a, Z_0 > 0$, while α and β remain constant. Then

$$T(0) = \frac{L^2}{4D} + \frac{\alpha Z_0}{\beta} \frac{L^{2+a}}{(4 + 4a + a^2)D}. \quad (6.19)$$

On short length scales the first term in Equation 6.19 dominates this expression, and we again have Brownian diffusion. However, on longer length scales the second term of Equation 6.19 dominates and we find $T^{2/(2+a)} \propto L^2$; i.e, the macroscopic transport of receptors is subdiffusive since the coefficient $2/(2+a)$ is less than one. This transition from Brownian to subdiffusion as the mean squared displacement of the particle increases fits very well with the data from single-particle experiments [132, 39].

6.3 Intrinsic and extrinsic noise

In this thesis we represented AMPA receptor trafficking in terms of a system of kinetic equations describing the temporal variation in receptor concentrations. These concentrations determine the mean receptor number across a population of synapses. In order for

this to be a good description of trafficking at a single synapse, the number of receptors within the synapse has to be sufficiently large, else random fluctuations about the mean receptor number can become significant (typically the size of fluctuations varies as $N^{-1/2}$ where N is the number of receptors). One way to determine both the mean and variance of the receptor number is to replace the kinetic equations by a corresponding master equation [143], which describes the temporal evolution of the probability distribution for the location of a single receptor within the spine. For fixed values of the various trafficking parameters, the resulting fluctuations reflect the inherent stochasticity or “intrinsic noise” of receptor trafficking. Such a study was attempted by Holcman and Triller (2006) wherein a Markov model of the transitions of a single receptor between the free and bound states and entering and leaving the PSD was proposed. However, the modeling paradigm of Holcman and Triller (2006) is very different from that presented in this thesis, and some of the assumptions made in that paper are questionable (e.g., treatment of the PSD as concentric regions of free and bound scaffolding proteins). In addition to intrinsic noise, there are sources of fluctuations associated with the underlying biochemical processes that regulate the trafficking parameters, and these represent forms of “extrinsic noise.” It would be interesting to investigate the relative contributions of intrinsic and extrinsic noise to AMPA receptor trafficking within the postsynaptic membrane, possibly along lines analogous to a recent study of gene expression [130] based on the Linear Noise Approximation of Van Kampen (1992).

6.4 Discrete synaptic states

Recent work suggests that synaptic plasticity at excitatory synapses in the CNS occurs as a transition between discrete, electrophysiologically-defined states [89, 96], and that the transition is expressed through AMPA receptor trafficking. Montgomery and Madison (2004) define five such states: active, potentiated, depressed, silent, and recently silent. The *active* state displays both AMPA and NMDA receptor responses and can undergo only NMDA receptor-mediated LTP or LTD. The active state can transition into the potentiated, depressed or silent state. The *potentiated* state can be depotentiated (i.e., return to the active state) only through metabotropic glutamate receptor-mediated depression. The *depressed* state is currently ill-defined and may differ little from the active state. The *silent* state manifests NMDA receptor responses, but not AMPA receptor responses due to the lack of membrane-expressed postsynaptic AMPA

receptors. Silent synapses cannot be depressed (they are in a sense already depressed), but can be potentiated, leading to the *recently silent* state. The recently silent state shows both AMPA and NMDA receptor responses like the active state, but, unlike the active state, it cannot be depressed. The recently silent state spontaneously transitions into the active state approximately 30 minutes after being unsilenced. Montgomery and Madison (2004) argue that the discrete synaptic state model improves upon the continuum model of synaptic strength by increasing the information-carrying capacity of a synapse, since a synapse retains a history of recent state transitions, and by providing a wider range of dynamic responses to pre- and postsynaptic activity. In terms of discrete states, we have studied in this thesis the active state of a synapse and its transitions into the potentiated or depressed state. One can also study the other four synaptic states and their possible transitions within our modeling framework by assigning parameter behaviors in each case. For instance, the silent synaptic state could be realized by decreasing the type II exocytic rate and removing active binding sites, while the transition from the silent into the recently silent state can be simulated in a manner similar to our LTP simulations. Using similar techniques, our model can also be used to simulate the results of O'Connor et al. (2005) in which the potentiation/depotentiation of a large population of synapses can be decomposed into discrete, step-like transitions of single synapses. As these transitions appear to occur stochastically, the modeling approach describing in Section 6.3 is particularly suited to exploring this data.

REFERENCES

- [1] H. D. I. ABARBANEL, R. HUERTA, AND M. I. RABINOVICH, *Dynamical model of long-term synaptic plasticity*, PNAS, 99 (2002), pp. 10132–10137.
- [2] H. ADESNIK, R. A. NICOLL, AND P. M. ENGLAND, *Photoinactivation of native ampa receptors reveals their real-time trafficking*, Neuron, 48 (2005), pp. 977–985.
- [3] M. C. ASHBY, S. R. MAIER, A. NISHIMUNE, AND J. M. HENLEY, *Lateral diffusion drives constitutive exchange of ampa receptors at dendritic spines and is regulated by spine morphology*, J. Neurosci., 26 (2006), pp. 7046–7055.
- [4] T. G. BANKE, D. BOWIE, H.-K. LEE, R. L. HUGANIR, A. SCHOUSBOE, AND S. F. TRAYNELIS, *Control of glur1 ampa receptor function by camp-dependent protein kinase*, J. Neurosci., 20 (2000), pp. 89–102.
- [5] E. C. BEATTIE, R. C. CARROLL, X. YU, W. MORISHITA, H. YASUDA, M. VON ZASTROW, AND R. C. MALENKA, *Regulation of ampa receptor endocytosis by a signaling mechanism shared with ltd*, Nat. Neurosci., 3 (2000), pp. 1291–1300.
- [6] T. A. BLANPIED, D. B. SCOTT, AND M. D. EHLERS, *Dynamics and regulation of clathrin coats at specialized endocytic zones of dendrites and spines*, Neuron, 36 (2002), pp. 435–449.
- [7] T. V. BLISS AND T. LOMO, *Long-lasting potentiation of synaptic transmission in the dentate area of the anaesthetized rabbit following stimulation of the perforant path.*, J. Physiol., 232 (1973), pp. 331–356.
- [8] T. V. P. BLISS AND G. L. COLLINGRIDGE, *A synaptic model of memory: long-term potentiation in the hippocampus*, Nature, 361 (1993), pp. 31–39.
- [9] A. J. BORGDORFF AND D. CHOQUET, *Regulation of ampa receptor lateral movements*, Nature, 417 (2002), pp. 649–653.
- [10] D. S. BREDT AND R. A. NICOLL, *Ampa receptor trafficking at excitatory synapses*, Neuron, 40 (2003), pp. 361–379.
- [11] P. C. BRESSLOFF, *Stochastic model of protein receptor trafficking prior to synaptogenesis*, Phys. Rev. E, 74 (2006), pp. 031910–+.
- [12] P. C. BRESSLOFF AND B. A. EARNSHAW, *Diffusion-trapping model of receptor trafficking in dendrites*, Phys. Rev. E, 75 (2007), pp. 041915–+.
- [13] R. C. CARROLL, E. C. BEATTIE, M. VON ZASTROW, AND R. C. MALENKA, *Role of ampa receptor endocytosis in synaptic plasticity*, Nat. Rev. Neurosci., 2 (2001), pp. 315–324.

- [14] R. C. CARROLL, E. C. BEATTIE, H. XIA, C. LUSCHER, Y. ALTSCHULER, R. A. NICOLL, R. C. MALENKA, AND M. VON ZASTROW, *Dynamin-dependent endocytosis of ionotropic glutamate receptors*, PNAS, 96 (1999), pp. 14112–14117.
- [15] R. C. CARROLL, D. V. LISSIN, R. A. VON ZASTROW, R. A. NICOLL, AND R. C. MALENKA, *Rapid redistribution of glutamate receptors contributes to long-term depression in hippocampal cultures*, Nat. Neurosci., 2 (1999), pp. 454–460.
- [16] G. C. CASTELLANI, E. M. QUINLAN, L. N. COOPER, AND H. Z. SHOUVAL, *A biophysical model of bidirectional synaptic plasticity: Dependence on ampa and nmda receptors*, PNAS, 98 (2001), pp. 12772–12777.
- [17] L. CHEN, D. M. CHETKOVICH, R. S. PETRALIA, N. T. SWEENEY, Y. KAWASAKI, R. J. WENTHOLD, D. S. BREDDT, AND R. A. NICOLL, *Stargazin regulates synaptic targeting of ampa receptors by two distinct mechanisms*, Nature, 408 (2000), pp. 936–943.
- [18] L. CHEN, T. TRACY, AND C. I. NAM, *Dynamics of postsynaptic glutamate receptor targeting*, Curr. Opin. Neurobiol., 17 (2006), pp. 53–38.
- [19] D. CHOQUET AND A. TRILLER, *The role of receptor diffusion in the organization of the postsynaptic membrane*, Nat. Rev. Neurosci., 4 (2003), pp. 251–265.
- [20] H. J. CHUNG, J. XIA, R. H. SCANNEVIN, X. ZHANG, AND R. L. HUGANIR, *Phosphorylation of the ampa receptor subunit glur2 differentially regulates its interaction with pdz domain-containing proteins*, J. Neurosci., 20 (2000), pp. 7258–7267.
- [21] M. COLLEDGE, E. M. SNYDER, R. A. CROZIER, J. A. SODERLING, Y. JIN, L. K. LANGEBERG, H. LU, M. F. BEAR, AND J. D. SCOTT, *Ubiquitination regulates psd-95 degradation and ampa receptor surface expression*, Neuron, 40 (2003), pp. 595–607.
- [22] G. L. COLLINGRIDGE, J. T. R. ISAAC, AND Y. T. WANG, *Receptor trafficking and synaptic plasticity*, Nat. Rev. Neurosci., 5 (2004), pp. 952–962.
- [23] J. R. COTTRELL, G. R. DUBE, C. EGLES, AND G. LIU, *Distribution, density, and clustering of functional glutamate receptors before and after synaptogenesis in hippocampal neurons*, J. Neurophysiol., 84 (2000), pp. 1573–1587.
- [24] G. W. DAVIS, *Homeostatic control of neural activity: From phenomenology to molecular design*, Annu. Rev. Neurosci., 29 (2006), pp. 307–323.
- [25] P. DAYAN AND L. F. ABBOTT, *Theoretical Neuroscience: Computational and Mathematical Modeling of Neural Systems*, The MIT Press, December 2001.
- [26] V. A. DERKACH, M. C. OH, E. S. GUIRE, AND T. R. SODERLING, *Regulatory mechanisms of ampa receptors in synaptic plasticity*, Nat. Rev. Neurosci., 8 (2007), pp. 101–113.
- [27] R. DINGLEDINE, K. BORGES, D. BOWIE, AND S. F. TRAYNELIS, *The glutamate receptor ion channels*, Pharmacol. Rev., 51 (1999), pp. 7–62.

- [28] S. DUDEK AND M. BEAR, *Bidirectional long-term modification of synaptic effectiveness in the adult and immature hippocampus*, J. Neurosci., 13 (1993), pp. 2910–2918.
- [29] S. M. DUDEK AND M. F. BEAR, *Homosynaptic long-term depression in area ca1 of hippocampus and effects of n-methyl-d-aspartate receptor blockade*, PNAS, 89 (1992), pp. 4363–4367.
- [30] B. A. EARNSHAW AND P. C. BRESSLOFF, *Biophysical model of ampa receptor trafficking and its regulation during long-term potentiation/long-term depression*, J. Neurosci., 26 (2006), pp. 12362–12373.
- [31] M. D. EHLERS, *Reinsertion or degradation of ampa receptors determined by activity-dependent endocytic sorting*, Neuron, 28 (2000), pp. 511–525.
- [32] ———, *Activity level controls postsynaptic composition and signaling via the ubiquitin-proteasome system*, Nat. Neurosci., 6 (2003), pp. 231–242.
- [33] A. E.-D. EL-HUSSEINI, E. SCHNELL, D. M. CHETKOVICH, R. A. NICOLL, AND D. S. BREDET, *Psd-95 involvement in maturation of excitatory synapses*, Science, 290 (2000), pp. 1364–1368.
- [34] A. E.-D. EL-HUSSEINI, E. SCHNELL, S. DAKOJI, N. SWEENEY, Q. ZHOU, O. PRANGE, C. GAUTHIER-CAMPBELL, A. AGUILERA-MORENO, R. A. NICOLL, AND D. S. BREDET, *Synaptic strength regulated by palmitate cycling on psd-95*, Cell, 108 (2002), pp. 849–863.
- [35] F. ENGERT AND T. BONHOEFFER, *Synapse specificity of long-term potentiation breaks down at short distances*, Nature, 388 (1997), pp. 279–284.
- [36] J. A. ESTEBAN, *Ampa receptor trafficking: a road map for synaptic plasticity*, Molecular Interventions, 3 (2003), pp. 375–385.
- [37] R. M. FITZSIMONDS, H.-J. SONG, AND M.-M. POO, *Propagation of activity-dependent synaptic depression in simple neural networks*, Nature, 388 (1997), pp. 439–448.
- [38] K. M. FRANKS AND T. J. SEJNOWSKI, *Complexity of calcium signaling in synaptic spines*, BioEssays, 24 (2002), pp. 1130–1144.
- [39] L. GROC, M. HEINE, L. COGNET, K. BRICKLEY, F. A. STEPHENSON, B. LOUNIS, AND D. CHOQUET, *Differential activity-dependent regulation of the lateral mobilities of ampa and nmda receptors*, Nat. Neurosci., 7 (2004), pp. 695–696.
- [40] E. HANSE AND B. GUSTAFSSON, *Postsynaptic, but not presynaptic, activity controls the early time course of long-term potentiation in the dentate gyrus*, J. Neurosci., 12 (1992), pp. 3226–3240.
- [41] K. HARRIS AND J. STEVENS, *Dendritic spines of ca 1 pyramidal cells in the rat hippocampus: serial electron microscopy with reference to their biophysical characteristics*, J. Neurosci., 9 (1989), pp. 2982–2997.
- [42] Y. HAYASHI, S.-H. SHI, J. A. ESTEBAN, A. PICCINI, J.-C. PONCER, AND R. MALINOW, *Driving ampa receptors into synapses by ltp and camkii: Requirement for glur1 and pdz domain interaction*, Science, 287 (2000), pp. 2262–2267.

- [43] A. HAYER AND U. S. BHALLA, *Molecular switches at the synapse emerge from receptor and kinase traffic*, PLoS Comput. Biol., 1 (2005), pp. 0137–0154.
- [44] J. HENLEY, *Surface expression and metabolic half-life of ampa receptors in cultured rat cerebellar granule cells*, Neuropharm., 37 (1998), pp. 1345–1353.
- [45] D. HOLCMAN AND Z. SCHUSS, *Escape through a small opening: Receptor trafficking in a synaptic membrane*, J. Stat. Phys., 117 (2004), pp. 975+.
- [46] D. HOLCMAN AND A. TRILLER, *Modeling synaptic dynamics driven by receptor lateral diffusion*, Biophys. J., 91 (2006), pp. 2405–2415.
- [47] W. R. HOLMES AND L. M. GROVER, *Quantifying the magnitude of changes in synaptic level parameters with long-term potentiation*, J. Neurophysiol., 96 (2006), pp. 1478–1491.
- [48] B. D. HUGHES, *Random Walks and Random Environments*, Clarendon Press, 1995.
- [49] A. INOUE AND S. OKABE, *The dynamic organization of postsynaptic proteins: translocating molecules regulate synaptic function*, Current Opinion in Neurobiology, 13 (2003), pp. 332–340.
- [50] W. JU, W. MORISHITA, J. TSUI, G. GAETTA, T. J. DEERINCK, S. R. ADAMS, C. C. GARNER, R. Y. TSIEN, M. H. ELLISMAN, AND R. C. MALENKA, *Activity-dependent regulation of dendritic synthesis and trafficking of ampa receptors*, Nat. Neurosci., 7 (2004), pp. 244–253.
- [51] E. R. KANDEL, *The molecular biology of memory storage: A dialogue between genes and synapses*, Science, 294 (2001), pp. 1030–1038.
- [52] E. R. KANDEL, J. H. SCHWARTZ, AND T. M. JESSELL, *Principles of Neural Science*, McGraw-Hill Medical, January 2000.
- [53] U. R. KARMARKAR AND D. V. BUONOMANO, *A model of spike-timing dependent plasticity: One or two coincidence detectors?*, J. Neurophysiol., 88 (2002), pp. 507–513.
- [54] H. KASAI, M. MATSUZAKI, J. NOGUCHI, N. YASUMATSU, AND H. NAKAHARA, *Structure-stability-function relationships of dendritic spines*, Trends Neurosci., 26 (July 2003), pp. 360–368(9).
- [55] R. J. KELLEHER, A. GOVINDARAJAN, AND S. TONEGAWA, *Translational regulatory mechanisms in persistent forms of synaptic plasticity*, Neuron, 44 (2004), pp. 59–73.
- [56] M. J. KENNEDY AND M. D. EHLERS, *Organelles and trafficking machinery for postsynaptic plasticity*, Annu. Rev. Neurosci., 29 (2006), pp. 325–362.
- [57] C.-H. KIM, H. J. CHUNG, H.-K. LEE, AND R. L. HUGANIR, *Interaction of the ampa receptor subunit *glur2/3* with *pdz* domains regulates hippocampal long-term depression*, PNAS, 98 (2001), pp. 11725–11730.

- [58] C.-H. KIM AND J. E. LISMAN, *A labile component of ampa receptor-mediated synaptic transmission is dependent on microtubule motors, actin, and n-ethylmaleimide-sensitive factor*, J. Neurosci., 21 (2001), pp. 4188–4194.
- [59] T. KITAJIMA AND K. HARA, *A generalized hebbian rule for activity-dependent synaptic modifications*, Neural Networks, 13 (2000), pp. 445–454.
- [60] A. B. KOLOMEISKY AND M. E. FISHER, *Extended kinetic models with waiting-time distributions: Exact results*, J. Chem. Phys., 113 (2000), pp. 10867–10877.
- [61] S. KONUR, D. RABINOWITZ, V. L. FENSTERMAKER, AND R. YUSTE, *Systematic regulation of spine sizes and densities in pyramidal neurons*, J. Neurobiol., 56 (2003), pp. 95–112.
- [62] R. LAMPRECHT AND J. LEDOUX, *Structural plasticity and memory*, Nat. Rev. Neurosci., 5 (2004), pp. 45–54.
- [63] D. LAUFFENBERGER AND J. LINDERMAN, *Receptors: models for binding, trafficking and signaling*, Oxford University Press, 1993.
- [64] H. LEE, K. KAMEYAMA, R. L. HUGANIR, , AND M. F. BEAR, *Nmda induces long-term synaptic depression and dephosphorylation of the glur1 subunit of ampa receptors in hippocampus*, Neuron, 21 (1998), pp. 1151–1162.
- [65] H.-K. LEE, M. BARBAROSIE, K. KAMEYAMA, M. F. BEAR, AND R. L. HUGANIR, *Regulation of distinct ampa receptor phosphorylation sites during bidirectional synaptic plasticity*, Nature, 405 (2000), pp. 955–959.
- [66] H.-K. LEE, K. TAKAMIYA, J.-S. HAN, H. MAN, C.-H. KIM, G. RUMBAUGH, S. YU, L. DING, C. HE, R. S. PETRALIA, R. J. WENTHOLD, M. GALLAGHER, AND R. L. HUGANIR, *Phosphorylation of the ampa receptor glur1 subunit is required for synaptic plasticity and retention of spatial memory*, Cell, 112 (2003), pp. 631–643.
- [67] S. H. LEE, L. LIU, Y. T. WANG, AND M. SHENG, *Clathrin adaptor ap2 and nsf interact with overlapping sites of glur2 and play distinct roles in ampa receptor trafficking and hippocampal ltd*, Neuron, 36 (2002), pp. 661–674.
- [68] J. W. LIN, W. JU, K. FOSTER, S. H. LEE, G. AHMADIAN, M. WYSZYNSKI, Y. T. WANG, AND M. SHENG, *Distinct molecular mechanisms and divergent endocytotic pathways of ampa receptor internalization*, Nat. Neurosci., 3 (2000), pp. 1282–1290.
- [69] J. LISMAN, *Long-term potentiation: outstanding questions and attempted synthesis*, Philos. Trans. R. Soc. Lond. B Biol. Sci., 358 (2003), pp. 829–842.
- [70] J. LISMAN, H. SCHULMAN, AND H. CLINE, *The molecular basis of camkii function in synaptic and behavioural memory.*, Nat. Rev. Neurosci., 3 (2002), pp. 175–190.
- [71] J. E. LISMAN AND A. M. ZHABOTINSKY, *A model of synaptic memory: a camkii/pp1 switch that potentiates transmission by organizing an ampa receptor anchoring assembly*, Neuron, 31 (2001), pp. 191–201.

- [72] W. LU AND E. B. ZIFF, *Pick1 interacts with abp/grip to regulate ampa receptor trafficking*, *Neuron*, 47 (2005), pp. 407–421.
- [73] C. LUSCHER, H. XIA, E. C. BEATTIE, R. C. CARROLL, M. VON ZASTROW, R. C. MALENKA, AND R. A. NICOLL, *Role of ampa receptor cycling in synaptic transmission and plasticity*, *Neuron*, 24 (1999), pp. 649–658.
- [74] G. S. LYNCH, T. DUNWIDDLE, AND G. V., *Heterosynaptic depression: a postsynaptic correlate of long-term potentiation*, *Nature*, 266 (1977), pp. 737–739.
- [75] R. C. MALENKA AND M. F. BEAR, *Ltp and ltd: An embarrassment of riches*, *Neuron*, 44 (2004), pp. 5–21.
- [76] R. C. MALENKA AND R. A. NICOLL, *Long-term potentiation—a decade of progress?*, *Science*, 285 (1999), pp. 1870–1874.
- [77] R. MALINOW, *Ampa receptor trafficking and long-term potentiation*, *Philos. Trans. R. Soc. Lond. B Biol. Sci.*, 358 (2003), pp. 707–714.
- [78] R. MALINOW AND R. C. MALENKA, *Ampa receptor trafficking and synaptic plasticity*, *Annu. Rev. Neurosci.*, 25 (2002), pp. 103–126.
- [79] H.-Y. MAN, J. W. LIN, W. H. JU, G. AHMADIAN, L. LIU, L. E. BECKER, M. SHENG, AND Y. T. WANG, *Regulation of ampa receptor-mediated synaptic transmission by clathrin-dependent receptor internalization*, *Neuron*, 25 (2000), pp. 649–662.
- [80] M. MARIN-PADILLA, *Number and distribution of the apical dendritic spines of the layer v pyramidal cells in man*, *J. Comp. Neurol.*, 131 (1967), pp. 475–489.
- [81] S. J. MARTIN, P. D. GRIMWOOD, AND R. G. M. MORRIS, *Synaptic plasticity and memory: An evaluation of the hypothesis*, *Annu. Rev. Neurosci.*, 23 (2000), pp. 649–711.
- [82] S. J. MARTIN AND R. G. M. MORRIS, *New life in an old idea: The synaptic plasticity and memory hypothesis revisited*, *Hippocampus*, 12 (2002), pp. 609–636.
- [83] MATLAB, *Partial Differential Equation Toolbox, User's Guide*, The Mathworks, Inc., Natick. Mass., 1996.
- [84] S. MATSUDA, T. LAUNNEY, S. MIKAWA, AND H. HIRAI, *Disruption of ampa receptor glur2 clusters following long-term depression induction in cerebellar purkinje neurons*, *EMBO J.*, 19 (2000), pp. 2765–1774.
- [85] A. MATUS, *Actin-based plasticity in dendritic spines*, *Science*, 290 (2000), pp. 754–758.
- [86] D. MAUCERI, F. CATTABENI, M. DI LUCA, AND F. GARDONI, *Calcium/calmodulin-dependent protein kinase ii phosphorylation drives synapse-associated protein 97 into spines*, *J. Biol. Chem.*, 279 (2004), pp. 23813–23821.
- [87] M. L. MAYER AND N. ARMSTRONG, *Structure and function of glutamate receptor ion channels*, *Annu. Rev. Physiol.*, 66 (2004), pp. 161–181.

- [88] S. G. MCCORMACK, R. L. STORNETTA, AND J. J. ZHU, *Synaptic ampa receptor exchange maintains bidirectional plasticity*, *Neuron*, 50 (2006), pp. 75–8.
- [89] J. M. MONTGOMERY AND D. V. MADISON, *State-dependent heterogeneity in synaptic depression between pyramidal cell pairs*, *Neuron*, 33 (2002), pp. 765–777.
- [90] R. MULKEY, C. HERRON, AND R. MALENKA, *An essential role for protein phosphatases in hippocampal long-term depression*, *Science*, 261 (1993), pp. 1051–1055.
- [91] R. M. MULKEY, S. ENDO, S. SHENOLIKAR, AND R. C. MALENKA, *Involvement of a calcineurin/ inhibitor-1 phosphatase cascade in hippocampal long-term depression*, *Nature*, 369 (1994), pp. 486–488.
- [92] V. N. MURTHY, *Synaptic plasticity: Neighborhood influences*, *Curr. Biol.*, 7 (1997), pp. 512–515.
- [93] E. A. NIMCHINSKY, B. L. SABATINI, AND K. SVOBODA, *Structure and function of dendritic spines*, *Annu. Rev. Physiol.*, 64 (2002), pp. 313–353.
- [94] Z. NUSSER, R. LUJAN, G. LAUBE, J. D. ROBERTS, E. MOLNAR, AND P. SOMOGYI, *Cell type and pathway dependence of synaptic ampa receptor number and variability in the hippocampus.*, *Neuron*, 21 (1998), pp. 545–559.
- [95] R. J. O’BRIEN, S. KAMBOJ, M. D. EHLERS, K. R. ROSEN, , G. D. FISCHBACH, AND R. L. HUGANIR, *Activity-dependent modulation of synaptic ampa receptor accumulation*, *Neuron*, 21 (1998), pp. 1067–1078.
- [96] D. H. O’CONNOR, G. M. WITTENBERG, AND S. S.-H. WANG, *Graded bidirectional synaptic plasticity is composed of switch-like unitary events*, *PNAS*, 102 (2005), pp. 9679–9684.
- [97] S. OKABE, H.-D. KIM, A. MIWA, T. KURIU, AND H. OKADO, *Continual remodeling of postsynaptic density and its regulation by synaptic activity*, *Nat. Neurosci.*, 2 (1999), pp. 804–811.
- [98] C. L. PALMER, L. COTTON, AND J. M. HENLEY, *The molecular pharmacology and cell biology of alpha-amino-3-hydroxy-5-methyl-4-isoxazolepropionic acid receptors*, *Pharmacol. Rev.*, 57 (2005), pp. 253–277.
- [99] M. PARK, E. C. PENICK, J. G. EDWARDS, J. A. KAUER, AND M. D. EHLERS, *Recycling endosomes supply ampa receptors for ltp*, *Science*, 305 (2004), pp. 1972–1975.
- [100] M. PASSAFARO, V. PIACH, AND M. SHENG, *Subunit-specific temporal and spatial patterns of ampa receptor exocytosis in hippocampal neurons.*, *Nat Neurosci.*, 4 (2001), pp. 917–926.
- [101] J. L. PEREZ, L. KHATRI, C. CHANG, S. SRIVASTAVA, P. OSTEN, AND E. B. ZIFF, *Pick1 targets activated protein kinase calpha to ampa receptor clusters in spines of hippocampal neurons and reduces surface levels of the ampa-type glutamate receptor subunit 2*, *J. Neurosci.*, 21 (2001), pp. 5417–5428.

- [102] C. C. PETERSEN, R. C. MALENKA, R. A. NICOLL, AND J. J. HOPFIELD, *All-or-none potentiation at $ca3$ - $ca1$ synapses*, PNAS, 95 (1998), pp. 4732–4737.
- [103] J. P. PIERCE, K. VAN LEYEN, AND J. B. MCCARTHY, *Translocation machinery for synthesis of integral membrane and secretory proteins in dendritic spines*, Nat. Neurosci., 3 (2000), pp. 311–313.
- [104] J. C. PONCER, J. A. ESTEBAN, AND R. MALINOW, *Multiple mechanisms for the potentiation of ampa receptor-mediated transmission by alpha - $ca2+$ /calmodulin-dependent protein kinase ii*, J. Neurosci., 22 (2002), pp. 4406–4411.
- [105] L. F. QUENZER AND R. S. FELDMAN, *Fundamentals of Neuropsychopharmacology*, Sinauer Associates Inc., 1984.
- [106] W. RALL, *Theory of physiological properties of dendrites.*, Ann. NY Acad. Sci., 96 (1962), pp. 1071–1092.
- [107] S. ROYER AND D. PARE, *Conservation of total synaptic weight through balanced synaptic depression and potentiation*, Nature, 422 (2003), pp. 518–522.
- [108] J. E. RUBIN, R. C. GERKIN, G.-Q. BI, AND C. C. CHOW, *Calcium time course as a signal for spike-timing-dependent plasticity*, J. Neurophysiol., 93 (2005), pp. 2600–2613.
- [109] J. RUBINSTEIN AND S. TORQUATO, *Diffusion-controlled reactions: Mathematical formulation, variational principles, and rigorous bounds*, J. Chem. Phys., 88 (1988), pp. 6372–6380.
- [110] J. R. SANES AND J. W. LICHTMAN, *Can molecules explain long-term potentiation?*, Nat. Neurosci., 2 (1999), pp. 597–604.
- [111] R. H. SCANNEVIN AND R. L. HUGANIR, *Postsynaptic organization and regulation of excitatory synapses*, Nat. Rev. Neurosci., 1 (2000), pp. 133–141.
- [112] M. SCANZIANI, R. C. MALENKA, AND R. A. NICOLL, *Role of intercellular interactions in heterosynaptic long-term depression*, Nature, 380 (1996), pp. 446–450.
- [113] H. SCHER AND E. W. MONTROLL, *Anomalous transit-time dispersion in amorphous solids*, Phys. Rev. B, 12 (1975), pp. 2455–2477.
- [114] E. SCHNELL, M. SIZEMORE, S. KARIMZADEGAN, L. CHEN, D. S. BREDT, AND R. A. NICOLL, *Direct interactions between $psd-95$ and stargazin control synaptic ampa receptor number*, PNAS, 99 (2002), pp. 13902–13907.
- [115] E. SCHUMAN AND D. MADISON, *Locally distributed synaptic potentiation in the hippocampus*, Science, 263 (1994), pp. 532–536.
- [116] M. SETOU, D.-H. SEOG, Y. TANAKA, Y. KANAI, Y. TAKEI, M. KAWAGISHI, AND N. HIROKAWA, *Glutamate-receptor-interacting protein $grip1$ directly steers kinesin to dendrites*, Nature, 417 (2002), pp. 83–87.
- [117] L. SHEN, F. LIANG, L. D. WALENSKY, AND R. L. HUGANIR, *Regulation of ampa receptor $glur1$ subunit surface expression by a $4.1n$ -linked actin cytoskeletal association*, J. Neurosci., 20 (2000), pp. 7932–7940.

- [118] M. SHENG, *Molecular organization of the postsynaptic specialization*, PNAS, 98 (2001), pp. 7058–7061.
- [119] M. SHENG AND M. J. KIM, *Postsynaptic signaling and plasticity mechanisms*, Science, 298 (2002), pp. 776–780.
- [120] M. SHENG AND S. H. LEE, *Ampa receptor trafficking and the control of synaptic transmission*, Cell, 105 (2001), pp. 825–828.
- [121] S.-H. SHI, Y. HAYASHI, J. A. ESTEBAN, AND R. MALINOW, *Subunit-specific rules governing ampa receptor trafficking to synapses in hippocampal pyramidal neurons*, Cell, 105 (2001), pp. 331–343.
- [122] H. Z. SHOUVAL, *Clusters of interacting receptors can stabilize synaptic efficacies*, PNAS, 102 (2005), pp. 14440–14445.
- [123] H. Z. SHOUVAL, M. F. BEAR, AND L. N. COOPER, *A unified model of nmda receptor-dependent bidirectional synaptic plasticity*, PNAS, 99 (2002), pp. 10831–10836.
- [124] H. Z. SHOUVAL, G. C. CASTELLANI, B. S. BLAIS, L. C. YEUNG, AND L. N. A. COOPER, *Converging evidence for a simplified biophysical model of synaptic plasticity*, Biol. Cyber., 87 (2002), pp. 383–391.
- [125] I. SONG AND R. L. HUGANIR, *Regulation of ampa receptors during synaptic plasticity*, Trends Neurosci., 25 (2002), pp. 578–588.
- [126] K. E. SORRA AND K. M. HARRIS, *Overview on the structure, composition, function, development, and plasticity of hippocampal dendritic spines*, Hippocampus, 10 (2000), pp. 501–511.
- [127] J. P. STEINBERG, K. TAKAMIYA, Y. SHEN, J. XIA, M. E. RUBIO, S. YU, W. JIN, G. M. THOMAS, D. J. LINDEN, AND R. L. HUGANIR, *Targeted in vivo mutations of the ampa receptor subunit glur2 and its interacting protein pick1 eliminate cerebellar long-term depression*, Neuron, 49 (2006), pp. 845–860.
- [128] R. STRAUBE, M. J. WARD, AND M. FALCKE, *Reaction rate of small diffusing molecules on a cylindrical membrane*, J. Stat. Phys., (2007).
- [129] M. A. SUTTON AND E. M. SCHUMAN, *Local translational control in dendrites and its role in long-term synaptic plasticity*, J. Neurobiol., 64 (2005), pp. 116–131.
- [130] P. S. SWAIN, M. B. ELWITZ, AND E. D. SIGGIA, *Intrinsic and extrinsic contributions to stochasticity in gene expression*, PNAS, 99 (2002), pp. 12795–12800.
- [131] J.-I. TANAKA, M. MATSUZAKI, E. TARUSAWA, A. MOMIYAMA, E. MOLNAR, H. KASAI, AND R. SHIGEMOTO, *Number and density of ampa receptors in single synapses in immature cerebellum*, J. Neurosci., 25 (2005), pp. 799–807.
- [132] C. TARDIN, L. COGNET, C. BATS, B. LOUNIS, AND D. CHOQUET, *Direct imaging of lateral movements of ampa receptors inside synapses*, EMBO J., 22 (2003), pp. 4656–4665.

- [133] D. B. TIKHONOV, J. R. MELLOR, P. N. R. USHERWOOD, AND L. G. MAGAZANIK, *Modeling of the pore domain of the *glur1* channel: Homology with k^+ channel and binding of channel blockers*, *Biophys. J.*, 82 (2002), pp. 1884–1893.
- [134] S. TOMITA, H. ADESNIK, M. SEKIGUCHI, W. ZHANG, K. WADA, J. R. HOWE, R. A. NICOLL, AND D. S. BREDT, *Stargazin modulates ampa receptor gating and trafficking by distinct domains*, *Nature*, (2005), pp. 1052–1058.
- [135] S. TOMITA, M. FUKATA, R. A. NICOLL, AND D. S. BREDT, *Dynamic interaction of stargazin-like tarps with cycling ampa receptors at synapses*, *Science*, 303 (2004), pp. 1508–1511.
- [136] S. TOMITA, V. STEIN, T. J. STOCKER, R. A. NICOLL, AND D. S. BREDT, *Bidirectional synaptic plasticity regulated by phosphorylation of stargazin-like tarps*, *Neuron*, 45 (2005), pp. 269–277.
- [137] S. TORQUATO, *Random Heterogeneous Materials: Microstructure and Macroscopic Properties*, Springer-Verlag, 2002.
- [138] A. TRILLER AND D. CHOQUET, *Synaptic structure and diffusion dynamics of synaptic receptors*, *Biol. Cell*, 95 (2003), pp. 465–476.
- [139] ———, *Surface trafficking of receptors between synaptic and extrasynaptic membranes: and yet they do move!*, *Trends Neurosci.*, 28 (2005), pp. 133–139.
- [140] H. C. TUCKWELL, *Introduction to Theoretical Neurobiology: Volume 1, Linear Cable Theory and Dendritic Structure (Cambridge Studies in Mathematical Biology)*, Cambridge University Press, April 1988.
- [141] G. G. TURRIGIANO, K. R. LESLIE, N. S. DESAI, L. C. RUTHERFORD, AND S. B. NELSON, *Activity-dependent scaling of quantal amplitude in neocortical neurons*, *Nature*, 391 (1998), pp. 892–896.
- [142] G. G. TURRIGIANO AND S. B. NELSON, *Homeostatic plasticity in the developing nervous system*, *Nat. Rev. Neurosci.*, 5 (2004), pp. 97–107.
- [143] N. G. VAN KAMPEN, *Stochastic Processes in Physics and Chemistry (North-Holland Personal Library)*, North Holland, July 2001.
- [144] M. J. WARD, *Diffusion and bifurcation problems in singularly perturbed domains*, *Natural Resource Modeling*, 13 (2000), pp. 271–302.
- [145] M. J. WARD, W. D. HESHAW, AND J. B. KELLER, *Summing logarithmic expansions for singularly perturbed eigenvalue problems*, *SIAM J. App. Math.*, 53 (1993), pp. 799–828.
- [146] P. WASHBOURNE, X.-B. LIU, E. G. JONES, AND A. K. MCALLISTER, *Cycling of *nmda* receptors during trafficking in neurons before synapse formation*, *J. Neurosci.*, 24 (2004), pp. 8253–8264.
- [147] D. G. WINDER AND J. D. SWEATT, *Roles of serine/threonine phosphatases in hippocampal synaptic plasticity*, *Nat. Rev. Neurosci.*, 2 (2001), pp. 461–474.

- [148] H. WU, J. E. NASH, P. ZAMORANO, AND C. C. GARNER, *Interaction of sap97 with minus-end-directed actin motor myosin vi. implications for ampa receptor trafficking*, J. Biol. Chem., 277 (2002), pp. 30928–30934.
- [149] A. M. ZHABOTINSKY, *Bistability in the ca(2+)/calmodulin-dependent protein kinase-phosphatase system.*, Biophys J, 79 (2000), pp. 2211–2221.
- [150] A. M. ZHABOTINSKY, R. N. CAMP, I. R. EPSTEIN, AND J. E. LISMAN, *Role of the neurogranin concentrated in spines in the induction of long-term potentiation*, J. Neurosci., 26 (2006), pp. 7337–7347.
- [151] E. B. ZIFF, *Enlightening the postsynaptic density*, Neuron, 19 (1997), pp. 1163–1174.